

THESIS

SIMULATIONS OF ARCTIC MIXED-PHASE CLOUDS USING A NEW AEROSOL-
LINKED ICE NUCLEI PARAMETERIZATION IN A PROGNOSTIC ICE PREDICTION
SCHEME

Submitted by

James Michael Carpenter

Department of Atmospheric Science

In partial fulfillment of the requirements

For the Degree of Master of Science

Colorado State University

Fort Collins, Colorado

Spring 2013

Master's Committee:

Advisor: Sonia M. Kreidenweis

Paul J. DeMott
David A. Randall
Richard Eykholt

Copyright by James Michael Carpenter 2013

All Rights Reserved

ABSTRACT

SIMULATIONS OF ARCTIC MIXED-PHASE CLOUDS USING A NEW AEROSOL- LINKED ICE NUCLEI PARAMETERIZATION IN A PROGNOSTIC ICE PREDICTION SCHEME

Despite the nearly universally-accepted notion that the Arctic is one of the most important areas to fully understand in the face of a changing global climate, observations from the region remain sparse, particularly of clouds and aerosol concentrations and sources. Low-level, mixed-phase clouds in the Arctic are capable of remarkable persistence, lasting for several days when our knowledge of the Wegener-Bergeron-Findeisen (WBF) process suggests that complete conversion to ice, or glaciation, should occur much faster, within a couple of hours. Multiple attempts at simulating these long-lived, mixed-phase clouds have been unable to accurately reproduce all cloud properties observed, with a major consequence being poor representation of radiative transfer, with important consequences for long-term climate simulations.

Recent observational campaigns have sought to characterize ice-nucleating particles (IN) not just in the Arctic, but around the planet. A product of these campaigns, the DeMott IN parameterization (*DeMott et al.*, 2010) seeks to provide a means for accurately implementing IN concentration calculations in a global model using minimal, readily-available proxy measurements or estimates of number concentrations of particles having diameters larger than 0.5 microns.

In this study, the performance of this parameterization is tested in a cloud-resolving model capable of high resolution simulations of Arctic mixed-phase boundary layer stratus

clouds. Three mixed-phase cloud case studies observed during the Indirect and Semi-Direct Aerosol Campaign (ISDAC) and Mixed-Phase Arctic Cloud Experiment (M-PACE) are simulated with varying complexity in their cloud microphysical packages. The goal is to test the new aerosol-linked parameterization as well as the sensitivity of the observed clouds to ice nuclei concentrations.

In an effort to increase the realism of the aerosol-cloud interactions represented in the cloud-resolving model, a new, simple prognostic scheme for the activation of ice nuclei is incorporated. The new scheme imposes a finite budget on potential ice nuclei, which are depleted through ice activation and growth, and can potentially be replenished by sublimating ice crystals. Results are contrasted with simulations in which no depletion of IN is assumed.

In this study, we found that while the DeMott IN parameterization successfully predicted available IN concentrations within observational error, the model was unable to predict sufficiently high pristine ice concentrations for one of the case studies. There were likely issues with the model or initialization in this case. For two of the case studies, the model performed exceptionally well, predicting accurate ice number concentrations as well as cloud droplet concentrations, leading to reasonable predictions of downwelling longwave radiation at the surface. In all cases, the model failed to predict reasonable cloud ice water contents. In the future, tests of ice crystal habits and growth rates may improve microphysical representation and predicted ice water contents. Replenishment of scavenged ice nuclei via surface fluxes and long-range transport can be included in the simulations to increase realism, but more observations are needed to accurately quantify these effects.

ACKNOWLEDGMENTS

I would like to thank Drs. Sonia Kreidenweis and Paul DeMott for their invaluable guidance and support over the course of this work. Additionally, Drs. David Randall and Richard Eykholt for their participation as members of my committee. I appreciate immensely the support provided by Mark Branson to further my understanding of the cloud model, and for his development of the visualization and analysis tools, which I have used extensively in pursuit of this research.

It is important for me to acknowledge the support of my parents, who instilled in me at an early age a love of science, which continues to drive my intellectual curiosity, and each of my friends who have provided helpful discussion, and occasional arguments. A special thanks to Allyson Clark, for supporting me all along the way.

This research was supported in part by the National Science Foundation Science and Technology Center for MultiScale Modeling of Atmospheric Processes, managed by Colorado State University under cooperative agreement ATM-0425247. Additional analyses used were also supported under the Department of Energy/Office of Science, Biological, and Environmental Research Division Contract SC00002354.

TABLE OF CONTENTS

| | |
|--|------|
| ABSTRACT..... | ii |
| ACKNOWLEDGMENTS..... | iv |
| TABLE OF CONTENTS..... | v |
| LIST OF TABLES..... | vii |
| LIST OF FIGURES..... | viii |
| Chapter 1: Introduction | 1 |
| 1.1: Issues and Motivation..... | 1 |
| 1.2: Arctic Clouds..... | 2 |
| 1.3: Arctic Cloud Modeling..... | 9 |
| 1.4: Ice Nuclei..... | 12 |
| 1.5: Objectives..... | 14 |
| Chapter 2: Methodology | 16 |
| 2.1: Analysis of ISDAC IN Data..... | 16 |
| 2.2: SAM Description and Setup..... | 23 |
| 2.3: Development of IN Budget Equations..... | 25 |
| 2.4: Case Study Days..... | 28 |
| Chapter 3: Case Study 1 – ISDAC Flight 16 | 30 |
| 3.1: Observations..... | 30 |
| 3.2: Model Initialization..... | 33 |
| 3.3: Diagnostic IN Simulations..... | 36 |
| 3.4: Prognostic IN Simulations..... | 43 |
| Chapter 4: Case Study 2 – ISDAC Flight 31 | 56 |
| 4.1: Observations..... | 56 |
| 4.2: Model Initialization..... | 60 |
| 4.3: Diagnostic IN Simulations..... | 61 |

| | |
|--|-----------|
| 4.4: Prognostic IN Simulations..... | 65 |
| Chapter 5: Case Study 3 – M-PACE..... | 78 |
| 5.1: Observations..... | 78 |
| 5.2: Model Initialization..... | 79 |
| 5.3: Diagnostic IN Simulations..... | 81 |
| 5.4: Prognostic IN Simulations..... | 84 |
| Chapter 6: Summary and Conclusions..... | 94 |
| REFERENCES..... | 101 |

LIST OF TABLES

| | |
|--|----|
| TABLE 2.1: Basic model parameters and aerosol distributions..... | 28 |
| TABLE 3.1: List of ISDAC Flight 16 (8 April 2008) SAM Simulations..... | 34 |
| TABLE 4.1: List of ISDAC Flight 31 (26 April 2008) SAM Simulations..... | 60 |
| TABLE 5.1: List of M-PACE (October 2004) SAM Simulations..... | 80 |

LIST OF FIGURES

Figure 2.1: Comparison of observed IN versus IN predicted on the basis of D10 (dashed curve) for ISDAC Flight 17 on April 8, 2008 (local time). UTC time is for the beginning of April 9, 2008. IN data are for one minute integral periods. IN processing temperatures ranged from -27 to -30°C during the period shown. PCASP aerosol concentrations at sizes above 0.5 μm and cloud phase (0 = no cloud; 1 = subcloud ice present) are also shown. An ambient pressure range from the surface to 450 mb is represented.....20

Figure 2.2: Comparison of observed IN versus predicted IN in a) for a portion of ISDAC Flight 31 on April 26, 2008. Gaps in IN data are periods of sampling from the counterflow virtual impactor inlet. PCASP aerosol concentrations at sizes larger than 0.5 μm and cloud phase (0 = no cloud; 1 = ice or sub-cloud precipitating ice present) are also shown. CFDC IN processing temperatures and RH are shown in b). A mix of above (~910 mb, highest T_{CFDC}) and below (~970 mb, lowest T_{CFDC}) sampling is represented.....22

Figure 2.3: Summary of ISDAC IN (red points) relation to IN predicted by the D10 parameterization, and including the original data from DeMott et al. (2010). All data are for standard temperature and pressure conditions. Dashed lines parallel to the 1:1 solid line bracket a factor of 5 times the standard relation.....23

Figure 3.1: Time series of (a) temperature in degrees Celsius, (b) liquid water content in g m⁻³, (c) cloud droplet number concentration in units cm⁻³, (d) ice water content in g m⁻³, (e) pristine ice number concentration in units L⁻¹, from onboard the Convair 580 during Flight 16. Data obtained from the DOE-ARM archive for the ISDAC project.....32

Figure 3.2: Vertical profiles of the initialization data used for simulations of cloud encountered during Flight 16. SAM is initialized with potential temperature instead of ambient temperature. Also shown are water vapor mixing ratio in g kg⁻¹, and averaged horizontal winds used to nudge the simulations.....36

Figure 3.3: Selected SAM output from the CTRL simulation. The horizontal axis is time, and the vertical axis is height; all fields were horizontally averaged at each time step to produce these and all subsequent modeled output figures, unless otherwise noted. The upper left panel is cloud ice mass in g kg⁻¹, the upper right panel is cloud water mass in g kg⁻¹, the lower left panel is cloud ice number concentration in cm⁻³, and the lower right panel is surface precipitation in mm day⁻¹. Color scales shown are consistent across all diagnostic mode simulations (Figures 3.3-3.6) for easy visual comparison.....37

| | |
|---|----|
| Figure 3.4: Selected SAM output from the DEMOTT simulation. The horizontal axis is time, and the vertical axis is height. Panels as in Figure 3.3..... | 39 |
| Figure 3.5: Selected SAM output from the DM_0.1. The horizontal axis is time, and the vertical axis is height. Panels as in Figure 3.3..... | 40 |
| Figure 3.6: Selected SAM output from the DM_10. The horizontal axis is time, and the vertical axis is height. Panels as in Figure 3.3. Note that the scales differ from Figures 3.3-3.5 to show detail..... | 41 |
| Figure 3.7: Selected SAM output from the prognostic IN simulation, where IN recycling due to sublimation is completely ignored. The horizontal axis is time, and the vertical axis is height. The upper left is cloud ice mass concentration in g kg^{-1} , the upper right panel is cloud liquid water mass concentration in g kg^{-1} , the lower left panel is cloud ice number concentration in cm^{-3} , and the lower right panel is potential IN concentration (tracer field) in L^{-1} | 43 |
| Figure 3.8: Selected SAM output from the prognostic IN simulation SNOSUB, where IN recycling due to sublimating snow only is considered. The horizontal axis is time, and the vertical axis is height. All panels as in Figure 3.7..... | 46 |
| Figure 3.9: Selected SAM output from the prognostic IN simulation SNOSUB_d, where IN recycling due to sublimating snow only is considered. The lowest 200m of the atmosphere have been totally dried, resulting most noticeably in the elimination of the surface fog. The horizontal axis is time, and the vertical axis is height. All panels as in Fig..... | 47 |
| Figure 3.10: Selected SAM output from the prognostic 8.65 L^{-1} IN simulation SUB_HI, where IN recycling due to all sublimating ice species is considered. The horizontal axis is time, and the vertical axis is height. All panels as in Fig. 3.7..... | 48 |
| Figure 3.11: Selected SAM output from the prognostic 4.325 L^{-1} IN simulation SUB_LO, where IN recycling due to all sublimating ice species is considered. The horizontal axis is time, and the vertical axis is height. All panels as in Figure 3.7..... | 49 |
| Figure 3.12: Selected SAM output from the prognostic 8.65 L^{-1} IN simulation SUB_HI_d, where IN recycling due to all sublimating ice species was considered. The lowest 200m of the atmosphere have been totally dried, resulting in the elimination of the surface fog seen in other simulations. The horizontal axis is time, and the vertical axis is height. All panels as in Fig. 3.7..... | 50 |
| Figure 3.13: Single vertical profiles for selected F16 simulations. Diagnostic simulations are from hour 11, and prognostic simulations from hour 7. Refined aircraft data from G. McFarquhar shown for reference, obtained from DOE-ARM archive..... | 52 |

Figure 4.1: Time series of (a) temperature in degrees Celsius, (b) liquid water content in g m^{-3} , (c) cloud droplet number concentration in units cm^{-3} , (d) ice water content in g m^{-3} , (e) pristine ice number concentration in units L^{-1} , from onboard the Convair 580 during Flight 31. Data obtained from the DOE-ARM archive for the ISDAC project.....59

Figure 4.2: Vertical profiles of the initialization data used for Flight 31. SAM is initialized with potential temperature instead of actual ambient temperature. Also shown are water vapor mixing ratio in g/kg , and averaged horizontal winds.....61

Figure 4.3: Selected SAM output from the CTRL simulation. The horizontal axis is time, and the vertical axis is height; all fields were horizontally averaged at each time step to produce these and all subsequent modeled output figures, unless otherwise noted. The upper left panel is cloud ice mass in g kg^{-1} , the upper right panel is cloud water mass in g kg^{-1} , the lower left panel is cloud ice number concentration in cm^{-3} , and the lower right panel is surface precipitation in mm day^{-1}62

Figure 4.4: Selected SAM output from the DEMOTT simulation. The horizontal axis is time, and the vertical axis is height. All panels as in Fig. 4.3.....63

Figure 4.5: Selected SAM output from the DM_0.1 simulation. The horizontal axis is time, and the vertical axis is height. All panels as in Fig. 4.3.....64

Figure 4.6: Selected SAM output from the DM_10 simulation. The horizontal axis is time, and the vertical axis is height. All panels as in Fig. 4.3.....65

Figure 4.7: Selected SAM output from the prognostic NOSUB simulation (5.0 L^{-1} IN, no IN recycling due to sublimation). The horizontal axis is time, and the vertical axis is height. The upper left is cloud ice mass concentration in g kg^{-1} , the upper right panel is cloud liquid water mass concentration in g kg^{-1} , the lower left panel is cloud ice number concentration in cm^{-3} and the lower right panel is potential IN concentration (tracer field) in L^{-1} . The color scales are consistent across the prognostic simulations for easy visual comparison.....66

Figure 4.8: Selected SAM output from the prognostic SNOSUB simulation (5.0 L^{-1} IN, including IN recycling due to sublimating snow only). The horizontal axis is time, and the vertical axis is height. All panels as in Fig. 4.7.....68

Figure 4.9: Selected SAM output from the prognostic SNOSUB_d simulation (5.0 L^{-1} IN, IN recycling due to sublimating snow only). The lowest 200m of the atmosphere have been totally dried, resulting in the elimination of the surface fog. The horizontal axis is time, and the vertical axis is height. All panels as in Fig. 4.7.....69

Figure 4.10: Selected SAM output from the prognostic SUB_HI simulation (5.0 L^{-1} IN, IN recycling due to all sublimating ice species). The horizontal axis is time, and the vertical axis is height. All panels as in Fig. 4.7.....70

Figure 4.11: Selected SAM output from SUB_LO simulation. The horizontal axis is time, and the vertical axis is height. All panels as in Fig. 4.7.....72

Figure 4.12: Selected SAM output from the prognostic SUB_HI_d simulation ($5.0 \text{ L}^{-1} \text{ IN}$, IN recycling due to all sublimating ice species). The lowest 200m of the atmosphere have been totally dried, resulting in the elimination of the surface fog. All panels as in Fig. 4.7.....73

Figure 4.13: Single vertical profiles for selected F31 simulations. Diagnostic simulations are from hour 11, and prognostic simulations from hour 4. Refined aircraft data from G. McFarquhar shown for reference, obtained from DOE-ARM archive.....75

Figure 5.1: Vertical profiles of the initialization data used for M-PACE. SAM is initialized with potential temperature instead of ambient temperature. Also shown are water vapor mixing ratio in g/kg, and averaged horizontal winds.....81

Figure 5.2: Selected SAM output from CTRL. The horizontal axis is time, and the vertical axis is height; all fields were horizontally averaged at each time step to produce these and all subsequent modeled output figures, unless otherwise noted. The upper left panel is cloud ice mass in g/kg, the upper right panel is cloud water mass in g/kg, the lower left panel is cloud ice number concentration in $\#/\text{cm}^3$, and the lower right panel is surface precipitation in mm/day. Color scales shown are consistent across all diagnostic mode simulations for easy visual comparison.....82

Figure 5.3: Selected SAM output from the DEMOTT simulation. The horizontal axis is time, and the vertical axis is height. All panels as in Fig. 5.2.....83

Figure 5.4: Selected SAM output from the prognostic NOSUB simulation ($4.04 \text{ L}^{-1} \text{ IN}$, no IN recycling due to sublimation). The horizontal axis is time, and the vertical axis is height. Upper left panel is cloud ice mass in g/kg, upper right panel is cloud water mass in g/kg, lower left panel is cloud ice number concentration in $\#/\text{cm}^3$, and lower right panel is potential IN concentration in $\#/\text{Liter}$. The color scales are consistent across the prognostic simulations for easy visual comparison.....84

Figure 5.5: Selected SAM output from the prognostic SNOSUB simulation ($4.04 \text{ L}^{-1} \text{ IN}$, IN recycling due to sublimating snow only). The horizontal axis is time, and the vertical axis is height. All panels as in Fig. 5.4.....86

Figure 5.6: Selected SAM output from the prognostic SNOSUB_d simulation ($4.04 \text{ L}^{-1} \text{ IN}$, IN recycling due to sublimating snow only). The lowest 200m of the atmosphere were totally dried in the initialization. All panels as in Fig. 5.4.....87

Figure 5.7: Selected SAM output from the prognostic $4.04 \text{ L}^{-1} \text{ IN}$ simulation, where IN recycling due to Selected SAM output from the prognostic SUB_HI simulation ($4.04 \text{ L}^{-1} \text{ IN}$, IN recycling due to all sublimating ice species). The horizontal axis is time, and the vertical axis is height. All panels as in Fig. 5.4.....88

Figure 5.8: Selected SAM output from the prognostic SUB_HI_d simulation ($4.04 \text{ L}^{-1} \text{ IN}$, IN recycling due to all sublimating ice species). The lowest 200m of the atmosphere were totally dried in the initialization. All panels as in Fig. 5.4.....89

Chapter 1

Introduction

1.1 Issues and Motivation

The sensitivity of the Arctic to changes in climate and circulation has been postulated for a number of years (IPCC 2007), and recent rapid declines in seasonal sea ice extent have increased interest in the factors controlling sea ice, circulations, and Arctic cloudiness. Sea ice variations have been linked to cloudiness in several studies (e.g., *Kay and Gettelman, 2009*). As of mid-October 2012, sea ice extent in the Arctic was 5.18 million square kilometers, 3.49 million square kilometers below the 1979-2000 mean for this time of year, and 70,000 square kilometers lower than the same date in 2007 (*National Snow and Ice Data Center*). The Arctic, in conjunction with the Antarctic, serves as a net sink of longwave energy, radiating more heat to space than is received via insolation as an annual average. With the tropics heating on average, an imbalance is created which drives Earth's weather systems, and subsequently clouds. A warming Arctic is a primary indicator that this radiative balance is changing (*Serreze et al., 2006; Garrett et al., 2009*), and it is not unreasonable to assume that corresponding changes in cloud cover will also be observed in the long term (*MacBean, 2004*). Both liquid and mixed-phase, low-level stratus have been shown to be the most important contributors to the surface radiation balance in the Arctic (*Shupe et al., 2003*).

Of particular interest are the processes that maintain mixed-phase clouds, which have frequently been observed in the Arctic and can persist for many hours (*Morrison et al., 2012*).

Due to the presence of liquid layers, these clouds have different radiative properties than their fully glaciated counterparts. At the cloud level, an area of active research is in elucidating the microphysical processes at work, which help determine the structure of the cloud, how much precipitation is produced, and how long the system can persist. Because of their direct link to hydrometeor formation, atmospheric aerosols play a large role in cloud microphysical processes, but sources of cloud-active particles to the Arctic are not well characterized. Long-range transport from the mid-latitudes may be a primary means of replenishing Arctic aerosols, but locally-sourced particles may also play a role. In the following, we review current understanding of low cloud formation and Arctic clouds in particular, as well as recent observational campaigns that were targeted at improving understanding of Arctic cloud processes. We conclude with an overview of the science questions to be addressed in this thesis.

1.2 Arctic Clouds

1.2.1 Climatology

Annual climatologies of stratus clouds derived from surface and satellite observations have shown that roughly one-third of the planet is covered in low-level stratus decks at any given time (*Klein et al.*, 1993). Stratus clouds can form over any location on Earth, but the majority occur at mid- to high latitudes, particularly over open ocean, with cloud amounts averaging 34%, compared to nearly 18% over land (*Klein et al.*, 1993). Stratus clouds are an important regulator of Earth's climate. Low-lying clouds tend to reflect a significant amount of incoming solar radiation during the daytime, leading to surface cooling; it has been estimated that a 4% increase in stratus coverage globally would be sufficient to offset the increased longwave heating

predicted to occur from a doubling of atmospheric carbon dioxide concentrations (*Randall et al.*, 1984). Whether Arctic cloud cover is changing is therefore a key question related to changes in the Earth's average albedo, especially when considering the impact of decreasing sea ice cover in the Arctic, since sea ice also serves to reflect incoming short-wave radiation whereas open water is strongly absorbing.

Stratus clouds typically cover large areas preferentially forming on the western side of continents where cold water upwelling is present. Stratus decks can form under a variety of circumstances, but similar base ingredients are required. A well-mixed boundary layer, relatively uniform wind field, a strong subsidence inversion, aerosol particles to serve as cloud condensation nuclei and ice nuclei, and sufficient moisture to condense into a cloud layer are required parts of the formation process. The lifting of relatively warm, moist air to the dew-point level, or the radiative cooling of air in place to its dew-point, are two common processes that can initiate the condensation of vapor into droplets, leading to stratus formation.

We separate stratus decks into three basic forms dependent on cloud phase. Warm stratus decks contain water only in liquid form, occur primarily in mid-latitudes, and do not frequently precipitate, but at times may produce light precipitation such as drizzle. Fully glaciated clouds consist only of ice crystals, and can result when a mixed-phase cloud exhausts its liquid water supply.

1.2.2 Mixed-phase clouds

Mixed-phase stratus clouds, which are examined in this study, contain both liquid and frozen water. Low-level, mixed-phase stratus clouds in the Arctic commonly appear as a shallow layer, topped with a supercooled liquid layer. The liquid layer is thought to be the region where

the activation of ice nuclei and initial growth of ice crystals occurs (*Morrison et al.*, 2012), and within the lower portion of the supercooled liquid layer exists the mixed-phase layer, where liquid droplets and pristine ice crystals are co-located. Closer to the surface, the mixed-phase layer transitions into an ice-only layer where the liquid droplets have been evaporated in favor of the vapor-condensational growth of ice crystals and aggregates. Updrafts of $\sim 0.4 \text{ m s}^{-1}$ within the clouds are a key component in sustaining the mixed-phase structure; ice crystal formation and growth typically occurs in these regions, and sufficiently large crystals fall out around the updrafts (*Shupe et al.*, 2008). If a mixed-phase stratus cloud exhausts the liquid water supply through ice formation, or if temperatures are sufficiently cold, then a mixed-phase stratus deck can transition into a glaciated stratus, where only frozen hydrometeors remain. Multiple field campaigns have been conducted over the last two decades to characterize the behavior and structure of Arctic mixed-phase stratus clouds, with an emphasis on furthering our understanding of the microphysical processes at work and how they relate to and interact with other factors in these clouds contributing to their prolonged lifetimes (*McFarquhar et al.*, 2007, 2011; *Jackson et al.*, 2012; *Morrison et al.*, 2012). The enhanced lifetimes of these mixed-phase clouds, frequently on the scale of days, is particularly troublesome to understand given our knowledge of ice-liquid relationships inside clouds. Known as the Wegener-Bergeron-Findeisen process, our current understanding of cloud physics indicates that cloud droplets are sacrificed in favor of ice crystal growth due to differences in vapor pressures above the hydrometeors. In theory, this process should glaciate a mixed-phase stratus cloud in a matter of hours (*Morrison et al.*, 2012), yet they persist for a significantly longer period of time. It has been suggested that three simple inequalities determine the fate of mixed-phase stratus (*Korolev*, 2007). When the vapor pressure is greater than both saturation vapor pressures for liquid and ice, the mixed-phase cloud can exist

for as long as the vapor pressure is sufficiently high. When actual vapor pressures are higher than the saturation vapor pressure for ice, but lower than the liquid saturation vapor pressure, the Wegener-Bergeron-Findeisen process is expected to dominate in the cloud. Third, when the actual vapor pressure is lower than both saturation vapor pressures for ice and liquid, the cloud is observed to dissipate due to evaporation of both ice and droplets (*Korolev, 2007*). Understanding the complex interactions that sustain the liquid layer in these clouds for such long periods of time is a priority, and an area of active research. Understanding mixed-phase clouds is of crucial importance to enhancing modeling capability, primarily in a climate prediction framework. Climate models depend on accurate representation of radiation balances, and cloud type has significant impact on the radiative transfer processes occurring at the surface, inside the cloud, and above cloud top. Liquid water has enhanced longwave absorptive properties, and increases in cloud liquid can increase return of longwave energy to the surface, resulting in additional surface warming. In a mixed-phase cloud, the relationship between liquid water droplets and ice crystals determines the radiative impact of the cloud, and impacts properties from cloud-scale dynamics to sea-ice coverage (*Curry et al., 1996; Harrington and Olsson, 2001; Jiang et al., 2000*). Radiative processes have also been indicated in determining the lifetime of the clouds, with longwave cooling suspected in decreasing the amount of time required for glaciation to occur, and shortwave heating leading to longer times before glaciation (*Lebo et al., 2008*).

1.2.3 Arctic Observations

The United States government Atmospheric Radiation Measurement (ARM) Program was founded in 1989 by the Department of Energy to establish multiple scientific research platforms for the study of clouds and cloud impacts on radiative processes in Earth's atmosphere. One such site, the North Slope of Alaska site (NSA) near Barrow, Alaska, has been a preferred

site for the study of mixed-phase arctic stratus decks. The NSA site is heavily instrumented with LIDAR, RADAR systems operating on different bands, precipitation sensors, radiometers, and sounding systems. For intensive field campaigns, instrumented aircraft can investigate clouds in the vicinity of the NSA site to supplement and validate remotely-sensed data from the ground.

The First ISCCP (International Satellite Cloud Climatology Project) Regional Experiment – Arctic Cloud Experiment (FIRE-ACE), conducted in April and July of 1998 sought to enhance understanding of Arctic cloud cover impacts on radiative transfer processes between the surface, atmosphere, and space, as well as how surface characteristics impact the cloud cover. The FIRE-ACE campaign focused on obtaining remote and in-situ measurements through use of multiple aircraft, including the ground-based NSA site. During the FIRE-ACE campaign, the first airborne measurements of ice nuclei for the Arctic were completed, providing insight into springtime concentrations of ice-nucleating aerosol particles (*Rogers et al.*, 2001). An important aspect of the FIRE-ACE study is its data overlap with the Surface Heat Budget of the Arctic field campaign (SHEBA).

The SHEBA field project, a year-long, multi-agency experiment that began in October 1997, headed by the National Science Foundation and Office of Naval Research, provided one of the early in-depth looks at annual mixed-phase arctic cloud cover properties and seasonality. Nearly an entire year of LIDAR and RADAR data was collected, which provided insight into the seasonality of arctic stratus clouds (*Intrieri et al.*, 2002). This study of arctic clouds revealed that the Arctic appears to exhibit a strong annual cycle in cloud cover and cloud properties. Late summer and early fall were found to be the cloudiest, with winter being the season with least cloud coverage. In general, the Arctic is cloudy more than not, with average total cloud cover at 84% for the year-long study (*Intrieri et al.*, 2002). Clouds containing liquid water occurred most

frequently in the summer, with lower occurrences in winter, though liquid water was still detected in winter clouds as frequently as 45% of the time. In the springtime, coinciding with FIRE-ACE/SHEBA and the later Indirect and Semi-Direct Aerosol Campaign (ISDAC), the presence of liquid water was detected in 73% of the observed clouds.

1.2.4 M-PACE Overview and Objectives

The Mixed-Phase Arctic Cloud Experiment (M-PACE) was conducted from late September through October 2004 at the ARM North Slope of Alaska site. During this seasonal transition, the M-PACE campaign sought to collect measurements to support further understanding of arctic mixed-phase cloud evolution, thermodynamics, microphysics, dynamics, and radiative properties (*Verlinde et al., 2007*). The primary science goals behind the M-PACE field study were to improve understanding of the links between radiative transfer, dynamics, and cloud microphysics, to evaluate the performance of surface-based remote sensing instrumentation in regards to mixed-phase clouds, and to understand the characteristics of midlevel clouds in the Arctic. The study set clear objectives in support of these goals, which included obtaining information on the spatial structure and distribution of cloud cover and microphysics, obtaining simultaneous radiation measurements above and below cloud cover with corresponding in-situ microphysical observations, and observing how varying surface conditions impact clouds. Of particular use to this study, M-PACE documented ice nuclei (IN) population characteristics, and vertical profiles of water vapor and other state variables, which are useful in developing initialization points for model simulations. Modeling studies utilizing the M-PACE dataset have since shown strong relationships between IN concentrations and resultant cloud properties, primarily in the form of fundamental alterations to the radiative balances at the

surface and within the cloud, but also the cloud structure itself can be altered drastically with small changes in IN concentrations (*Prenni et al., 2007; Fridlind et al., 2007*).

1.2.5 ISDAC Overview and Objectives

The ISDAC field study was conducted along the North Slope of Alaska from March 29 through April 30 of 2008, coinciding with the International Polar Year, resulting in increased observational capacity through the support of other sites conducting measurements. The ISDAC Campaign itself utilized the ARM Climate Research Facility's Barrow, Alaska site to deploy a suite of ground instruments to measure atmospheric, aerosol, and cloud properties, as well as the Canadian National Research Council's Convair 580 aircraft, upon which nearly 40 instruments were used to measure aerosol parameters including composition, concentration, and size distribution, ice nuclei concentration, supercooled liquid concentration, radiative properties, and state variables including humidity, temperature, and vertical velocity. The ISDAC Campaign set out to accomplish varied tasks, the most relevant of those including comparison of aerosol properties in springtime to those measured in the fall, during the Mixed-Phase Arctic Cloud Experiment (M-PACE). Additional tasks, relevant to this work, included evaluating changes in cloud structure and behavior due to aerosol changes and sea surface phase between fall and spring, and evaluating the performance of cloud models and cloud parameterizations, including how well they capture seasonally-varying differences in arctic clouds.

1.3 Arctic Cloud Modeling

1.3.1 Model types and characteristics

Multiple types of models exist for studying clouds, each with their own set of benefits and drawbacks. The simplest of these, one-dimensional layer-averaged models where cloud layer response to stimuli can be easily studied, lack versatility required to study much else. With increasing complexity comes more scientific utility, at the cost of increased computational requirements. Large-eddy simulations, or cloud-resolving models such as the one used in this study are capable of explicitly resolving some forms of turbulent mixing, but require many more calculations per time step. For this reason, large-eddy simulations are generally conducted with a vertical domain consisting of the lowest several kilometers of the atmosphere; to resolve cloud-scale motions over the entire depth of the atmosphere would require prohibitive amounts of computer time. In general, computer modeling proves to be an imprecise art. Finite differencing, parameterization, and overlying assumptions are just a few of the things that introduce computational error. In turn, errors can compound over time, resulting in poor model performance with outputs straying far from the intended results. To add to these inherent difficulties, different types of clouds are formed under different atmospheric conditions, and computer models must have the flexibility to model these different circumstances. For example, low-lying, weakly-forced clouds such as fog tend to be dominated by microphysical and radiative processes, whereas a mesoscale convective system is driven more by larger scale dynamical motions such as updrafts and vertical wind shear. An effective computer model must be able to accurately represent each of these driving forces appropriately for the type of cloud being studied. Of course, the underlying knowledge of the processes at work and which

dominate, if any, for each cloud type must be present, and this is an active, ongoing area of research.

Mixed-phase Arctic stratus decks form under unique circumstances, and cloud processes which may be treated as less important with minimal effect in other cloud types often prove to be essential. As an example, in a more dynamically-driven cloud such as a rotating supercell, the vertical wind shear is more important in prolonging the lifetime of the main updraft. In Arctic mixed-phase stratus clouds, vertical accelerations are more subtle, and intimately linked to longwave radiative cooling at cloud top. An incorrect or incomplete assumption regarding any single process can have repercussions for the entire cloud system, since the dynamical, radiative, and microphysical processes are tightly coupled in these clouds (*Morrison et al.*, 2012). As will be shown in the results of this study, modifying a single parameter in the model can drastically change the structure and behavior of the modeled Arctic stratus, requiring careful inspection of the model setup, assumptions, and cloud observations to provide insight into cloud behavior.

Turbulence is one of many essential processes occurring in persistent, mixed-phase stratus decks that contribute to cloud lifetime and precipitation production, so the ability to properly capture turbulent motions is a priority. Grid sizing plays an important role in representing small-scale turbulent motions that are important in these clouds; when grid boxes are too large, contributions by eddy transport will be incorrectly represented or altogether missed. Of course, choosing smaller grid-boxes comes at a computational cost, and modeling clouds is a balancing act in which the domain must be filled with sufficient grid boxes to capture most of the motion explicitly while maintaining a reasonable level of computational efficiency.

Turbulence which cannot be resolved based on the model resolution must be parameterized, but the effectiveness of these turbulence parameterizations is also limited by the desired efficiency of the model. This issue relates to what is often referred to as the turbulence closure problem, where the non-linear nature of the fluid motion creates complications when attempting to linearize dynamical equations to function in a finite-differencing model. Further, generally-applied turbulence closure schemes that work well in many applications are not appropriate to the stably stratified conditions frequently found in the Arctic (*Olsson et al.*, 1998).

1.3.2 Prior Arctic modeling

In general, research in the Arctic and modeling of arctic clouds was limited prior to several global climate modeling studies that indicated the Arctic to be an area of concern that warrants further investigation (*Walsh et al.*, 2002). Despite limited observations, early cloud-resolving model studies of Arctic mixed-phase stratus showed that cloud sustainability is dependent on several factors such as ice concentrations and growth habits, temperature, and available ice nuclei (*Harrington et al.*, 1999). Several modeling studies of the field study cases presented here have been conducted, in attempts to improve understanding of the processes that maintain long-lived mixed-phase clouds in the Arctic. In particular, there is a present lack of understanding of the key interactions between the dynamical and microphysical processes occurring within these clouds. Model intercomparison studies have shown large variations, up to five orders of magnitude, between cloud resolving models and single column models in predictions of ice crystal number concentrations, despite general agreement in ice water contents and ice water path (*Klein et al.* 2009). Individual studies have focused on particular processes ranging from the impact of changing ice number concentrations on mixed-phase cloud dynamics (*Ovchinnikov et al.*, 2011), to the relationship between hydrometeor types (*Larson et al.*, 2011).

Examples of prior modeling of the same case studies presented here will be discussed in conjunction with our results.

1.4 Ice Nuclei

At temperatures warmer than approximately $-35\text{ }^{\circ}\text{C}$, liquid droplets will freeze only if they contain particles capable of nucleating ice. Except in winter, temperatures lower than $-35\text{ }^{\circ}\text{C}$ are not often observed in Arctic clouds. Thus the presence of ice nuclei is important to ice formation, especially in mixed-phase clouds. Ice production in clouds is an important regulator of precipitation, and only a few IN particles per liter are required to explain observed precipitation rates (*Prenni et al.*, 2007). Although ice nucleation can proceed by a variety of mechanisms (*DeMott et al.*, 2010; *Rogers et al.*, 2001), we focus here on immersion-freezing nuclei, those particles that catalyze ice formation in supercooled liquid droplets. The activity of immersion-freezing ice nuclei (IN) is a function of temperature, with IN abundance generally increasing as temperature decreases. The identification and activity of these particles can be measured in real-time, including from aircraft, using a Continuous Flow Diffusion Chamber (CFDC) developed at Colorado State University (*Rogers et al.*, 1988). The CFDC measures IN concentrations by focusing aerosols within a vapor supersaturated region between two ice-coated cylinders, each with a different temperature. If active IN are present in the air flowing through the chamber, they will nucleate and grow into ice crystals of about 3 microns diameter or larger by the time they exit the chamber and are counted (*Rogers et al.*, 2001). The precise nature of the counted IN is a topic actively being pursued, as new measurement techniques have enabled the collection of more data on IN concentrations and compositions (*Kreidenweis et al.*, 1997) around

the globe and as a function of altitude. It is clear that some dust particles are active IN (*DeMott et al.*, 2003; *Prenni et al.*, 2009a), and biological particles are also important, especially at warmer temperatures (*Möhler et al.*, 2008). Other particle types that have been implicated in ice crystal nucleation include metal oxides and soot (*Prenni et al.*, 2009b; *Archuleta et al.*, 2005). The remote location of the Arctic and the lack of highly productive local dust and biological sources, particularly in colder seasons, means that IN are mostly likely present due to long range transport. Very little about the global sources and budgets of IN is known at present, and the budget for the Arctic is similarly unconstrained (*Prenni et al.*, 2007; *Fridlind et al.*, 2007). However, recent field studies have made in situ observations of IN concentrations so these can be used in modeling simulations to estimate their impacts on cloud phase, and also to estimate the rate at which they may be removed from the arctic boundary layer via interactions with clouds. These elements are important in building an understanding of the arctic IN budget. In some recent prior studies, ice initiation in models was constrained directly by such case-specific IN observations (*Avramov et al.*, 2011; *Morrison et al.*, 2008; *Fridlind et al.*, 2007). The recent development of an independent parameterization (*DeMott et al.*, 2010) to calculate the number of IN activating at each time step based on not just temperature, but on the ambient aerosol distribution itself, represents an important step in predicting ice properties in any cloud system, beyond those directly observed. For global models in particular, this method has inherent benefits considering the current limited capacity to monitor or predict source-specific IN concentrations in the global atmosphere.

1.5 Objectives

This work seeks to contribute to improved understanding of Arctic mixed-phase clouds in two ways. First, we employ a two-dimensional large-eddy model (horizontal grid spacing ~ 10 m; System for Atmospheric Modeling, SAM; Khairoutdinov et al., 2003) in case study mode to explore the aerosol-cloud microphysics-precipitation linkages described above. A unique contribution here is the incorporation into the model microphysical routines of a recent ice nuclei parameterization developed by DeMott et al. (2010) from multiple aerosol size-distribution datasets. This parameterization was also used in a new, prognostic IN prediction scheme that incorporated a finite budget on total available ice nuclei. This prognostic scheme was tested in multiple ways, from functioning essentially as an upper limit on the total available ice nuclei, to a fully interactive mode in which sublimating frozen hydrometeors can be recycled back into the simulated cloud system, potentially prolonging cloud lifetime and providing insight into the longevity of Arctic mixed-phase stratus clouds. This is a step forward in the world of computer simulations of the atmosphere, since there is a finite reservoir of ice-nucleating particles on the cloud scale. As particles are activated and grow to fall out of the cloud, they are efficiently removed from the atmosphere, and can only be replaced by continuing fluxes of particles from the Earth's surface entrained into cloud tops, or by evaporative processes potentially leading to particle recycling. For comparison, we also conducted simulations in which available ice nuclei were not depleted; hence, when ice crystals were removed from a volume of air by precipitation, new ice formation was allowed to occur to replenish the lost ice hydrometeors. We note that the original implementation of ice formation in the model followed a temperature-only formulation, that is, when the temperature dropped low enough, supercooled water was converted into ice.

This representation fails for the Arctic (*Morrison et al.*, 2006; *Liu et al.*, 2011; *DeMott et al.*, 2010).

The second contribution of this work is to demonstrate that SAM can accurately represent Arctic mixed-phase cloud formation when used in cloud-resolving mode (horizontal grid space ~100 m). SAM is the model embedded in the Multiscale Modeling Framework (MMF) used for a global representation of the effects of cloud-scale motions on the general circulation (*Khairoutdinov et al.*, 2002; *Randall et al.*, 2003) The MMF is a ‘model within a model’ in which the two-dimensional cloud-resolving model is inserted in a global model gridbox, initialized with the environmental conditions within the gridbox, and run to simulate the development of smaller-scale motions and clouds. The approach to ice nucleation used in this study improves SAM’s ability to represent mixed-phase clouds, and does so in a manner which does not significantly impact computational efficiency, thus maintaining the model in a state that can be used in a super-parameterization framework.

Chapter 2

Methodology

2.1 Analysis of ISDAC IN Data

The nucleation and growth of ice in arctic mixed-phase clouds remains under active investigation. Ice nucleation is typically parameterized in cloud models based on temperature, and prior methods of converting supercooled liquid water to ice in models have been based solely on temperature, or on estimated abundance of IN (as a function of temperature) that was obtained from a limited number of observations, neglecting the local aerosol environment. In an aerosol-deficient region such as the Arctic, we might expect such methods to overpredict IN number concentrations.

In cases where ice nuclei measurements were available, these have been used for one-to-one specification or constraint of predicted ice crystal concentrations in diagnostic or prognostic schemes (*Prenni et al., 2007; Avramov et al., 2011*). Other studies have employed known or hypothesized ice nucleation mechanisms and allowed the cloud microphysical observations to dictate parameters. This approach assumes that the IN measurements were possibly inadequate to explain observed ice formation (*Fridlind et al., 2007*).

In this study, we employed a recent parameterization of IN availability, based on more current and detailed field observations, that links the number concentrations of ice nuclei to not just temperature, but also to the concentrations of aerosol particles with diameters larger than 0.5 μm (*DeMott et al., 2010*). In this study, this activation parameterization is of the form

$$n_{IN} = a(273.16 - T_k)^b (n_{aer,0.5})^{(c(273.16 - T_k) + d)}, \quad (2.1)$$

where n_{IN} is the predicted number concentration of ice nuclei per standard Liter, T_k is the environmental temperature in Kelvins, and $n_{aer,0.5}$ is the number concentration of particles larger than 0.5 μm per standard cubic centimeter. Thus the predicted number concentrations of IN reflect the ambient aerosol number concentrations, so that in very clean regions, the available IN are not overpredicted. The constant coefficients a, b, c, and d may change based on the composition of the ambient aerosol, enabling even further sensitivity to the local aerosol environment. For a global average aerosol, ignoring variability due to chemical composition, these constants were set to $a = 0.0000594$, $b = 3.33$, $c = 0.0264$, and $d = 0.0033$.

DeMott et al. (2010) showed that equation 2.1 generally reproduces observations within a factor of ~ 5 , and also reduced unexplained variability in ice nuclei concentrations at a given temperature from 10^3 to on the order of 10, indicating that particle size is a major explanatory variable for IN concentrations. When compared to observations of ice nuclei obtained over multiple field studies, the D10 parameterization was shown to more accurately predict the number of ice nuclei available when compared to a parameterization responsive to temperature alone (DeMott et al., 2010). The aerosol-linked parameterization was shown to significantly alter cloud ice and liquid contents when incorporated into a global climate model, relative to simulations using the temperature-only ice activation parameterization. The changes in global ice and liquid water contents led to changes in global net radiative forcing large enough to suggest that the simulated phase of Arctic clouds has significant consequences for climate predictions (Liu et al., 2007).

In this study, it was desired to test if ice crystal formation could be accurately predicted in specific cloud cases on the basis of the parameterization put forth in *DeMott et al. (2010)*, hereafter referred to as D10. This choice is motivated by the obvious benefit of a globally-applicable ice nuclei parameterization, but especially the System for Atmospheric Modeling (SAM), since if successful it would represent a step toward linking aerosols and IN in future Super-Parameterized Community Atmosphere Model (SPCAM) simulations. Furthermore, even if IN data were available globally on a climatological basis, some framework for its application and prediction in models is desirable. For example, although IN data were collected in the ISDAC study (*Jackson et al., 2012*), their utility for single case study constraint can be limited. The measurements can only be made where the aircraft flies, and for the conditions that the ice nucleation instrument is processing aerosols at any time. In other words, IN data are seldom comprehensive as regards relevance to the thermodynamic and cloud conditions that occurred in each case. Thus, in contrast to the approach used in *Avramov et al. (2012)*, IN data collected during ISDAC will not be utilized in this work to specifically constrain IN activation in the SAM. Instead, IN will be predicted based on aerosol concentrations measured in and around the time periods of cloud case studies. Since previous ice nuclei concentration data collected in Arctic studies were included in the analyses used in D10, it is reasonable to assume that it should be valid to employ this parameterization along with observed aerosol and cloud thermodynamic data for diagnostic or prognostic prediction of IN in simulations. Nevertheless, we will compare predictions to ISDAC IN data to test consistency with and justification for the use of the D10 parameterization for general application in ISDAC.

For the parameterization evaluation, ISDAC IN data were provided by Andrew Glen and Dr. Sarah Brooks of Texas A&M University, whose CFDC flew on the Canadian Convair

aircraft and sampled via a forward facing and approximately isokinetic air inlet. Aerosol data from a wing-mounted Passive Cavity Aerosol Spectrometer Probe (PCASP) were provided by Dr. Peter Liu and Mr. Michael Earle of Environment Canada. Analyses followed procedures used by D10. Cloudy periods were first omitted from consideration using a cloud mask analyses provided by Dr. Greg McFarquhar and Mr. Robert Jackson of the University of Illinois. IN data during cloud-free periods were then combined for all flights and further segregated for times when the CFDC was processing aerosol above water saturation, thus representative of immersion freezing nuclei. PCASP aerosol concentrations above $0.48 \mu\text{m}$ (closest lower bin limit to the D10 parameterization size condition) were determined for the same time periods that satisfied the cloud-free and CFDC water supersaturated conditions required.

Figure 2.1 shows a time series of data from one flight segment for the April 8, 2008 case. Predicted IN are shown in comparison to observed IN data prior to application of the water supersaturation and cloud-free masks. Only periods of aircraft passage through precipitating ice crystals are included and the CFDC was operating in supersaturated conditions through the entire period shown. Good agreement is seen between observed and predicted IN values, and the presence of precipitating ice crystals in the sample appears to have only a modest influence on the intercomparison. Similar results are shown for a period on April 26, 2008 in Figure 2.2. In this case, CFDC water saturation values deviated substantially from supersaturated conditions at times, although most times was within 5% of water saturated conditions (100% RH). Agreement in predicted and observed IN is again reasonably good, easily within the uncertainty involved in the D10 parameterization. These results are encouraging for use of the parameterization to describe ambient IN concentrations in these specific cases.

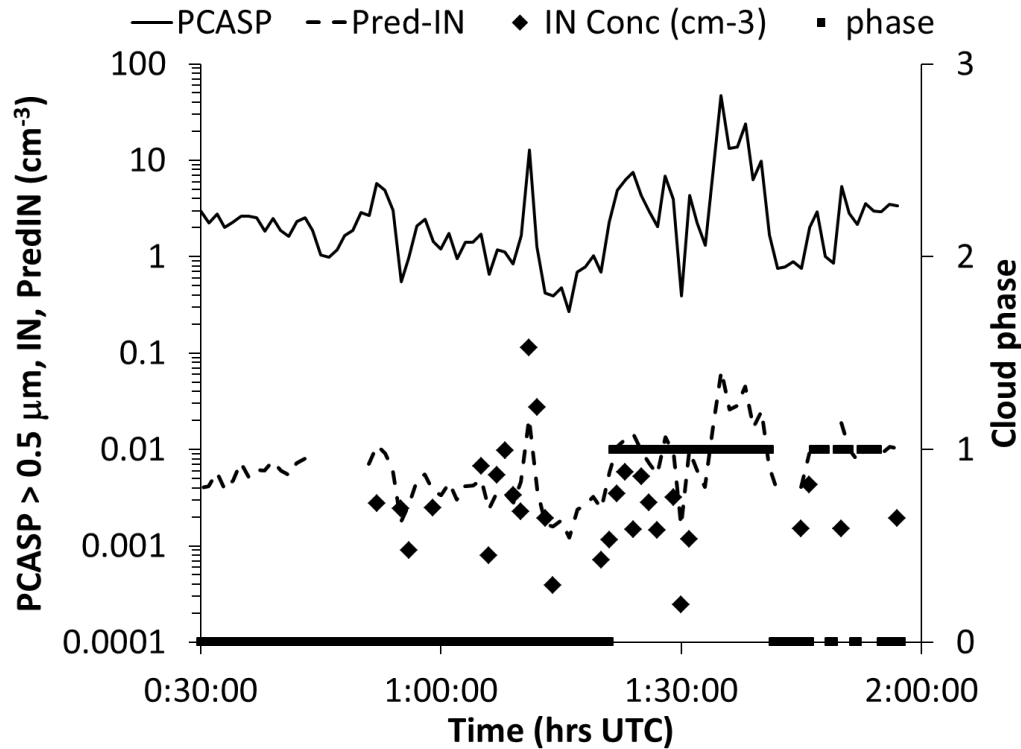


Figure 2.1. Comparison of observed IN versus IN predicted on the basis of D10 (dashed curve) for ISDAC Flight 17 on April 8, 2008 (local time). UTC time is for the beginning of April 9, 2008. IN data are for one minute integral periods. IN processing temperatures ranged from -27 to -30°C during the period shown. PCASP aerosol concentrations at sizes above $0.5\ \mu\text{m}$ and cloud phase (0 = no cloud; 1 = subcloud ice present) are also shown. An ambient pressure range from the surface to 450 mb is represented.

A project summary comparison of ISDAC IN data and the D10 parameterization for conditions meeting the criteria used in D10 is shown in Figure 2.3. In keeping with the single case examples shown in Figures 2.1 and 2.2, Figure 2.3 indicates that the ISDAC project data set as a whole is consistent with the compendium of data used for the D10 parameterization development. Only a very few data points fall outside the bounds of a factor of 5 range about the values predicted by D10. Data points shown in blue in Figure 2.3 are one-minute data from above cloud top at around 2200 to 2230 UTC on April 8, 2008 when the CFDC was processing at below 90% RH. The highest IN concentrations during this period were used by Avramov et al.

(2011) to constrain IN for simulations of the April 8 case. In consideration of the historical data used in formulating D10, and the good agreement of the ISDAC IN data with the parameterization overall, these data points represent outlier high IN concentrations for the aerosol concentrations present and CFDC processing temperatures (-21 to -23°C) used at the time. These data also exceed IN concentrations measured above cloud at similar aerosol concentrations, but at much lower processing temperatures, just a few hours later (Figure 2.1).

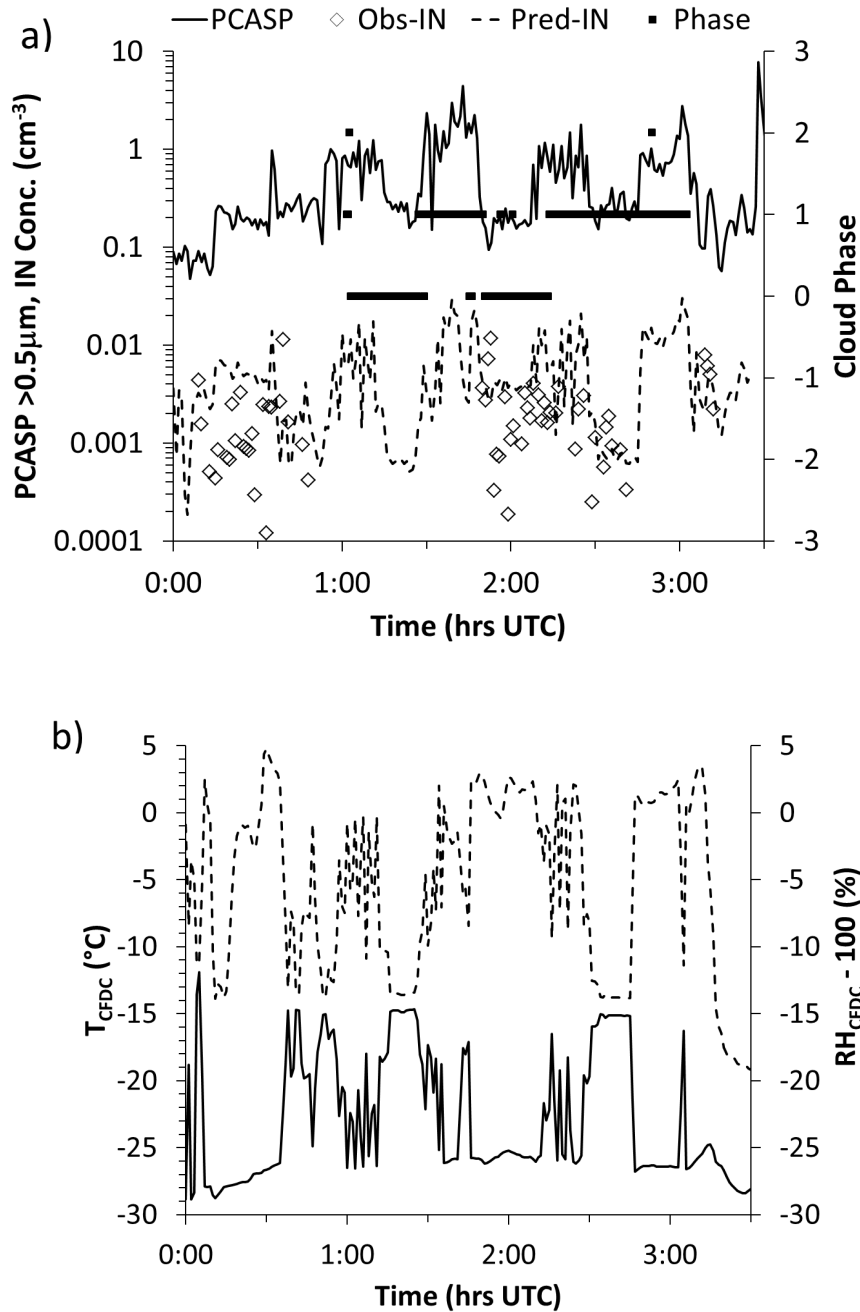


Figure 2.2. Comparison of observed IN versus predicted IN in a) for a portion of ISDAC Flight 31 on April 26, 2008. Gaps in IN data are periods of sampling from the counterflow virtual impactor inlet. PCASP aerosol concentrations at sizes larger than 0.5 μm and cloud phase (0 = no cloud; 1 = ice or sub-cloud precipitating ice present) are also shown. CFDC IN processing temperatures and RH are shown in b). A mix of above (~ 910 mb, highest T_{CFDC}) and below (~ 970 mb, lowest T_{CFDC}) sampling is represented.

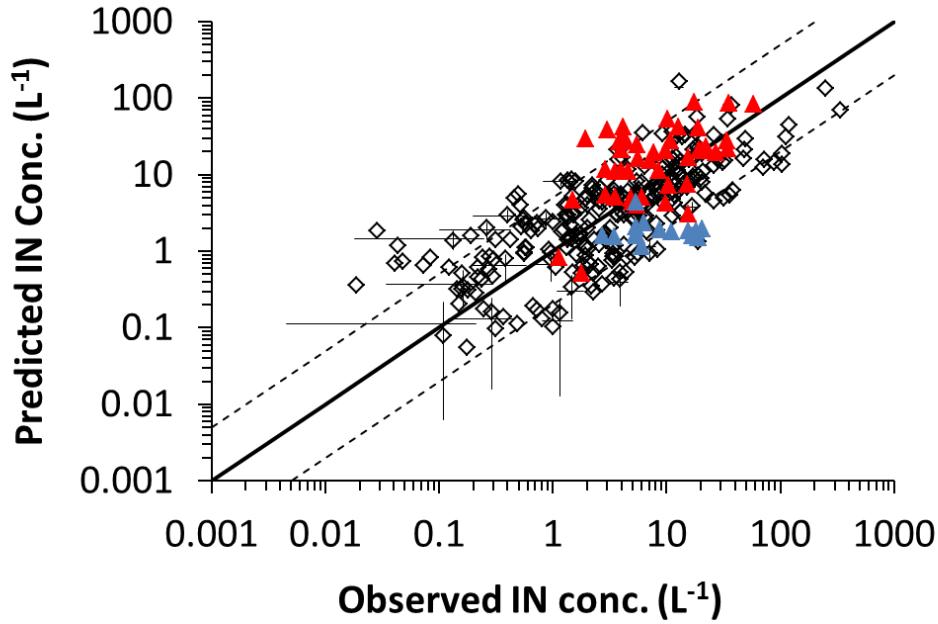


Figure 2.3. Summary of ISDAC IN (red points) observed and predicted by the D10 parameterization, and including the original data from DeMott et al. (2010). All data are for standard temperature and pressure conditions. Dashed lines parallel to the 1:1 solid line bracket a factor of 5 times the standard relation.

2.2 SAM Description and Setup

This study utilized a cloud-resolving model (CRM), known as the System for Atmospheric Modeling (SAM), to model persistent arctic stratus decks observed over the North Slope of Alaska. SAM is a versatile model originally developed by Khairoutdinov at the University of Oklahoma (*Khairoutdinov et al.*, 2003), and revised extensively at Colorado State University. For the purposes of this study, SAM was run with the NCAR CAM3 interactive radiation package, and used a two-moment bin microphysics scheme developed by Morrison (*Morrison et al.*, 2005, 2005a, 2005b, 2008), in which the number concentrations and mass mixing ratios of pristine cloud ice, snow, cloud droplets, and rain are treated prognostically. Dry aerosol is initially described by a lognormal distribution, and assumed to be composed entirely of

ammonium sulfate. Any changes in particle size or chemical composition, due to cloud processing for example, are neglected. Cloud droplet activation occurs following the Abdul-Razzak and Ghan scheme (*Abdul-Razzak et al.*, 2000), in which the aerosol size distribution is related to the number activated through Köhler theory, as a function of maximum supersaturation. Five species of hydrometeors are included in the microphysics package: cloud droplets, pristine ice, rain, snow, and graupel. For computational simplicity, all hydrometeors are treated as spheres so that the capacitance, used in the condensational growth calculations, is set equal to 1, with assigned densities of 997 kg/m^3 for liquid water, 500 kg/m^3 for pristine ice and graupel, and 100 kg/m^3 for snow. An option to include hail processes has been added to the microphysics package, but is ignored in these simulations. Hail was not observed in the clouds, nor is it expected that riming was significant enough to produce solid ice spheres larger than graupel. Warm-rain processes are also ignored in the simulations. Heterogeneous ice nucleation is the dominant mode of nucleation and is assumed to occur by condensation/immersion freezing of an insoluble nucleus surrounded by soluble material (*Morrison et al.*, 2005). In the original model, IN number concentrations were a fixed subset of the total aerosol, and were a function of temperature.

In the simulations presented here, SAM was configured to run in Large-Eddy Simulation (LES) mode, with surface fluxes of sensible and latent heats prescribed, using observations when available. Mean values for the horizontal winds were continually nudged towards the observed values. To best simulate the clouds encountered during the ISDAC campaign, SAM was run with an ice-covered ocean surface, as the mixed-phase, low-level stratus decks were encountered and sampled over frozen ocean regions. Subgrid-scale processes were parameterized via the prognostic TKE 1.5 order closure scheme. Longwave and shortwave radiation were computed

prognostically within the model, and surface latent and sensible heat fluxes were prescribed. Also prescribed, and crucial to these simulations, is the large-scale forcing, but Coriolis forcing was neglected. Gravity waves were damped at the top of the model domain, which is 3 kilometers in the following simulations.

Simulations were conducted in two dimensions. After comparing a simulation with the same initial conditions, the only difference being one simulation run in 3-dimensions and the other in 2-D, it was determined that with a sufficiently large domain, differences in simulated cloud properties were minor. The model exhibits notably enhanced computational efficiency when the extra horizontal dimension is removed, and this is the way that the SAM is run in the super-parameterization framework. All simulations were initialized on a horizontal domain of 3 kilometers on a 10 m grid, and 3 kilometers vertically, also with 10 m grid spacing. ISDAC simulations were 12 hours of simulated time with a time step of 1 second; the M-PACE simulations were run with 0.25 second time steps for a total simulated time of six hours. Output variables were horizontally-averaged and saved every 600 time steps, or 10 minutes of simulated time for ISDAC simulations, and 2.5 minutes for M-PACE simulations.

2.3 Development of IN Budget Equations

Initially, the D10 parameterization was configured in the SAM in a way that mostly left unbounded the ice production in the simulated cloud. While the model would prohibit the production of further ice if the total number of ice species present in the grid-box equaled the total predicted IN concentrations, as hydrometeors were advected or fell out of the gridbox, more activation was allowed, assuming constant total available potential IN in the domain.

To allow for depletion of IN during the simulation, the model microphysics package was modified to communicate with and make use of a pre-existing tracer subroutine that can advect and diffuse an unreactive tracer throughout the model domain. The tracer subroutine was populated above and below the cloud deck with an initial concentration of potential ice nuclei using equation (2.1) and based on the coldest observed in-cloud temperature. It was found that populating the entire domain, including the ice-activating liquid layer, with potential ice nuclei led to an instantaneous pulse of ice nucleation and rapid crystal growth within the layer, which caused faster than expected depletion of the cloud through snowfall. Because of this effect, and since ice activation within the model occurs in the cloud supercooled liquid layer, the potential ice nuclei layers were necessarily separated from the liquid layer by approximately 50 meters so that potential IN needed to advect and turbulently entrain into the cloud. This separation allowed ice formation to proceed more slowly as the model spun up.

In our modified IN treatment, a first guess of the activated number concentration of ice nuclei at a position and time was calculated from equation (2.1) using the ambient aerosol concentrations larger than 0.5 micrometers and local temperature. This proposed ice crystal concentration was then checked against the pool of available nuclei. If there were sufficient nuclei available, the model activated all of the proposed ice nuclei, and this number concentration was then deducted from the available pool in that grid box. If there were fewer IN available than the proposed, all available were activated and the gridbox would be totally depleted of IN. Activation of additional ice nuclei would then not occur in this grid box unless more potential IN were advected or diffused in to replenish the available supply.

Following a set of simulations for all case studies following this method, the microphysics package was again modified to allow for sublimating crystals to be an additional

source of potential ice nuclei. Previous modeling studies have concluded that available IN are rapidly consumed, and IN sources many times higher than observed are required to reproduce reasonable, sustained cloud properties (*Fridlind et al., 2007; Fridlind et al., 2012*). In this case, recycled IN due to sublimating crystals could potentially serve as a portion of the additional IN required. Another study noted that the presence of a reservoir of IN below the well-mixed cloud may in some cases mix slowly vertically into the cloud, helping maintain ice concentrations (*Avramov et al., 2011*). Sublimating ice crystals falling out below the cloud would establish an enhanced reservoir of IN in the same manner, and could be reintroduced into the cloud at some point as mixing occurs. Since temperatures in the domain did not approach the threshold for homogeneous freezing, all pristine crystals that formed aggregates were assumed to have formed initially on an ice nucleus. The model calculated rates of snow number concentration loss due to sublimation at each grid point each time step; the snow number loss was set equal to the IN number gain. With this treatment, an aggregate such as snow, when sublimated, returned a solitary IN particle to the domain. Since an unknown number of crystals combined to form the original snow aggregate, a net loss of IN in the domain would still occur even if all of the snow crystals were sublimated. It is not clear if sublimation in an actual cloud would result in the return of multiple IN, in which case our treatment would underestimate this source of regenerated ice nuclei. We also extended this IN regeneration scheme to other hydrometeors, but since snow is the dominant precipitation species in these simulations, those pathways did not contribute significantly to the total regeneration rates, as will be shown.

2.4 Case Study Days

In order to test the efficacy of the prognostic ice scheme, a range of environmental conditions to test the model in was necessary. We chose three case studies from two field campaigns. Flight 16 of the ISDAC field campaign, which was the second research flight conducted on April 8 lifted off at 19:54Z for a 3.9 hour flight which made several passes above, below, and within a large cloud deck observed to occupy the entire visual range of the aircraft. These passes to measure aerosol properties were followed by spiral maneuvers over the Barrow ground site and additional passes above and below cloud, as well as a “porpoising run” through cloud to produce a vertical profile of parameters. This flight was later established as a “Golden Day” of the campaign, and one of the case studies chosen for our study. General model setup parameters are displayed in Table 2.1 for reference.

Table 2.1. Basic model parameters and aerosol distributions.

| | ISDAC Flight 16 | ISDAC Flight 31 | MPACE-B |
|--|-----------------|-----------------|---------|
| Domain [km] | 3x3 | 3x3 | 3x3 |
| Simulated Time [hrs] | 12 | 12 | 6 |
| Grid boxes | 300x300 | 300x300 | 300x300 |
| Δx [m] | 10 | 10 | 10 |
| Δz [m] | 10 | 10 | 10 |
| Δt [s] | 1 | 1 | 0.25 |
| Aerosol Mode 1 Geometric Mean Radius [μm] | 0.1 | 0.1 | 0.052 |
| Aerosol Mode 1 σ | 1.43 | 1.5 | 2.04 |
| Aerosol Mode 1 N [cm^{-3}] | 171.7 | 200 | 72.2 |
| Aerosol Mode 2 Geometric Mean Radius [μm] | 0.55 | 0.75 | 1.3 |
| Aerosol Mode 2 σ | 2.35 | 2 | 2.5 |
| Aerosol Mode 2 N [cm^{-3}] | 5 | 2 | 1.8 |

On April 26, Flight 31 of the ISDAC Campaign took off at 23:38Z for a 4.2 hour research flight to sample an area of cloud cover observed to be of uniform height and exhibiting

significant precipitation of ice. During the flight, multiple passes were made above and below a large cloud deck to measure aerosol properties, followed by level passes through the cloud deck and porpoising maneuvers to obtain vertical profiles. Flight 31 is considered to be an additional “Golden Day” of observations, and has been used as the basis of several modeling studies (*Ovchinnikov et al.*, 2011; *Fan et al.*, 2011). This flight is included as the initialization for the second of our case studies.

The third case study is derived from the initialization data used to model a single layer mixed-phase stratocumulus cloud encountered during the M-PACE field campaign. This initialization data stems from what is referred to as Intercomparison Period B, with the intent of representing a single layer cloud which was observed between roughly 17Z on 9 October 2004, through approximately 5Z on 10 October. The observed cloud system formed under a different synoptic situation than either of the clouds encountered during the ISDAC campaign; when northeasterly flow advected cold air located above sea ice over the relatively warmer, ice-free Beaufort Sea (*Klein et al.*, 2009). This resulted in large surface fluxes of heat which led to the creation of a single-layer mixed-phase stratus cloud that exhibited ‘cloud streets,’ narrow strips of parallel cloud separated by equally narrow cloud-free regions, a phenomenon often observed in this situation (*Klein et al.*, 2009).

Chapter 3

Case Study 1: ISDAC Flight 16

3.1 Observations

Throughout the 24-hour period beginning just before 10Z on 8 April 2008, as well as during the ~4 hour flight, a ground-based Vaisala FD12P Weather Sensor deployed at the NSA site near Barrow, Alaska reported light snow with an average precipitation rate of about 0.25 mm/hour. The NSA site is located at 71.323° N latitude, 156.616° W longitude. A field log noted the presence of an ice fog consisting of small ice crystals from midnight until morning local time, which was replaced by dendritic crystals precipitating until late afternoon. A European Center for Medium-Range Weather Forecasts (ECMWF) analysis conducted for the period showed agreement with the Moderate Resolution Imaging Spectroradiometer (MODIS) imagery that substantive cloud cover existed for the region in which aircraft operations were conducted, which consisted primarily of a line extending from the NSA site at Barrow to the north-northwest over the sea surface for about 120 kilometers. The cloud was observed to be well-established several hours before Research Flight 16, and portions of the same cloud mass were sampled over land during the transit flight from Fairbanks to the Barrow area. Flight 16 followed the transit flight, and the same cloud deck persisted for the duration of the approximately 4-hour research flight. Observational data from the research flight, but not the transit flight, are used to compare with simulated clouds.

Onboard the Convair 580 aircraft, multiple instruments collected data on cloud properties. Figure 3.1 shows relevant microphysical observations. Cloud droplet number concentrations obtained from the Forward Scattering Spectrometer Probe Model 100x (FSSP-100x) over a number of cloud descent and ascent profiles show that droplets were observed between about 500 and 1200 meters. As discussed, the layer consisting of only supercooled liquid droplets is in the upper region of these bounds, with the mixed-phase region below. Cloud droplet concentrations within the cloud had an upper limit of nearly 200 cm^{-3} , and ranged down to $\sim 0 \text{ cm}^{-3}$ for the same level, suggesting wide variability temporally and spatially within the cloud. Multiple instruments onboard the aircraft were capable of estimating concentrations of ice crystals, with some size-related caveats and with processing to attempt to differentiate liquid from ice particles. Such processing, as described by Jackson et al. (2012) yielded measurements ranging from 0 to 160 cm^{-3} for liquid cloud droplets, and cloud liquid water contents ranging from 0 to 0.3 g m^{-3} . Jackson et al. (2012) also reported pristine cloud ice concentrations between 0 and 0.001 cm^{-3} , with many measurements near 0.0005 cm^{-3} , and ice water contents from 0 to 0.06 g m^{-3} for the duration of the flight.

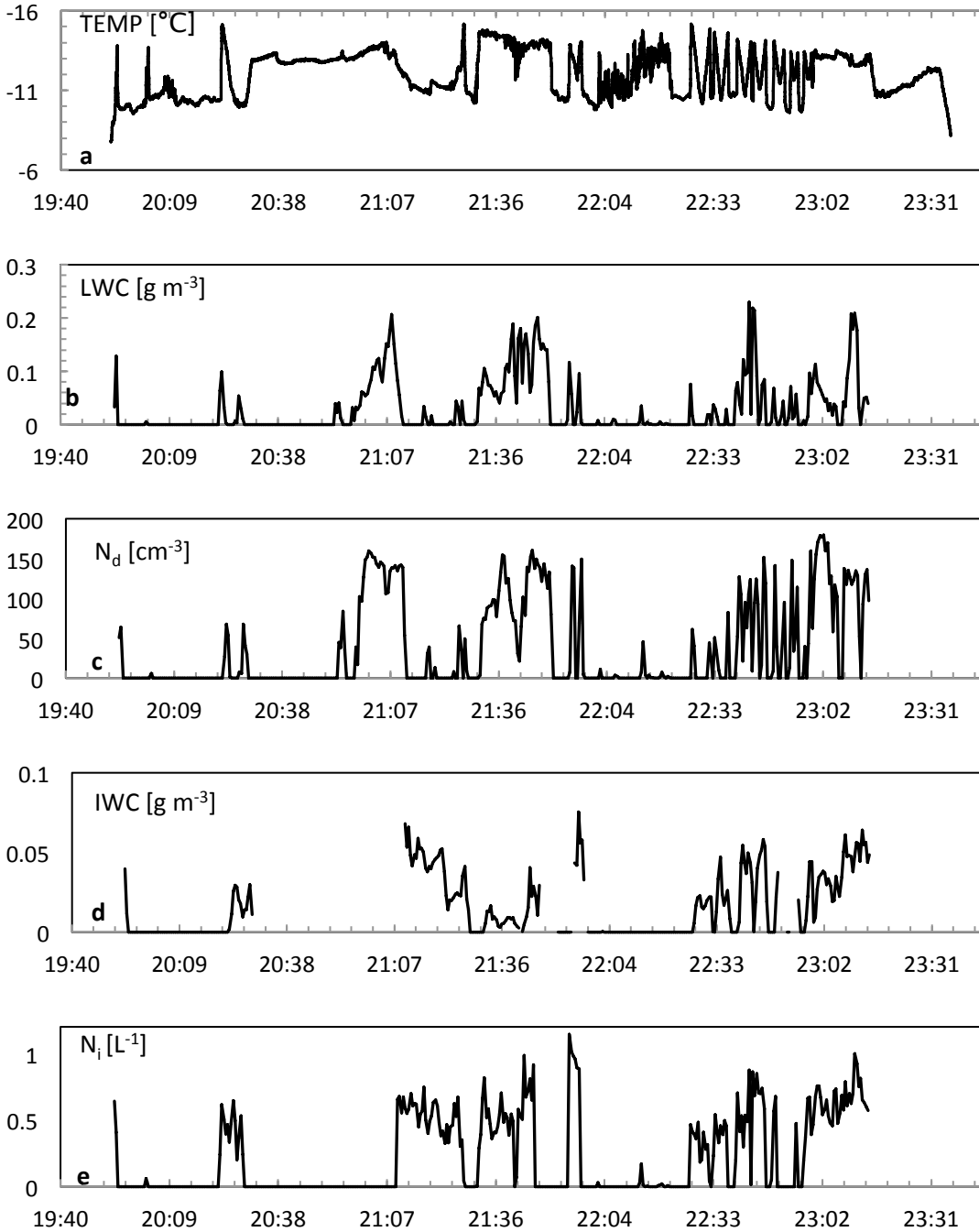


Figure 3.1. Time series of (a) temperature in degrees Celsius, (b) liquid water content in g m^{-3} , (c) cloud droplet number concentration in units cm^{-3} , (d) ice water content in g m^{-3} , (e) pristine ice number concentration in units L^{-1} , from onboard the Convair 580 during Flight 16. Data obtained from the DOE-ARM archive for the ISDAC project.

3.2 Model Initialization

In total, ten simulations representing both diagnostic and prognostic treatments of potential ice nuclei were performed for the 8 April ISDAC Flight 16 initialization (Table 3.1). These simulations representing the environmental conditions and resulting mixed-phase stratus cloud cover on 8 April were initialized with vertical profiles of potential temperature, water vapor mixing ratio, and horizontal wind fields derived from a sounding launched from the NSA ground site at 17:30 UTC.

Figure 3.2 shows the vertical profiles of moisture, temperature, and winds that were used to initialize all Flight 16 simulations. The horizontal wind fields were initialized using a constant value with height, representative of the average winds observed by the sonde. Based on observations, the sea surface temperature was prescribed to be 264.7 K. Additionally, surface sensible and latent heat fluxes were prescribed at 0 W m^{-2} and 10 W m^{-2} , respectively. The decision to prescribe these values was motivated by the recent Ovchinnikov et al. model intercomparison which noted that under the conditions observed during the ISDAC campaign, sensible and latent heat fluxes from the ice covered ocean surface would be on the order of $\sim 10 \text{ W m}^{-2}$. Additionally, when the cloud layer is decoupled from the surface, the impact of the surface heat fluxes is minimized further. Large-scale subsidence was imposed to reflect the impacts of the observed high pressure center on the cloud system. The case-study specific value for $n_{aer,0.5}$ from equation 2.1, to be used when the D10 parameterization is active, was determined to be 4.903 per standard cubic centimeter.

According to equation 2.1, the maximum potential ice nuclei present at the temperatures observed at cloud top in the simulations is then about 0.86 per standard Liter. Prognostic

simulations initialized with this value of potential IN, assumed constant throughout the depth of the model domain, produced a short-lived cloud with lower than observed ice contents and number concentrations. Simulations with a factor of 5 increase in the IN concentrations produced clouds with enhanced longevity and increased ice mass and number contents. Increases of a factor of 10 further increases ice mass concentrations toward observations, including in simulations that allowed IN recycling for all ice hydrometeors active in the model. Hence, one simulation with a factor of 5 increase in predicted IN is included in the set summarized in Table 3.1, but most prognostic simulations were conducted with a factor of 10 increase in potential IN. This treatment also provides some insight into claims that an IN source stronger than observed may be needed to accurately describe ice evolution in Arctic clouds (*Fridlind et al.*, 2007).

Table 3.1. List of ISDAC Flight 16 (8 April 2008) SAM Simulations

| Simulation | Acronym | IN Treatment | Max Initial IN | Activation |
|---------------------------------|----------------|---------------------|---|-------------------|
| Control | CTRL | Diagnostic | T-dependent (500 L ⁻¹ max) | Cooper |
| DeMott | DEMOTT | Diagnostic | 0.865 L ⁻¹ (constant) | D10 |
| 0.1x DeMott | DM_0.1 | Diagnostic | 0.0865 L ⁻¹ (constant) | 0.10 * D10 |
| 10x DeMott | DM_10 | Diagnostic | 8.65 L ⁻¹ (constant) | 10.0 * D10 |
| No Sublimation | NOSUB | Prognostic | 8.65 L ⁻¹ | D10 |
| Snow Sublimation | SNOSUB | Prognostic | 8.65 L ⁻¹ | D10 |
| Snow Sublimation, Dried Profile | SNOSUB_d | Prognostic | 8.65 L ⁻¹ | D10 |
| All Sublimation | SUB_HI | Prognostic | 8.65 L ⁻¹ | D10 |
| All Sublimation | SUB_LO | Prognostic | 4.325 L ⁻¹ | D10 |
| All Sublimation, Dried Profile | SUB_HI_d | Prognostic | 8.65 L ⁻¹ | D10 |

Four of the ten simulations utilized a diagnostic treatment of ice crystal activation: the Control simulation (CTRL), which used a temperature-dependent ice activation scheme; a

simulation using a standard implementation of the D10 parameterization (DEMOTT); and two simulations modifying the D10 parameterization by factors of 0.1 and 10 to test the simulated cloud's sensitivity (DM_0.1, DM_10). The six other simulations utilized the new prognostic scheme, which specifies ambient concentrations of potential IN by level. The first prognostic simulation (NOSUB) ignored recycling of IN due to the sublimation of ice crystals, while the next two simulations (SNOSUB) allowed snow sublimation to recycle IN particles. One of these simulations (SNOSUB_d) was conducted with the lowest 200 meters of the atmosphere dried out, by setting initial water vapor mixing ratios to zero, to emphasize the role of sublimating crystals and observe the impacts on cloud structure and longevity. The final set of simulations incorporated all sublimating ice crystals as IN regenerators, which includes pristine ice and graupel in addition to snow (SUB_LO, SUB_HI, SUB_HI_d, indicating perturbations to initial potential IN and thermodynamic structure similar to the other runs described above).

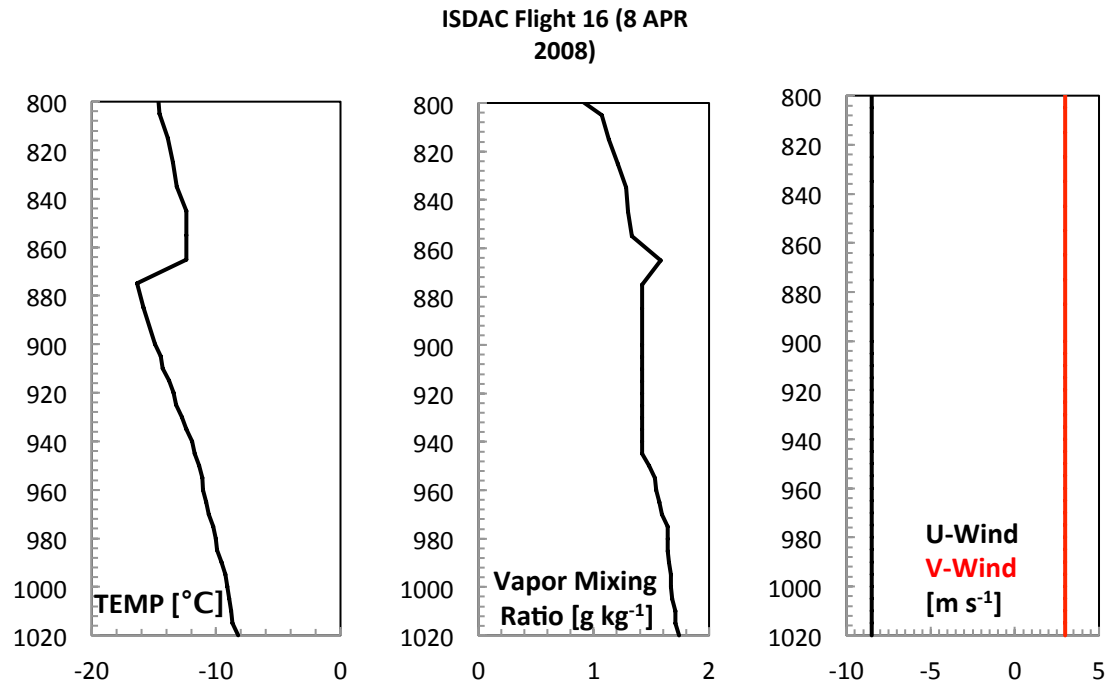


Figure 3.2. Vertical profiles of the initialization data used for simulations of cloud encountered during Flight 16. SAM is initialized with potential temperature (not shown) instead of ambient temperature. Also shown are water vapor mixing ratio in g kg⁻¹, and averaged horizontal winds used to nudge the simulations.

3.3 Diagnostic IN Simulations

In CTRL, ice nuclei activation via the DeMott parameterization was shut off, and instead, predicted activation followed the default scheme, where

$$n_{IN} = 0.005 * \exp [0.304(T_0 - T)] \quad (3.1)$$

is the concentration of activated ice nuclei according to the Cooper scheme (*Cooper*, 1986; *Morrison and Gettelman*, 2008), and n_{IN} was limited in the model to a maximum of 500 L⁻¹ per time step. T_0 is the reference temperature of 273.15 K, and T is the local ambient temperature, also in Kelvin. Note that the activated ice nuclei determined by the Cooper scheme are predicted solely based on temperature, and are not linked to the ambient aerosol. Furthermore, this

parameterization has its basis in ice number concentration data measured in cloud from many locales, under conditions where secondary ice formation was deemed not to be favored. It is not specific to the Arctic.

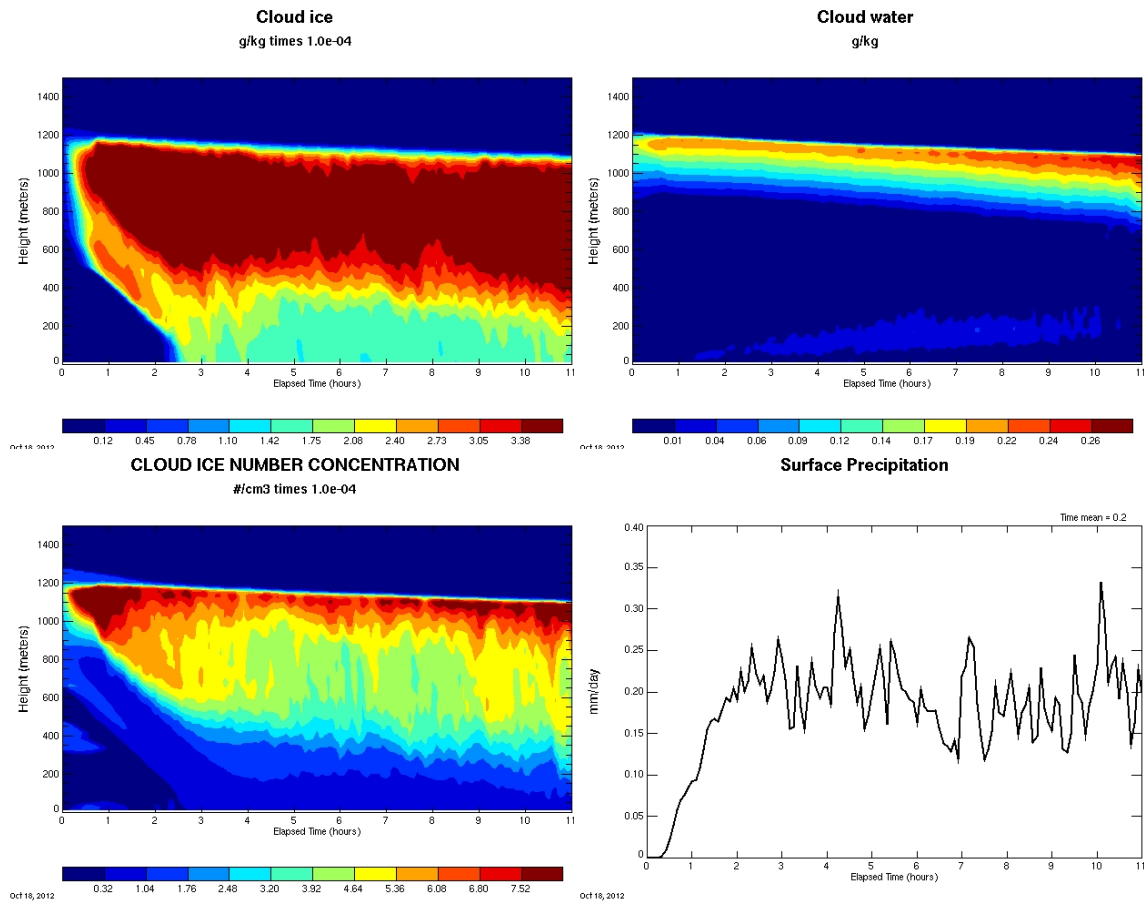


Figure 3.3. Selected SAM output from the CTRL simulation. The horizontal axis is time, and the vertical axis is height; all fields were horizontally averaged at each time step to produce these and all subsequent modeled output figures, unless otherwise noted. The upper left panel is cloud ice mass in g kg^{-1} , the upper right panel is cloud water mass in g kg^{-1} , the lower left panel is cloud ice number concentration in cm^{-3} , and the lower right panel is surface precipitation in mm day^{-1} . Color scales shown are consistent across all diagnostic mode simulations (Figures 3.4-3.7) for easy visual comparison.

Results from CTRL are shown in Figure 3.3. In CTRL, the cloud liquid layer existed between about 800 and 1200 meters, with maximum droplet concentrations at cloud top and a

gradual decrease in altitude over time due to the imposed subsidence profile. The mixed-phase region existed within the lower portion of the liquid layer, in agreement with observations. The region of the cloud containing pristine ice existed between about 500 and 1200 meters, and after the initial model spin-up, stabilized around hour 4 with a maximum concentration of about $7.5 \times 10^{-4} \text{ cm}^{-3}$, near the high end but within the range of aircraft observations. Simulated ice water contents exceeding $3.4 \times 10^{-4} \text{ g m}^{-3}$ in the same region of the cloud are much lower than typical measurements made onboard the aircraft. Liquid water contents of about 0.24 g m^{-3} at cloud top are in good agreement with observations, and droplet concentrations of about 170 cm^{-3} are just slightly higher than the average observed in the liquid layer.

The DEMOTT simulation was conducted in the same fashion as CTRL, with the only change being the replacement of the default ice activation scheme with the D10 parameterization. Results from the diagnostic DEMOTT simulation are shown in Figure 3.4. Changing the IN activation scheme resulted in a cloud with modestly lower pristine ice mass and number concentrations than the CTRL simulation. Higher liquid droplet mass concentrations in the upper region of the liquid layer by the end of the simulation indicated less liquid water depletion in favor of the ice growth, likely due to the lowered ice crystal concentrations. Maximum average ice water contents in the cloud exceeded $3.4 \times 10^{-4} \text{ g m}^{-3}$ for a brief time at mid-levels later in the simulation, but were sustained throughout most of the cloud layer for the duration of the simulation at values closer to $3 \times 10^{-4} \text{ g m}^{-3}$, still much lower than observed values. Cloud ice number concentrations approaching a sustained value of about $6.5 \times 10^{-4} \text{ cm}^{-3}$ remained in agreement with observations. Surface precipitation values were similar to the control simulation. Average surface precipitation values fell to 0.1 mm day^{-1} in DEMOTT simulation,

compared to 0.2 mm day^{-1} in the CTRL. Both rates are much lower than the average $0.25 \text{ mm hour}^{-1}$ reported at Barrow.

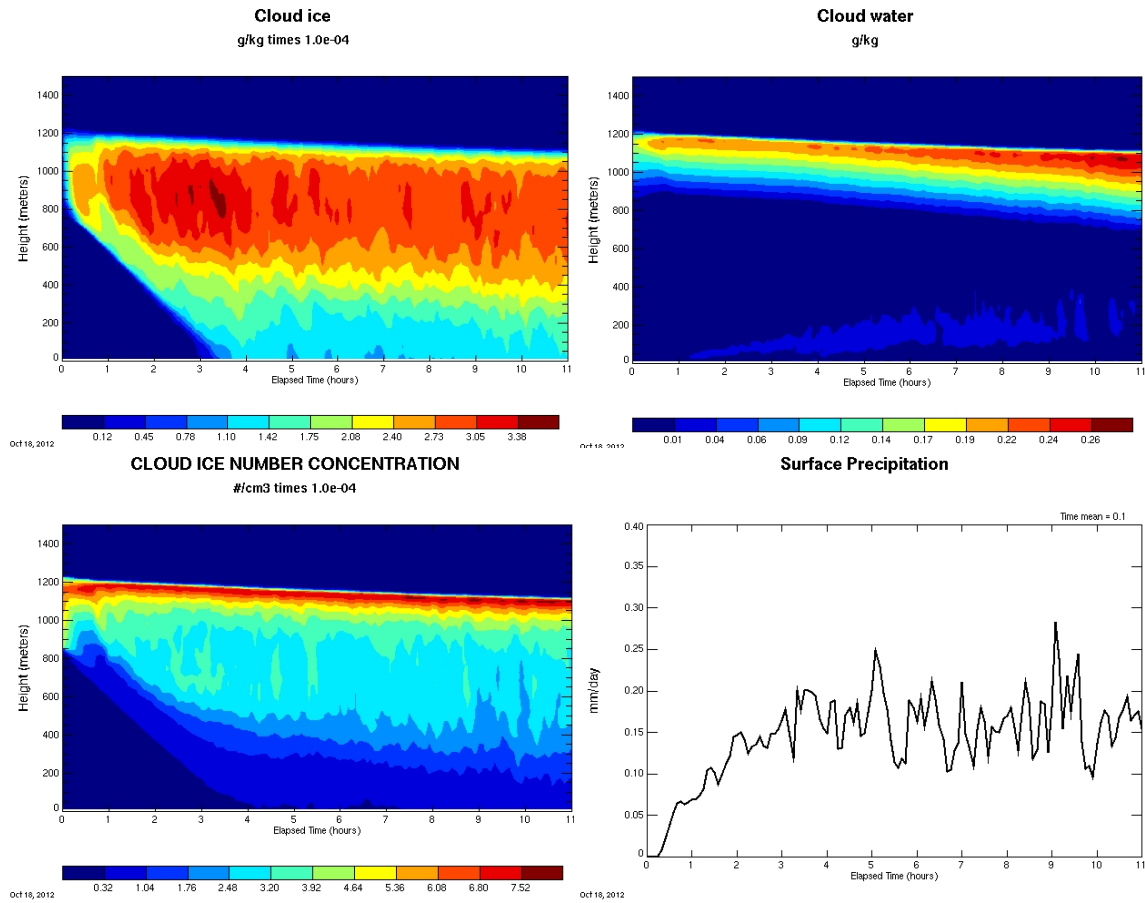


Figure 3.4. Selected SAM output from the DEMOTT simulation. The horizontal axis is time, and the vertical axis is height. Panels as in Figure 3.3.

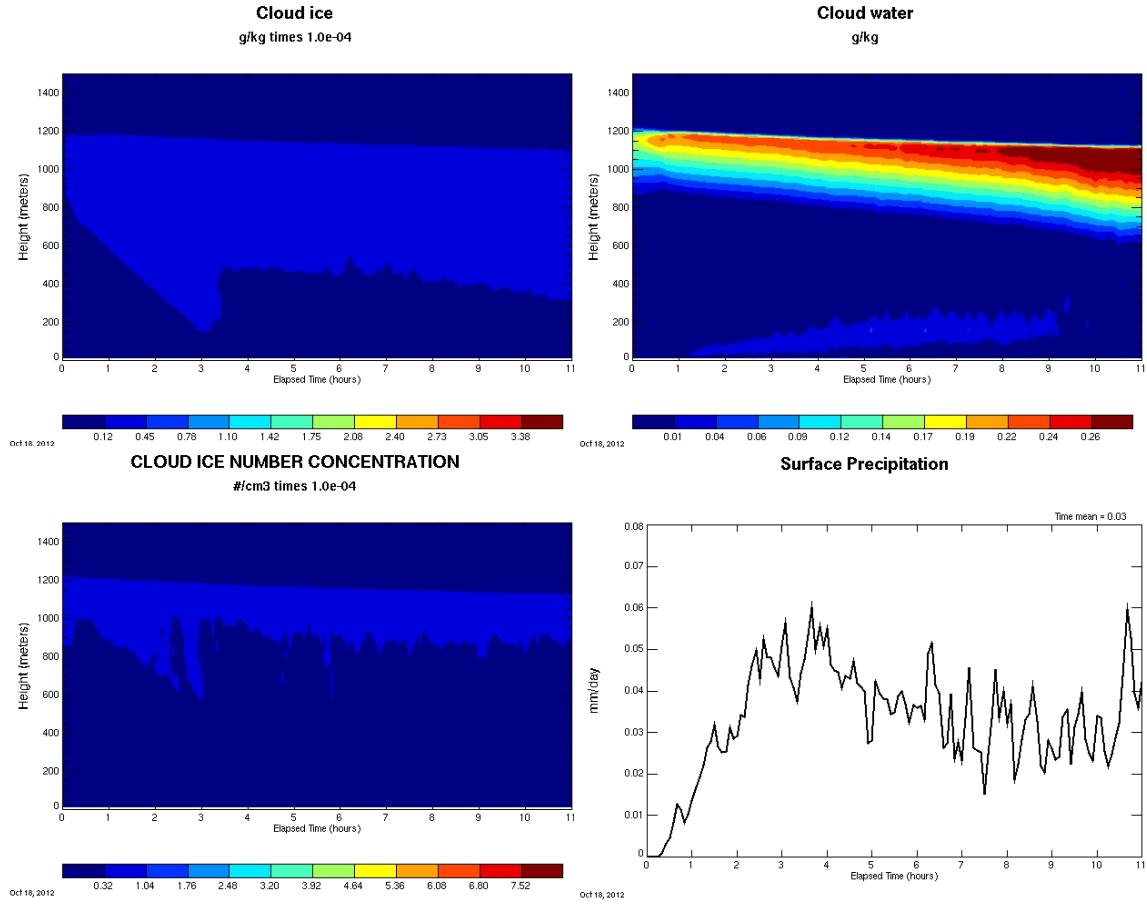


Figure 3.5. Selected SAM output from the DM_0.1. The horizontal axis is time, and the vertical axis is height. Panels as in Figure 3.3.

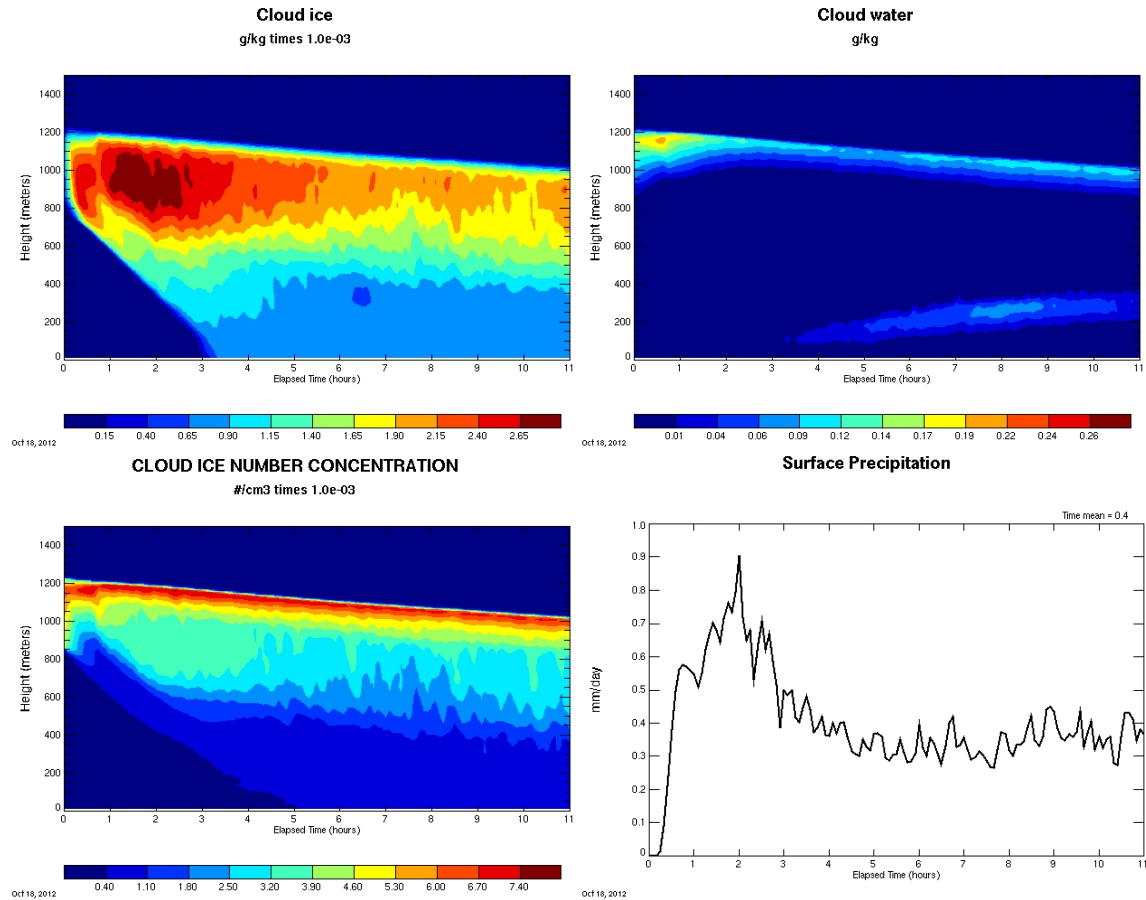


Figure 3.6. Selected SAM output from the DM_10. The horizontal axis is time, and the vertical axis is height. Panels as in Figure 3.3. Note that the scales differ from Figures 3.4-3.6 to show detail.

The D10 parameterization was modified to predict activated nuclei to be a factor of 10 lower (DM_01) and higher (DM_10) to test the sensitivity of the cloud properties to the IN predictions. Results from these sensitivity simulations, shown in Figures 3.5 and 3.6 respectively, showed reasonable and expected trends, suggesting a strong sensitivity of cloud and precipitation characteristics to the IN population. For the DM_0.1 simulation, almost nothing resembling observed clouds was formed, with the exception of very few pristine ice crystals, about $4.0 \times 10^{-5} \text{ cm}^{-3}$, and a supercooled liquid layer which appeared to be intensifying in time, likely due to lack of vapor scavenging by growing ice crystals, and

exceeding 0.30 g m^{-3} by the end of the simulation. Surface precipitation values fell to 0.03 mm day^{-1} . In DM_10, a substantially more active ice-forming cloud was observed, and the liquid layer was shown to be less persistent due to the rapid formation and growth of ice crystals, with maximum liquid water contents less than half those observed in the previous simulations. Peak ice water contents exceeded $2.65 \times 10^{-3} \text{ g m}^{-3}$ but remained below peak observed values, with corresponding ice number concentrations of about $7.0 \times 10^{-3} \text{ cm}^{-3}$, a factor of 7 increase over the peak observed concentrations. Interestingly, a factor of 10 increase in the ice activation scheme resulted in only a factor of four increase in surface precipitation rates, producing a 12-hour average rate of 0.4 mm day^{-1} .

3.4 Prognostic IN Simulations

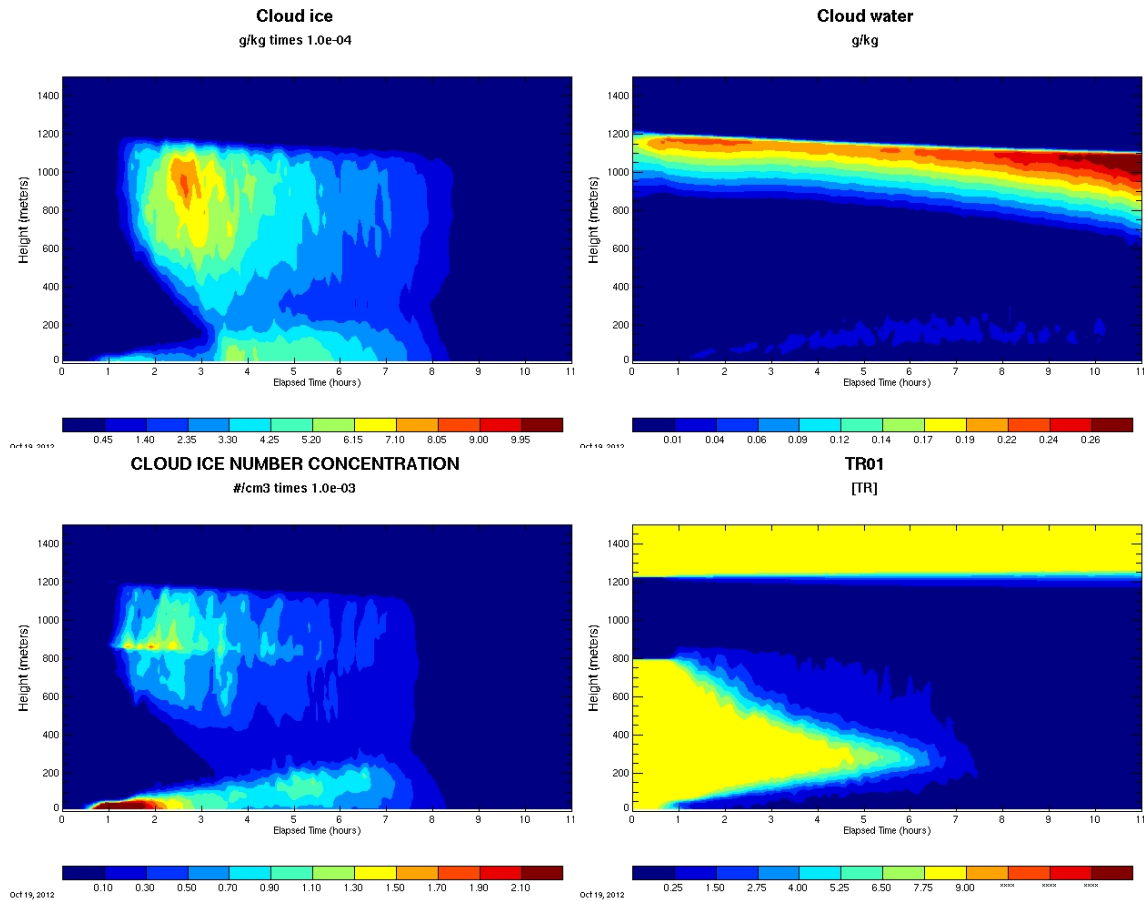


Figure 3.7. Selected SAM output from the prognostic IN simulation, where IN recycling due to sublimation is completely ignored. The horizontal axis is time, and the vertical axis is height. The upper left is cloud ice mass concentration in g kg^{-1} , the upper right panel is cloud liquid water mass concentration in g kg^{-1} , the lower left panel is cloud ice number concentration in cm^{-3} , and the lower right panel is potential IN concentration (tracer field) in L^{-1} .

When the model was modified to make use of the prognostic ice nuclei scheme (NOSUB), drastic changes in the structure and behavior of the cloud were observed. A distinguishing characteristic of the prognostic simulations, markedly more prominent than in any of the diagnostic simulations was the early formation of a dense surface fog. The formation of this fog in the model was not positively verified by the observations, and is likely an artifact of

the prognostic ice activation scheme. Figure 3.7 depicts the results of this simulation. In the following figures, ‘TR01’ refers to the model’s tracer field, used to track potential IN concentrations, and [TR] denotes the concentration of the tracer, in these simulations reported in units of L^{-1} . Onset of ice formation in NOSUB was delayed relative to the diagnostic simulations, due to the deliberate spatial separation of the potential IN layers from the supercooled liquid droplets; the IN had to be mixed into the cloud layer before activation and growth of ice could occur. Early in the simulation, cloud ice mixing ratios peaked at nearly $8.0 \times 10^{-4} \text{ g m}^{-3}$, but trailed off into lower values after about five hours, just three hours after initial formation. Pristine ice number concentrations peaked early in the simulation, and maximum simulated concentrations were about $1.5 \times 10^{-3} \text{ cm}^{-3}$, only slightly higher than peak observed values. Ice number concentrations in good agreement with typical observed values were not sustained more than ~6 hours, in similar fashion to ice mass concentrations. This fairly rapid depletion behavior occurs due to the consumption of ice nuclei, which were not replenished by entrainment quickly enough. When simulations were extended past 12 hours, this mixed-phase cloud was observed to fully dissipate. The liquid layer remained similar to all previous simulations, and surface precipitation rates averaged 0.1 mm day^{-1} .

When the model in prognostic mode was further modified (SNOSUB) to account for recycling of potential ice nuclei from sublimating snow aggregates, but not other ice species, the evolution of the potential IN field was visibly different (Fig. 3.8). Peak ice mass and number concentrations were similar to the NOSUB simulation, but were sustained for longer periods, resulting in a noticeable temporal extension of the cloud. Surface precipitation rates averaged 0.2 mm day^{-1} , but peaked at nearly 0.5 mm day^{-1} at hour 3, still much lower than observed precipitation rates at Barrow. To enhance observability of the impacts of potential recycling of

IN by sublimation, and to examine the evolution of the moisture profile due to hydrometeor formation and sublimation, a subsequent simulation was performed in which the lowest 200 meters of the atmosphere were completely dried at model initialization (SNOSUB_d).

As expected, in SNOSUB_d, sublimation was greatly enhanced, as shown in Fig. 3.9. Potential IN concentrations below the cloud level increased by nearly a factor of two compared with SNOSUB. In addition, surface precipitation averaged only 0.04 mm day^{-1} , evidence of the effect the dried profile had on sublimating precipitating ice before it reached the surface. Peak pristine ice mass mixing ratios and number concentrations were moderated towards slightly lower average values in the cloud. Up to about 800 meters, potential IN concentrations had remarkable stability at the 1 L^{-1} level, unseen in previous simulations, indicating that the ability to sustain this particular simulated cloud past the 12-hour mark was possible. The enhanced lifetime of the simulated cloud resulted from the combination of the enhanced sublimation, plus additional available IN in the lower boundary layer, as the fog was eliminated and unable to scavenge those IN.

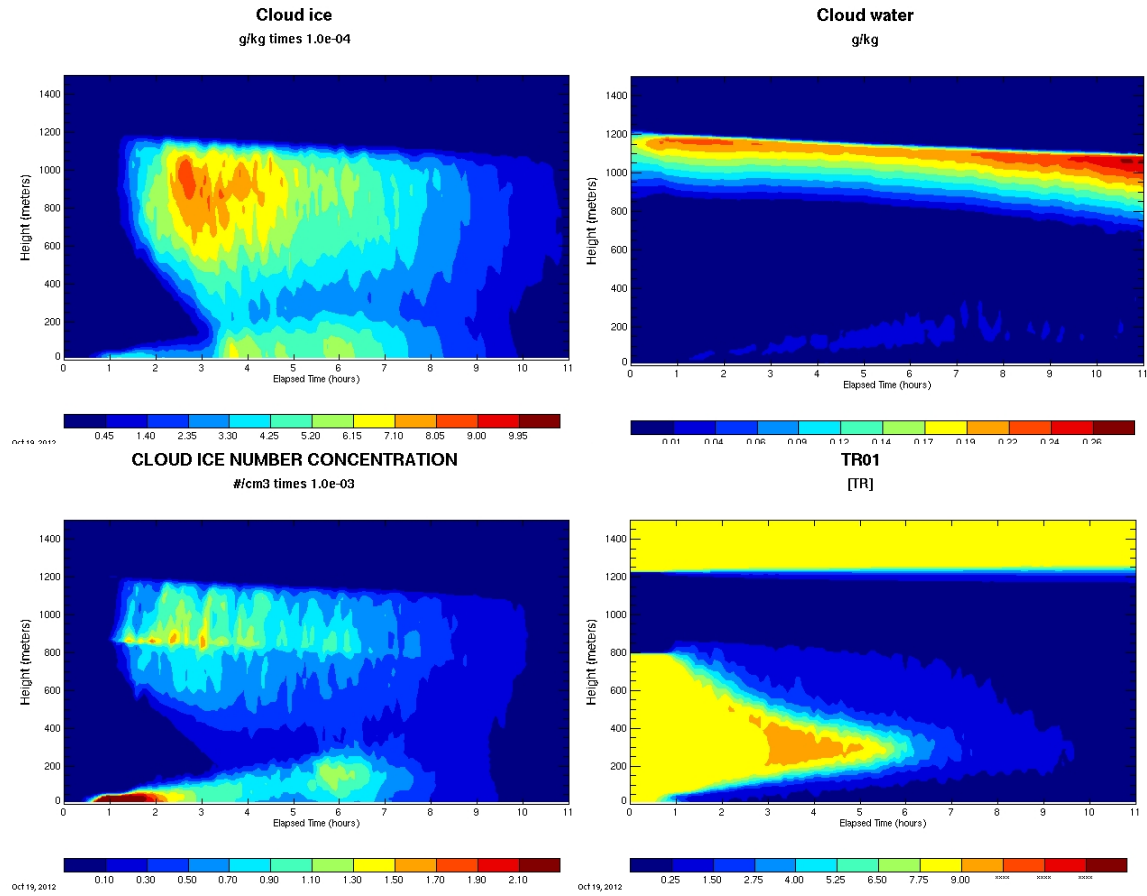


Figure 3.8. Selected SAM output from the prognostic IN simulation SNOSUB, where IN recycling due to sublimating snow only is considered. The horizontal axis is time, and the vertical axis is height. All panels as in Figure 3.7.

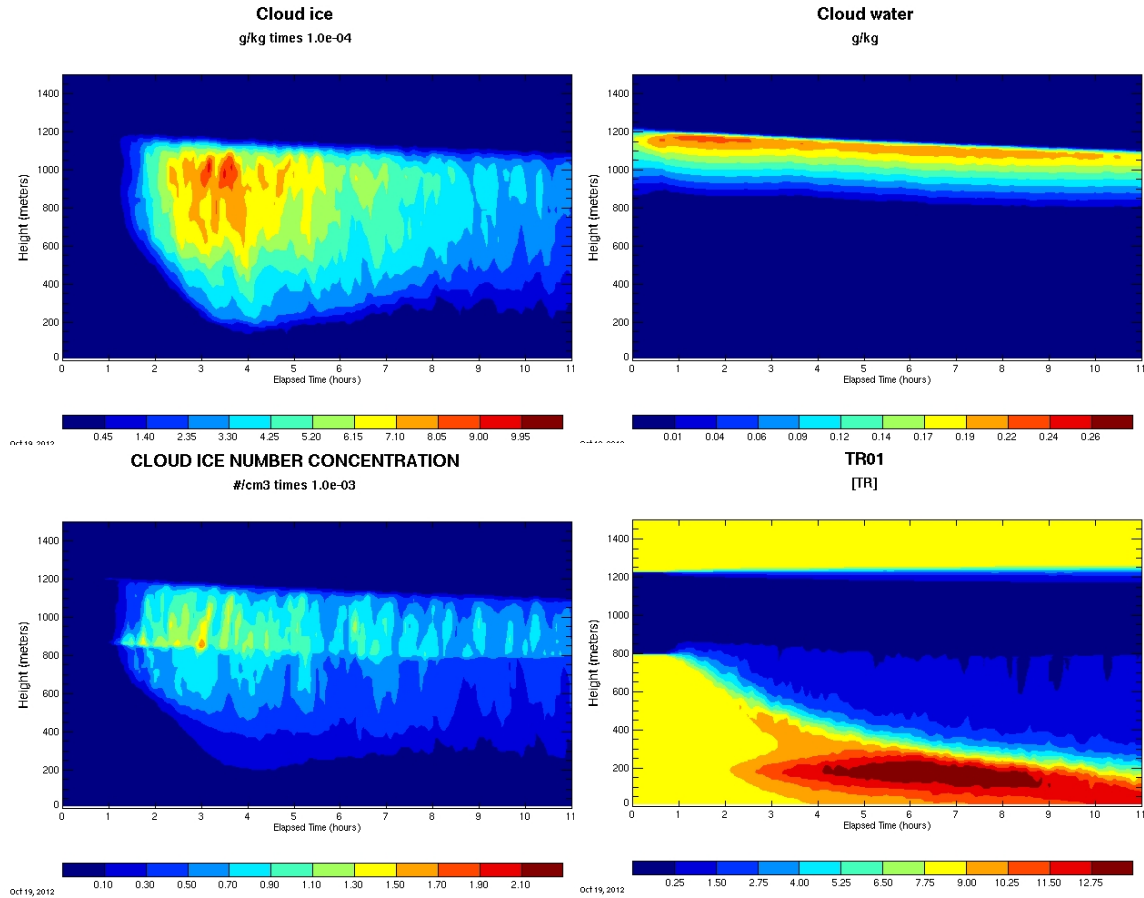


Figure 3.9. Selected SAM output from the prognostic IN simulation SNOSUB_d, where IN recycling due to sublimating snow only is considered. The lowest 200m of the atmosphere have been totally dried, resulting most noticeably in the elimination of the surface fog. The horizontal axis is time, and the vertical axis is height. All panels as in Fig. 3.7.

In the lowest 200 meters of the domain in SNOSUB and SNOSUB_d, snow was observed to be the dominant form of precipitation, responsible for 50-80% of the hydrometeors reaching the surface. To determine the relative importance of IN recycling due to evaporation of ice species other than snow, the prognostic scheme was again modified to allow IN recycling due to any sublimating frozen hydrometeor (SUB_LO, SUB_HI, and SUB_HI_d runs).

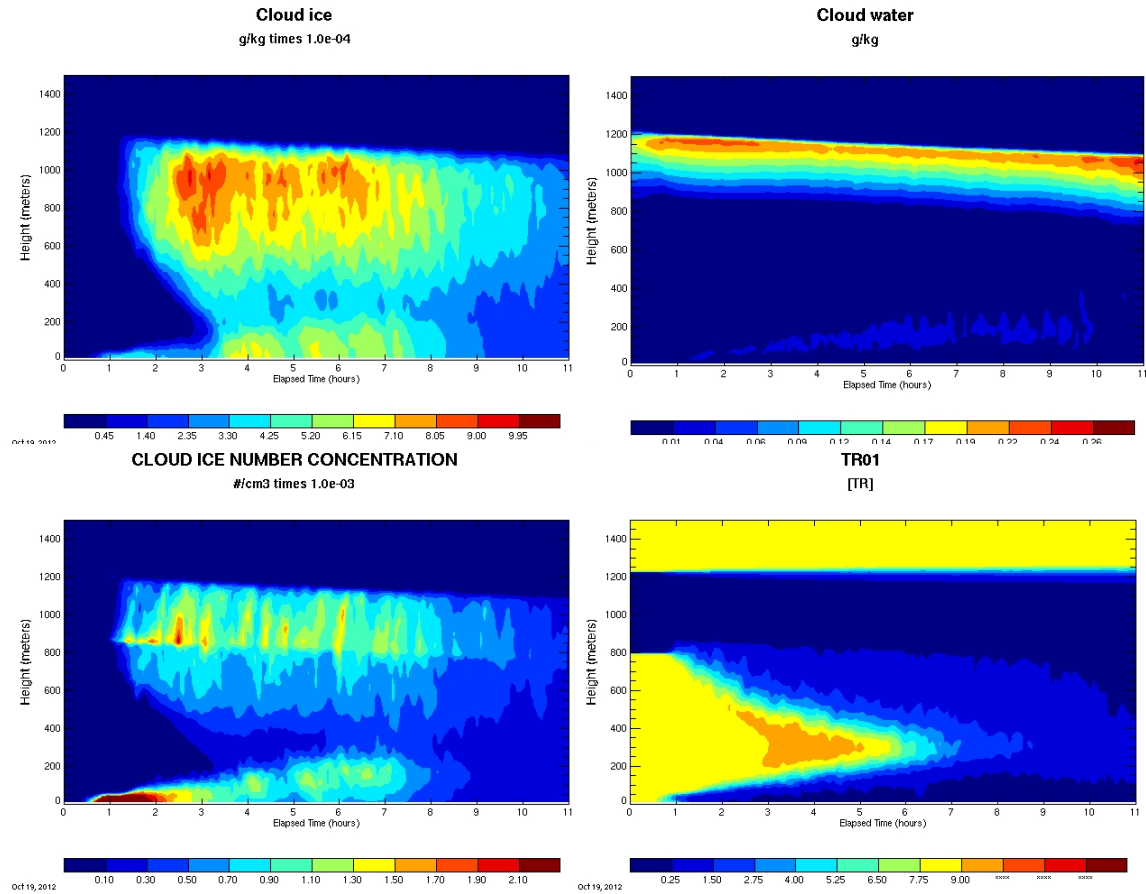


Figure 3.10. Selected SAM output from the prognostic 8.65 L^{-1} IN simulation SUB_HI, where IN recycling due to all sublimating ice species is considered. The horizontal axis is time, and the vertical axis is height. All panels as in Fig. 3.7.

Leaving the initial potential IN field set to the values used in the SNOSUB runs produced a more vigorous cloud in SUB_HI (Fig. 3.10), with higher ice number concentrations at all times and levels throughout the simulation. The span of simulated time showing ice contents in good agreement with observations is longer, by at least one hour, than in any of the previous prognostic simulations. The potential IN field (lower right panel) showed that potential IN concentrations of about 1 L^{-1} were better sustained in the lower region of the cloud in the SUB_HI simulations than in other simulations. In fact, potential IN concentrations higher than the initially specified concentrations existed close to the surface between hours 3 and 5 of the

simulation. These locally high concentrations were generated via the redistribution of IN via incorporation into ice particles and subsequent settling and sublimation. Since SUB_HI simulated a cloud with higher ice mass and number concentrations for an extended period, recycling of IN due to all sublimating species of ice is an important process to consider, and clearly assisted in sustaining the mixed-phase cloud in this case.

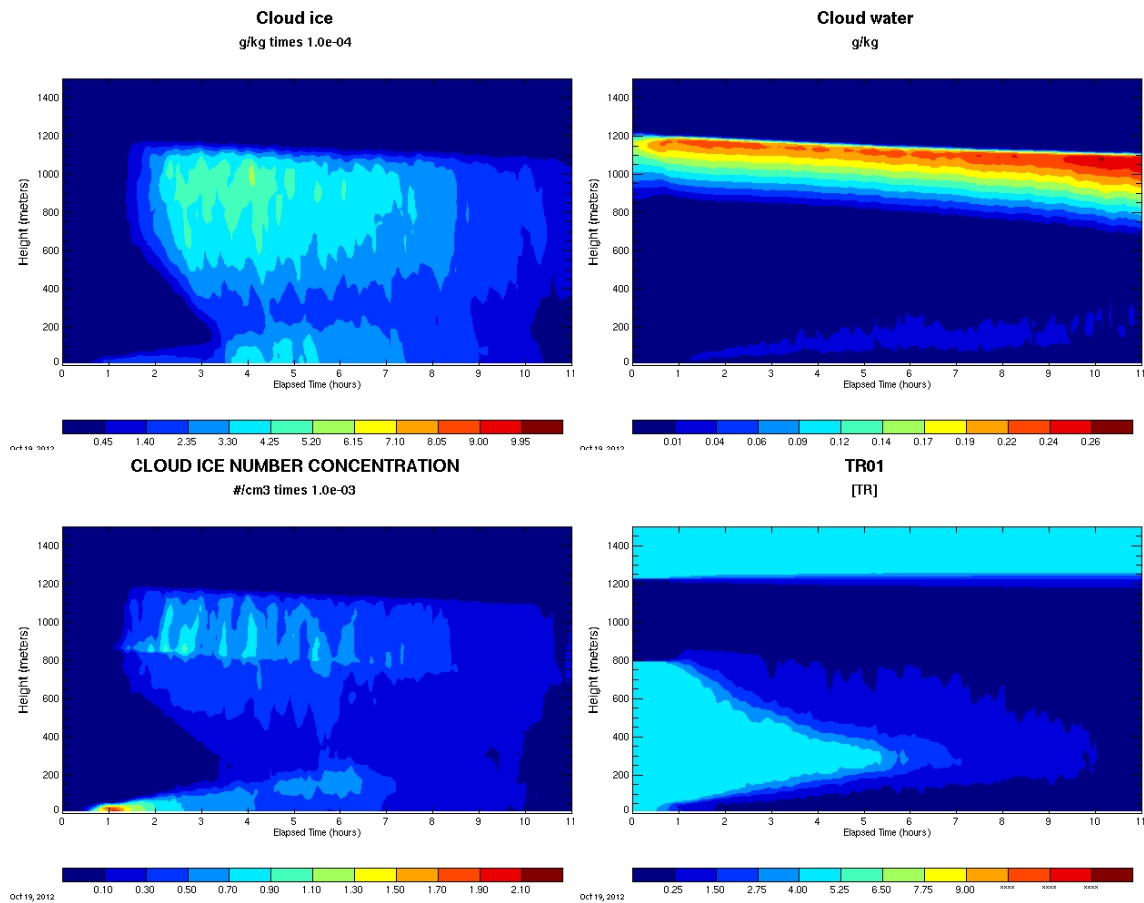


Figure 3.11. Selected SAM output from the prognostic 4.325 L^{-1} IN simulation SUB_LO, where IN recycling due to all sublimating ice species is considered. The horizontal axis is time, and the vertical axis is height. All panels as in Figure 3.7.

Results from the simulation SUB_LO, which used a factor of 5 increase over the predicted potential IN concentration according to equation 2.1, are shown in Fig. 3.11. Peak ice

water contents of about $5.7 \times 10^{-4} \text{ g m}^{-3}$ are only about 30% less than those obtained in the SUB_HI simulation. Ice number concentrations in the middle of the cloud layer from about $5.0 \times 10^{-4} \text{ cm}^{-3}$ to $8.0 \times 10^{-4} \text{ cm}^{-3}$ remain in good agreement with observations. Interestingly, surface precipitation rates for both the SUB_HI and SUB_LO simulations averaged 0.2 mm day^{-1} , even with enhanced peak pristine ice concentrations in the SUB_HI case.

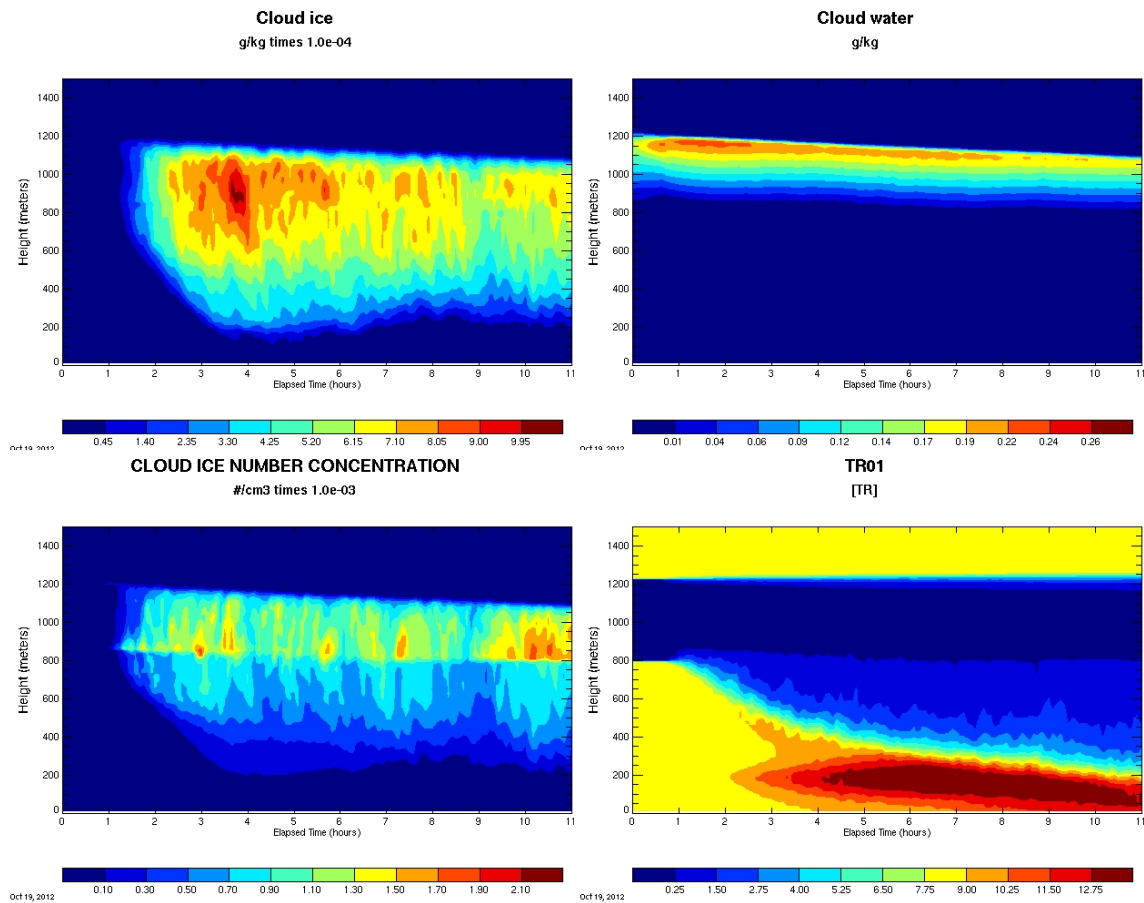


Figure 3.12. Selected SAM output from the prognostic 8.65 L^{-1} IN simulation SUB_HI_d, where IN recycling due to all sublimating ice species was considered. The lowest 200m of the atmosphere have been totally dried, resulting in the elimination of the surface fog seen in other simulations. The horizontal axis is time, and the vertical axis is height. All panels as in Fig. 3.7.

The SUB_HI simulation was repeated in SUB_HI_d, but with the lowest 200 meters of the atmosphere dried as in the SNOSUB_d simulation; results are shown in Fig. 3.12. Average

mixing ratios and number concentrations in the active, ice-forming region of the cloud increased relative to the SUB_HI simulation. Similar to SNOSUB_d, the peak values of ice mixing ratios increased to $\sim 1.0 \times 10^{-3} \text{ g m}^{-3}$, the highest values of any simulation excluding DM_10, but still below observed values by about a factor of ~ 50 . Surface precipitation rates decreased due to the enhanced sublimation, averaging 0.06 mm day^{-1} over the course of the simulation. Peak ice number concentrations are similar to the other prognostic simulations utilizing a factor of 10 increase in initial potential IN. In fact, ice formation within the cloud appeared to occur in a second pulse later in the simulation, as indicated by elevated ice number concentrations near the end of the 12-hour simulation. This simulation was the only Flight 16 simulation with this behavior. The ice nucleation was supported by the higher concentrations of potential IN, relative to SUB_HI, generated by sublimation below cloud and lifted to near cloud base by mixing. Indeed, the SUB_HI simulation with the original moisture profile had the most prominent decreases in cloud ice production when the potential IN concentrations near 800 m began to decrease near the end of the simulation, preventing the additional activation required to sustain ice formation.

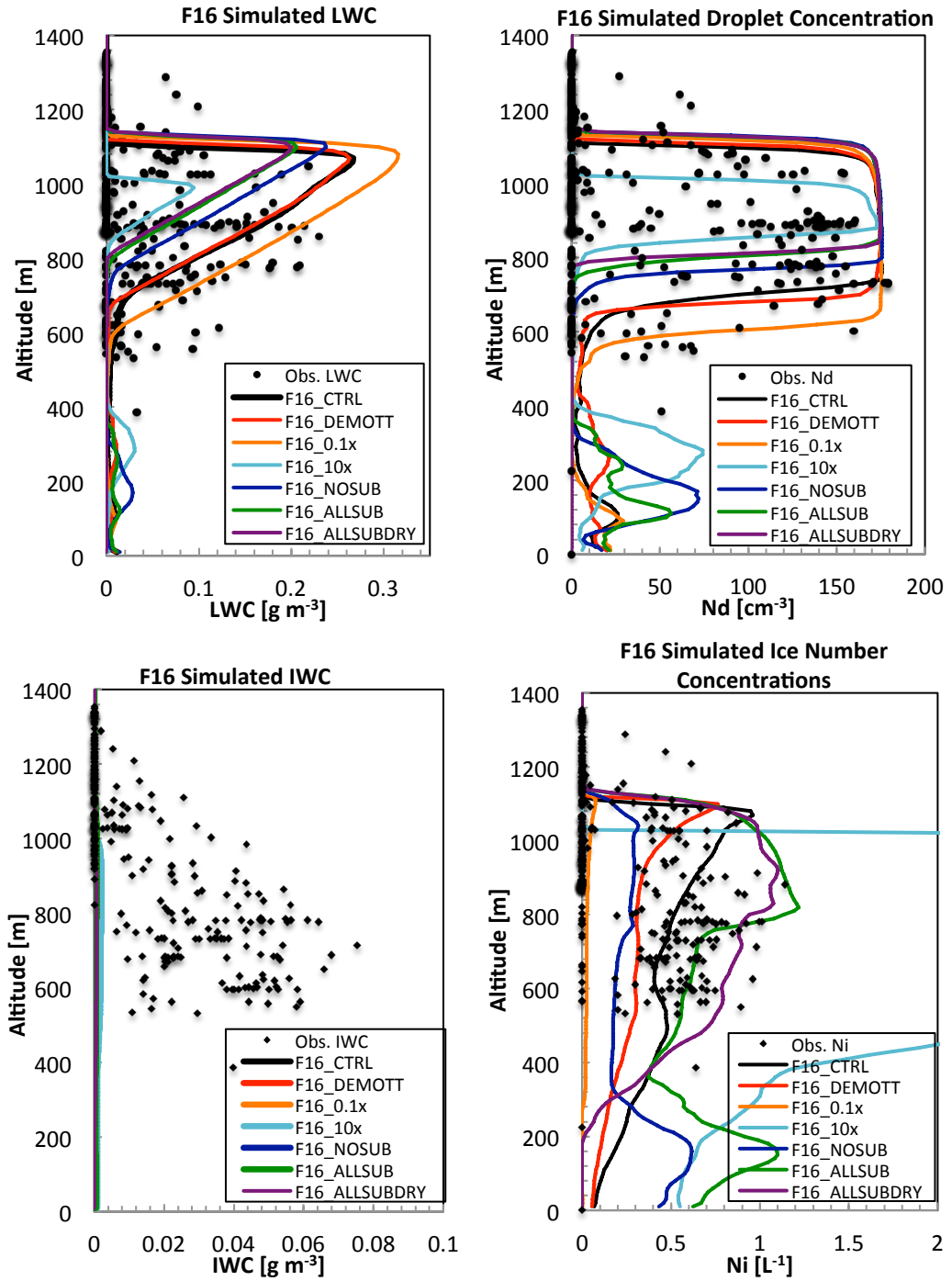


Figure 3.13. Single vertical profiles for selected F16 simulations. Diagnostic simulations are from hour 11, and prognostic simulations from hour 7. Refined aircraft data from G. McFarquhar shown for reference, obtained from DOE-ARM archive.

Selected profiles from the Flight 16 simulations are shown in Figure 3.13 for visual comparison to observations and to demonstrate the variability between all simulations. Both the diagnostic DEMOTT and prognostic SUB_HI_d simulations present a “best-case” representation of the observed cloud system on 8 April. The DEMOTT simulation exhibited a steady-state cloud with ice mass and number concentrations in reasonable agreement with observations, as well as supercooled liquid water contents. In the SUB_HI_d simulation, reasonable ice mass and number concentrations were also achieved, but small-scale variability in cloud structure was also observed, a feature present in the observations, but less so in the DEMOTT simulation. This indicates that the prognostic scheme, while unable to produce long-lived mixed-phase clouds that persist beyond several hours, is capable of representing physical processes in which IN are introduced to the cloud layer, removed by precipitation, and potentially re-introduced through sublimation.

In our simulations, cloud liquid water contents closely resembled the observed values, and downwelling longwave radiation at the surface ranged from $\sim 262 \text{ W m}^{-2}$ to 270 W m^{-2} , compared to peak radiation measured on 8 April of $\sim 260 \text{ W m}^{-2}$. A study utilizing the Community Atmosphere Model version 5 (CAM5) to simulate the entire time period of the ISDAC campaign found that the model was capable of resolving the types of mixed-phase stratus clouds that we focus on in this study (*Liu et al.*, 2011). However, it was concluded that while the model produced reasonable ice water contents, it underpredicted cloud liquid water mixing ratios with values of about $\sim 0.1 \text{ g m}^{-3}$, resulting in underestimation of radiative forcings. Downward longwave radiation was underestimated by 20-40 W m^{-2} . (*Liu et al.*, 2011). When a new ice nucleation parameterization developed by Phillips et al. (2008) was utilized, cloud liquid water

contents increased marginally due to fewer predicted pristine ice crystals, slowing the Wegener-Bergeron-Findeisen process responsible for liquid water depletion.

Additionally, a recent study utilizing a different large-eddy simulation model simulated the 8 April case specifically, providing comparison results for use in our study (*Avramov et al.*, 2011). The model, the Distributed Hydrodynamic Aerosol and Radiative Modeling Application (DHARMA) uses different microphysical and radiative packages than SAM, and was setup to run in 3-dimensional mode with 50 meter horizontal grid spacing and 15 meters vertically, with a maximum time step of 5 seconds. The study hypothesized that observed IN concentrations could explain the ice properties of the cloud system encountered during Flight 16. Various initial profiles of IN concentrations were used, ranging from simulations with initial concentrations of 10 L^{-1} above the temperature inversion, with 1 L^{-1} below, to 40 L^{-1} above the inversion, keeping 1 L^{-1} below. Additional simulations used a constant vertical profile of 10 L^{-1} throughout the domain (*Avramov et al.*, 2011). The study concluded that while the model reasonably predicted ice number concentrations regardless of assumed crystal density, ice water contents were underestimated. Furthermore, the study found that utilizing a uniform vertical profile of initial IN concentrations led to a reservoir of IN below the cloud, which were slowly mixed into the cloud, maintaining ice number concentrations.

In contrast, our study found that initially uniform vertical profiles of IN caused SAM to simulate a short-lived (less than 1 hour) pulse of ice activation and growth which depleted the boundary layer of IN, preventing the formation of a sustained cloud layer. However, when we dried the lowest 200 meters of the boundary layer and allowed ice to sublimate and return IN, a strong reservoir of potential IN did form, and was slowly mixed into the cloud layer, helping to

sustain ice number concentrations in good agreement with observations. SAM also produced ice water contents that were lower than peak values observed during the flight.

Chapter 4

Case Study 2: ISDAC Flight 31

4.1 Observations

The cloud system observed and investigated on 26 April exhibited some differences from the cloud observed less than three weeks prior, despite having established itself under a similar synoptic pattern. Both cloud systems formed under the influence of a deep high pressure system circulating over the North Pole, but while the cloud system on 8 April was observed to persist for the entire day, not fully dissipating until 9 April, the cloud system sampled on 26 April persisted for about 15 hours (*Jackson et al.*, 2012). Several 6-day back-trajectory analyses showed that the air mass in place at cloud level over the study area on 26 April likely originated from the Arctic Ocean, while the air mass above the inversion originated from the Pacific Ocean (*Jackson et al.*, 2012). This strong near-term oceanic influence is in contrast to the air mass in place during the 8 April cloud episode in that the air mass at that time likely originated from northern Canada and the above-cloud air mass from western Alaska. In addition, with the progressing springtime ice melt, surface fluxes from the ocean would be quantifiably larger on 26 April compared with 8 April, which might influence the microphysical properties of the clouds (*Morrison et al.*, 2008; *Jackson et al.*, 2012). Ideally these different fluxes of sensible and latent heat would be incorporated into the SAM simulation setup, but our ISDAC simulations used the same values for surface heat fluxes. This followed previous studies and intercomparisons, discussed later, and limits present insight into resultant effects on cloud cover between the two ISDAC cases. McFarquhar et al. (2011) suggest that CFDC measurements of IN concentrations were near 1 L^{-1}

during Flight 31, in contrast with values of 10 L^{-1} observed during a brief period of Flight 16. As discussed in chapter 2, the higher values assumed for Flight 16 appear suspect in consideration of inspecting the overall ISDAC data set. While the coarse mode concentration peaked at 2 cm^{-3} for Flight 31, compared to 5 cm^{-3} for Flight 16, the number of aerosol particles larger than 0.5 microns by volume, $n_{aer,0.5}$, was calculated to be 4.348 cm^{-3} for Flight 31, nearly equivalent to the value of 4.903 cm^{-3} for Flight 16.

Fine-mode aerosol size distributions were similar for the two days, with both cases exhibiting a number mean geometric radius of 0.1 microns, with sigma values of 1.5 for Flight 31 and 1.43 for Flight 16. Averaged fine-mode aerosol number concentrations do show minor differences between the cases, with 200 cm^{-3} during Flight 31 and 172 cm^{-3} during Flight 16, but overall, both cases are very similar in terms of aerosol concentrations. Both 8 April and 26 April represented ‘cleaner’ days from the ISDAC campaign, markedly different from the more polluted period of 18-21 April. While it is widely accepted that marine and continentally-sourced air masses exhibit distinctly different particle compositions and concentrations with marine air typically cleaner, the modest differences between Flight 16 and Flight 31 are expected to be reflected primarily in the activation of cloud droplets.

The primary result of implementing different aerosol size distributions will be manifested in the two-moment SAM by predicted cloud droplet number concentrations. In the observations, a thin layer of cloud droplet number concentrations occurred between 300 – 400 m above the surface, with most observations at 700-900 m and no drops observed above about 1000 meters. Drop number concentrations peaked near 248 cm^{-3} at ~700 meters, with one measurement of 286 cm^{-3} at 800 meters, both larger than the observed total aerosol number concentrations. This is likely due to the failure of the single aerosol distribution to reflect true spatial variability. During

Flight 16, concentrations peaked at about the same altitude at 225 cm^{-3} , so the difference in observed droplet concentrations between the two cases is consistent in direction and magnitude with the small difference in fine-mode aerosol number concentrations. Average cloud liquid water contents peaked at about 800 meters above ground, at nearly 0.05 g m^{-3} , with lowest values of about 0.02 g m^{-3} . Virtually no liquid water existed below about 600 meters, indicating the location of the transition to the ice-phase region of the cloud.

In general, ice number concentrations reported in the DOE-ARM archive for the ISDAC project were similar to those observed during Flight 16. Following screening and processing, only two datapoints remained for the mixed-phase portion of the cloud, with ice number concentrations $\sim 0.015 \text{ L}^{-1}$. Lower, in the ice-phase region of the cloud, ice number concentrations ranged from about 0.015 L^{-1} to nearly 3 L^{-1} . Most measurements, however, were between roughly 0.03 L^{-1} and 0.3 L^{-1} , very similar to the concentrations observed during Flight 16. Average ice water contents within the cloud ranged from about 0.02 g m^{-3} in the lowest levels of the cloud, to around 0.01 g m^{-3} in the mixed-phase region, roughly one-third the typical ice water contents observed during Flight 16. Average precipitation rates measured at the NSA site near Barrow by the FD12P instrument were about $\sim 0.06 \text{ mm hr}^{-1}$ for the 24-hour period beginning just after 9:30Z. The average precipitation rate from the same instrument during the period of Flight 31 increased to $\sim 0.12 \text{ mm hr}^{-1}$.

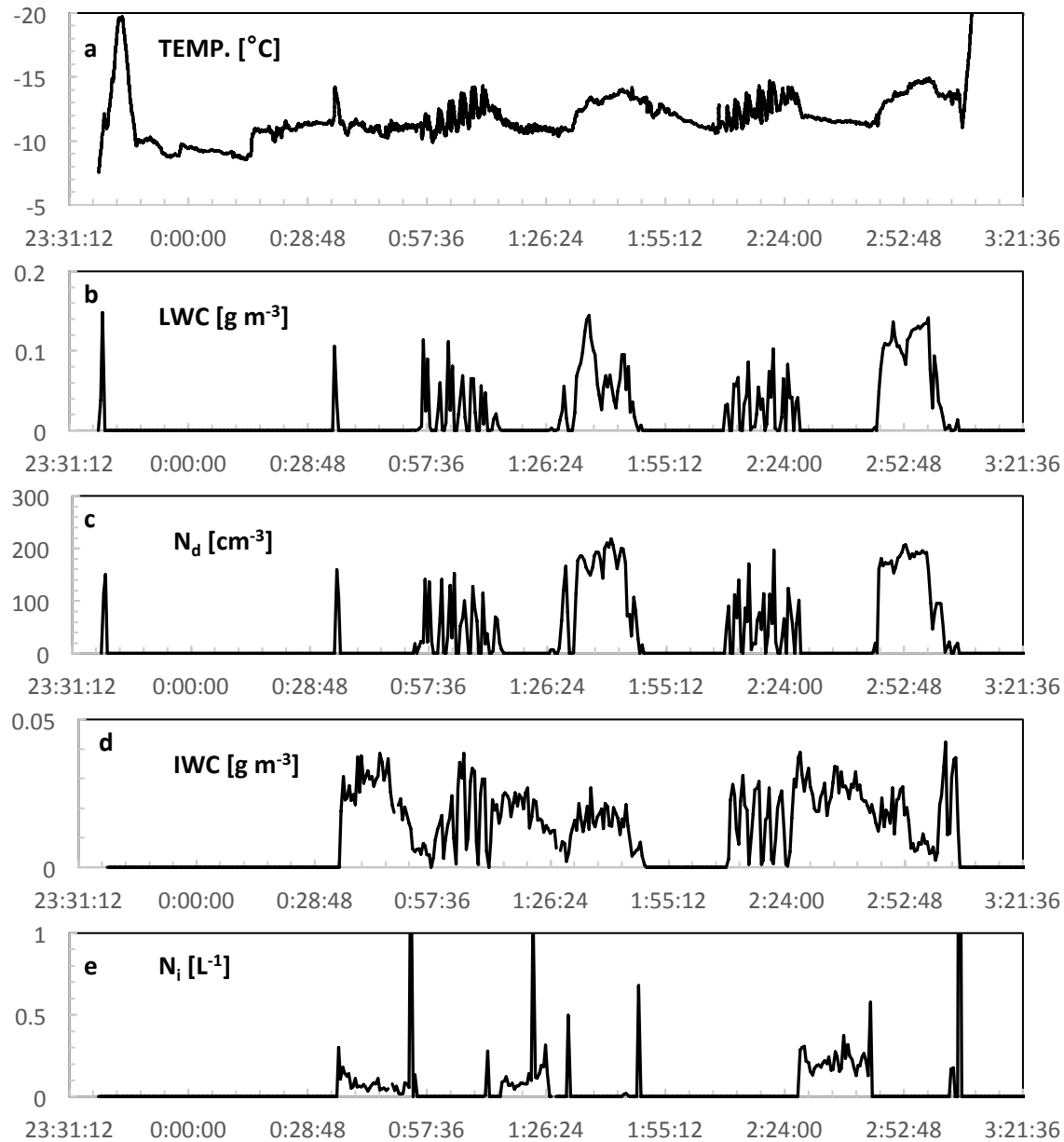


Figure 4.1. Time series of (a) temperature in degrees Celsius, (b) liquid water content in g m^{-3} , (c) cloud droplet number concentration in units cm^{-3} , (d) ice water content in g m^{-3} , (e) pristine ice number concentration in units L^{-1} , from onboard the Convair 580 during Flight 31. Data obtained from the DOE-ARM archive for the ISDAC project.

4.2 Model Initialization

The initial forcing data for the 26 April case, simulating Flight 31, were derived from a model intercomparison developed by Ovchinnikov et al. (2012) for the PAN-GASS conference. The initial profiles for temperature and water vapor were defined by a best fit profile between the Barrow surface sounding and the average conditions experienced by the aircraft at the time of the flight and are shown in Fig. 4.2, together with the wind fields applied (nudged to) in the model runs. The partial profile obtained by the aircraft agreed well with the land-based sounding launched at 5:42Z on environmental conditions, despite the fact that the aircraft-generated profile used measurements collected between 1:06 and 1:09Z, and about 120 kilometers north of Barrow (*Ovchinnikov et al.* Intercomparison 2012).

Table 4.1. List of ISDAC Flight 31 (26 April 2008) SAM Simulations

| Simulation | Acronym | IN Treatment | Max Initial IN | Activation |
|---------------------------------|----------------|---------------------|---|-------------------|
| Control | CTRL | Diagnostic | T-dependent (500 L ⁻¹ max) | Cooper |
| DeMott | DEMOTT | Diagnostic | 0.50 L ⁻¹ | D10 |
| 0.1x DeMott | DM_0.1 | Diagnostic | 0.050 L ⁻¹ | 0.10 * D10 |
| 10x DeMott | DM_10 | Diagnostic | 5.0 L ⁻¹ | 10.0 * D10 |
| No Sublimation | NOSUB | Prognostic | 5.0 L ⁻¹ | D10 |
| Snow Sublimation | SNOSUB | Prognostic | 5.0 L ⁻¹ | D10 |
| Snow Sublimation, Dried Profile | SNOSUB_d | Prognostic | 5.0 L ⁻¹ | D10 |
| All Sublimation | SUB_HI | Prognostic | 5.0 L ⁻¹ | D10 |
| All Sublimation | SUB_LO | Prognostic | 2.5 L ⁻¹ | D10 |
| All Sublimation, Dried Profile | SUB_HI_d | Prognostic | 5.0 L ⁻¹ | D10 |

For the coldest temperatures observed at the top of the cloud, equation 2.1 predicts a maximum available potential IN concentration of 0.5 L⁻¹, in good agreement with the ~1 L⁻¹ IN concentrations measured onboard the aircraft. In similar fashion to the Flight 16 case study, a

total of ten simulations are presented in this Chapter, following the same conventions. The simulations with their assigned acronyms are listed in Table 4.1.

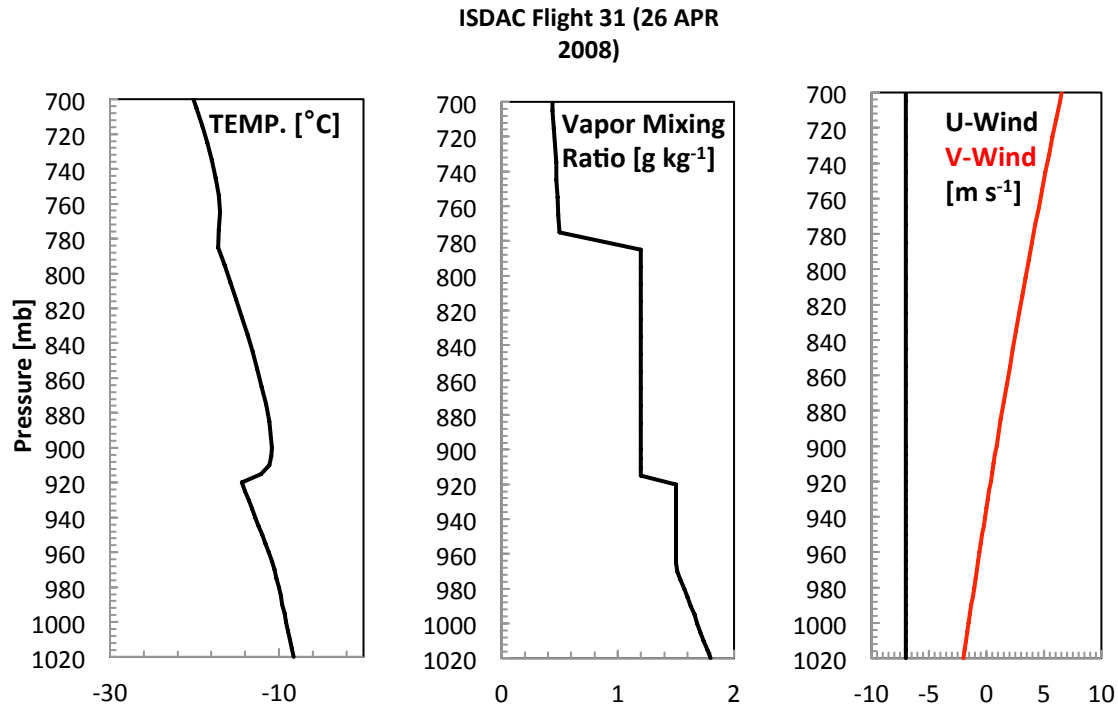


Figure 4.2. Vertical profiles of the initialization data used for Flight 31. SAM is initialized with potential temperature (not shown) instead of actual ambient temperature. Also shown are water vapor mixing ratio in g kg^{-1} , and averaged horizontal winds.

4.3 Diagnostic IN Simulations

In the CTRL simulation, the development of the simulated cloud occurred more slowly than in the CTRL simulation of Flight 16. Ice content of the cloud averaged about $1.25 \times 10^{-4} \text{ g m}^{-3}$, with short periods approaching $2.0 \times 10^{-4} \text{ g m}^{-3}$, particularly near the end of the simulation, an underprediction of a factor of 100 when compared to the observations. Ice number concentrations peaked near the end of the model run, with values at cloud top of about $5.5 \times 10^{-4} \text{ cm}^{-3}$, in good agreement with the wide range of ice number concentrations reported during the

flight. Peak liquid water contents were found near the end of the simulation as well, at about 0.3 g m^{-3} , nearly a factor of 10 higher than observed. It is important to note that the simulated cloud activity was observed to increase throughout the model run, with every indication that ice water contents and number concentrations would continue to rise past the 12-hour mark, but with increasing cloud water contents as well. The simulations suggest that due to the slow spinup, longer simulation times than used here are required to model the cloud peak and decay.

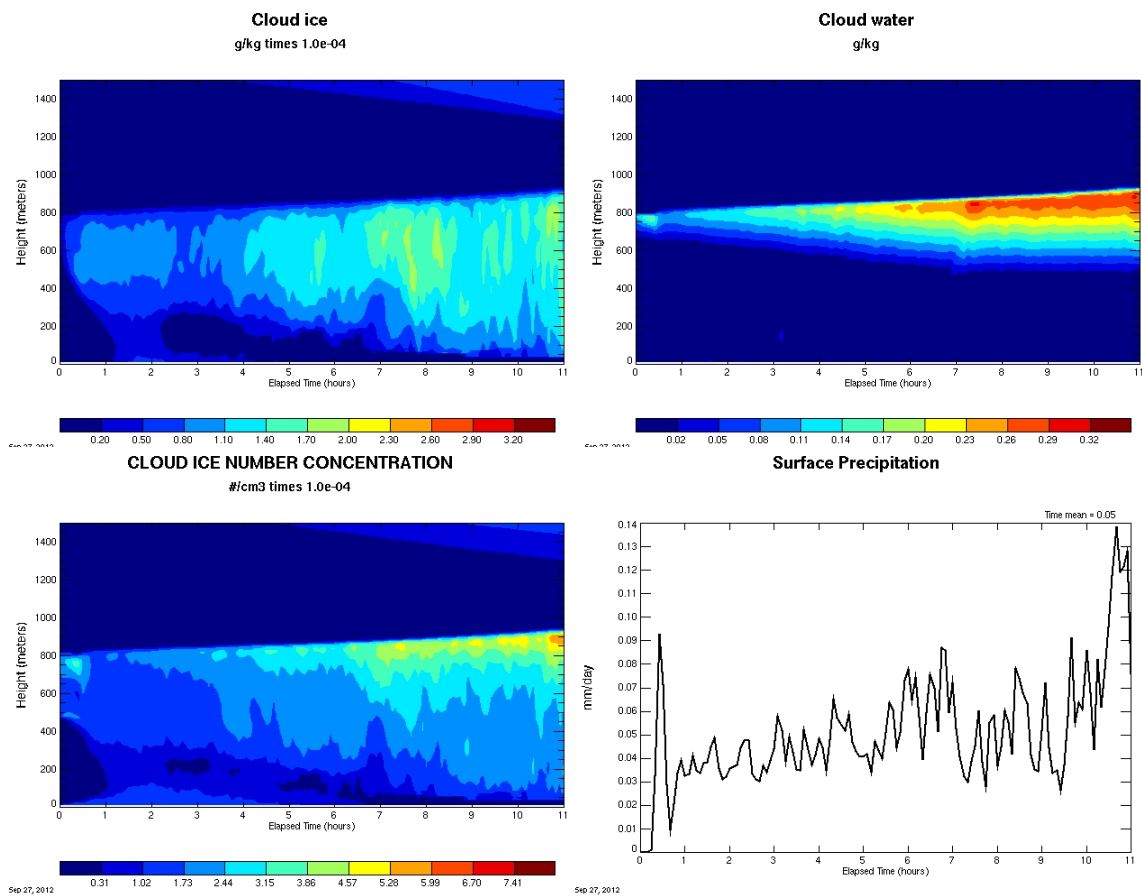


Figure 4.3. Selected SAM output from the CTRL simulation. The horizontal axis is time, and the vertical axis is height; all fields were horizontally averaged at each time step to produce these and all subsequent modeled output figures, unless otherwise noted. The upper left panel is cloud ice mass in g kg^{-1} , the upper right panel is cloud water mass in g kg^{-1} , the lower left panel is cloud ice number concentration in cm^{-3} , and the lower right panel is surface precipitation in mm day^{-1} .

In the diagnostic DEMOTT simulation, the cloud approached in about four hours a state similar to the CTRL simulation at 8 hours, indicating faster cloud development. The cloud was visibly more stratified, and the region containing about $5.0 \times 10^{-4} \text{ cm}^{-3}$ pristine cloud ice particles was more temporally stable, but occupied a thinner portion of the upper regions of the cloud. The cloud water contents were similar between the CTRL and DEMOTT simulations.

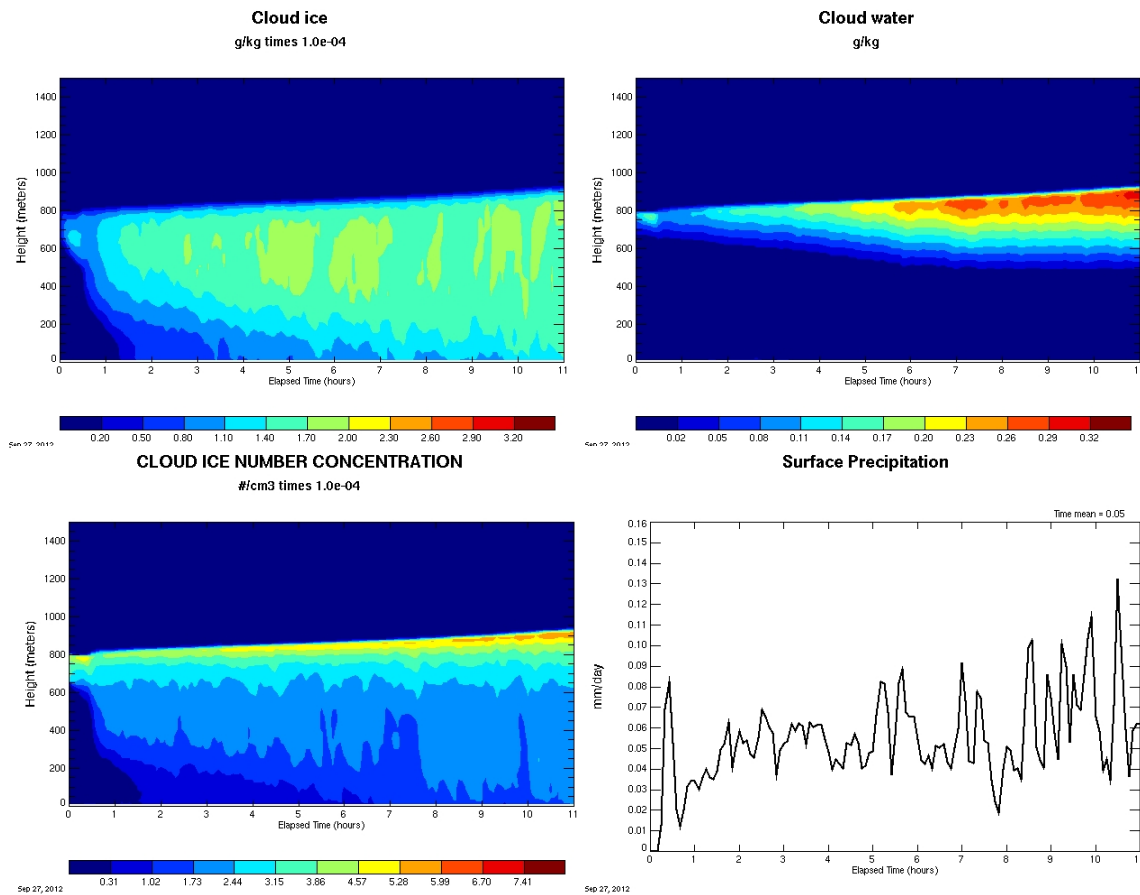


Figure 4.4. Selected SAM output from the DEMOTT simulation. The horizontal axis is time, and the vertical axis is height. All panels as in Fig. 4.3.

The results for DM_0.1 were similar to the sensitivity tests conducted for Flight 16. The cloud was significantly less active with lower surface precipitation for the duration of the simulation, eventually reaching negligible amounts of precipitation by hour seven. The liquid

layer was thicker, containing more liquid on average, than both the DEMOTT and CTRL simulations, due to the forced suppression of ice activation. This case demonstrates that the absence of a high-enough threshold concentration of IN can result in only small number concentrations of nucleated ice, that are unable to scavenge available water vapor, thus leading to growth and persistence of a deeper supercooled liquid cloud.

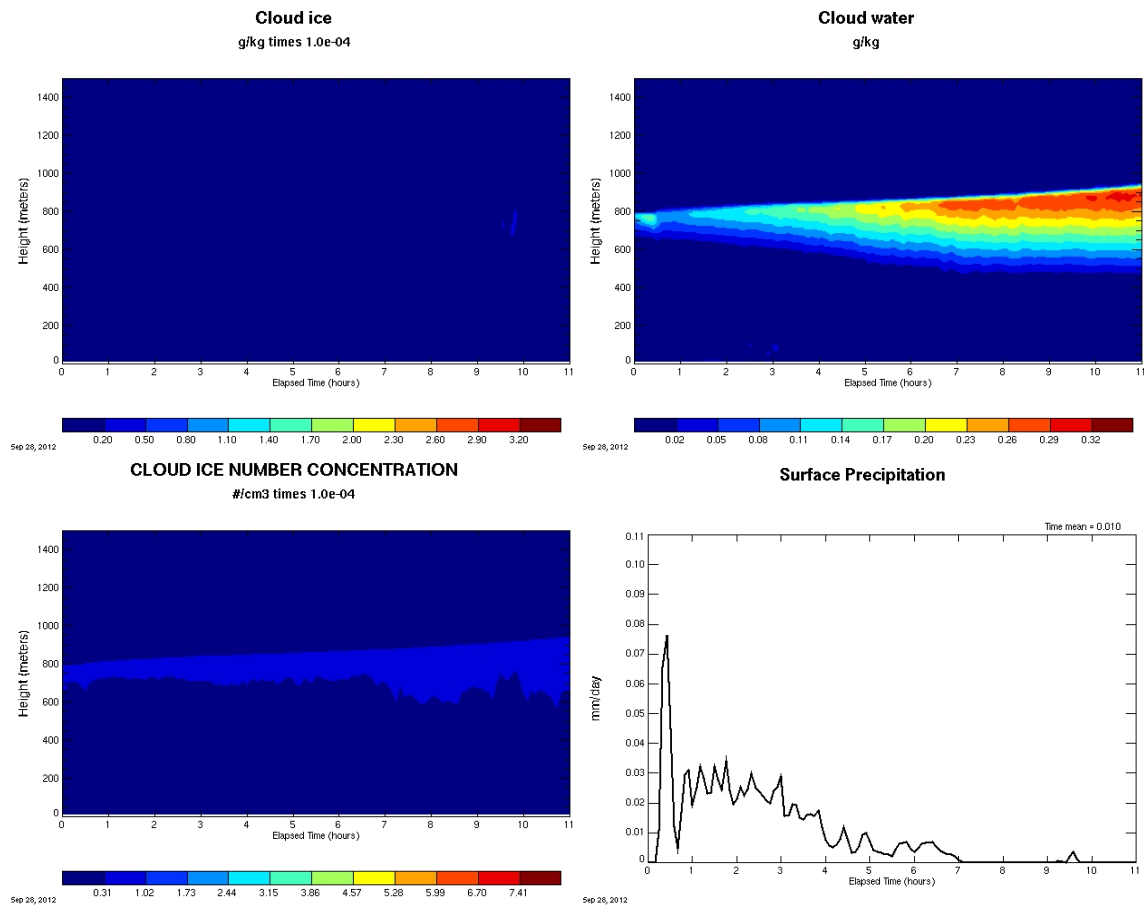


Figure 4.5. Selected SAM output from the DM_0.1 simulation. The horizontal axis is time, and the vertical axis is height. All panels as in Fig. 4.3.

Results from the DM_10 simulation are shown in Fig. 4.6. The cloud exhibited similar structure to the DEMOTT simulation, but with much higher concentrations of both ice mass and number concentrations. The liquid layer was observed to contain less liquid water than

DEMOTT at all times in the simulation, due to depletion by ice activation and growth.

Precipitation at the surface midway through the simulation was about 0.3 mm per day, compared to about 0.06 mm day⁻¹ for DEMOTT, a factor of 5 increase in precipitation rates corresponding to a factor of ten increase, on average, in ice crystal number concentrations.

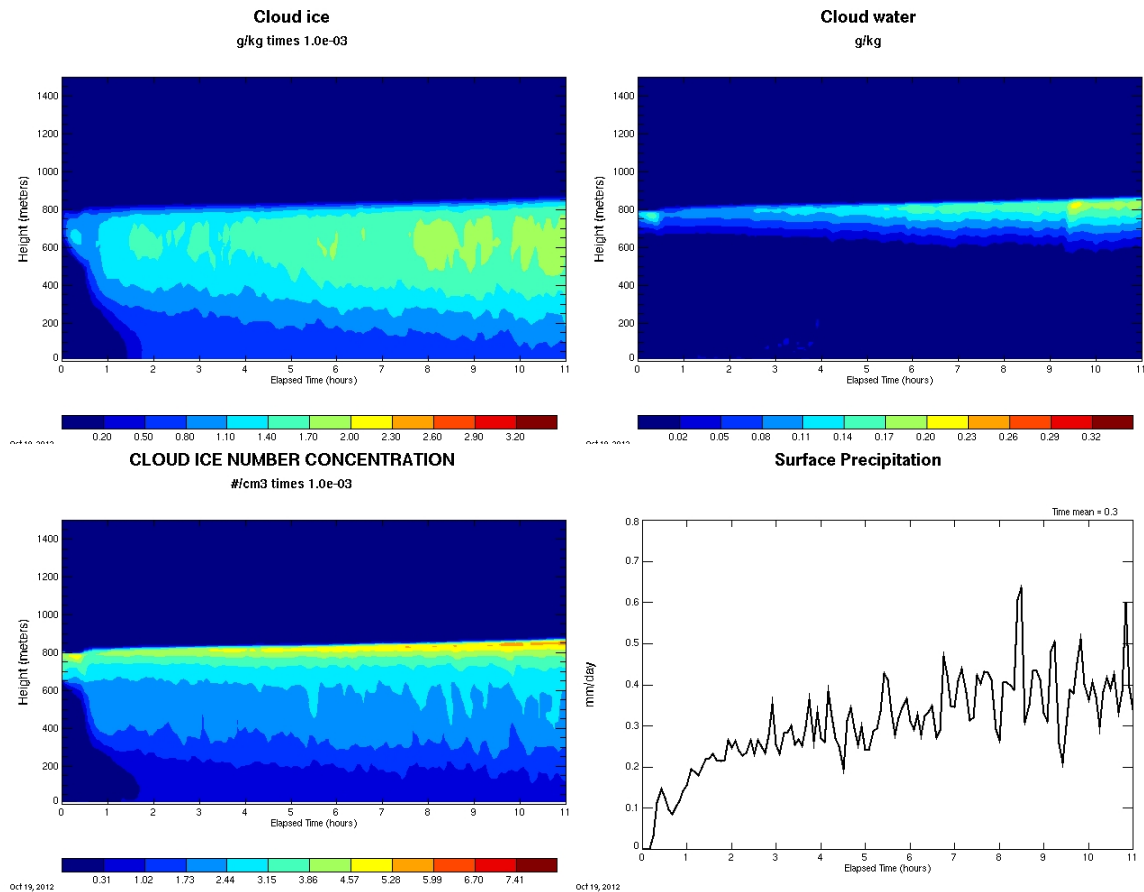


Figure 4.6. Selected SAM output from the DM_10 simulation. The horizontal axis is time, and the vertical axis is height. All panels as in Fig. 4.3.

4.4 Prognostic IN Simulations

In the series of simulations in which the prognostic ice nuclei scheme was active, the cloud exhibited fundamental differences in behavior from the diagnostic runs. In the NOSUB

simulation, in which potential IN recycling due to sublimation was neglected, the effective lifetime of the ice phase of the cloud was less than three hours.

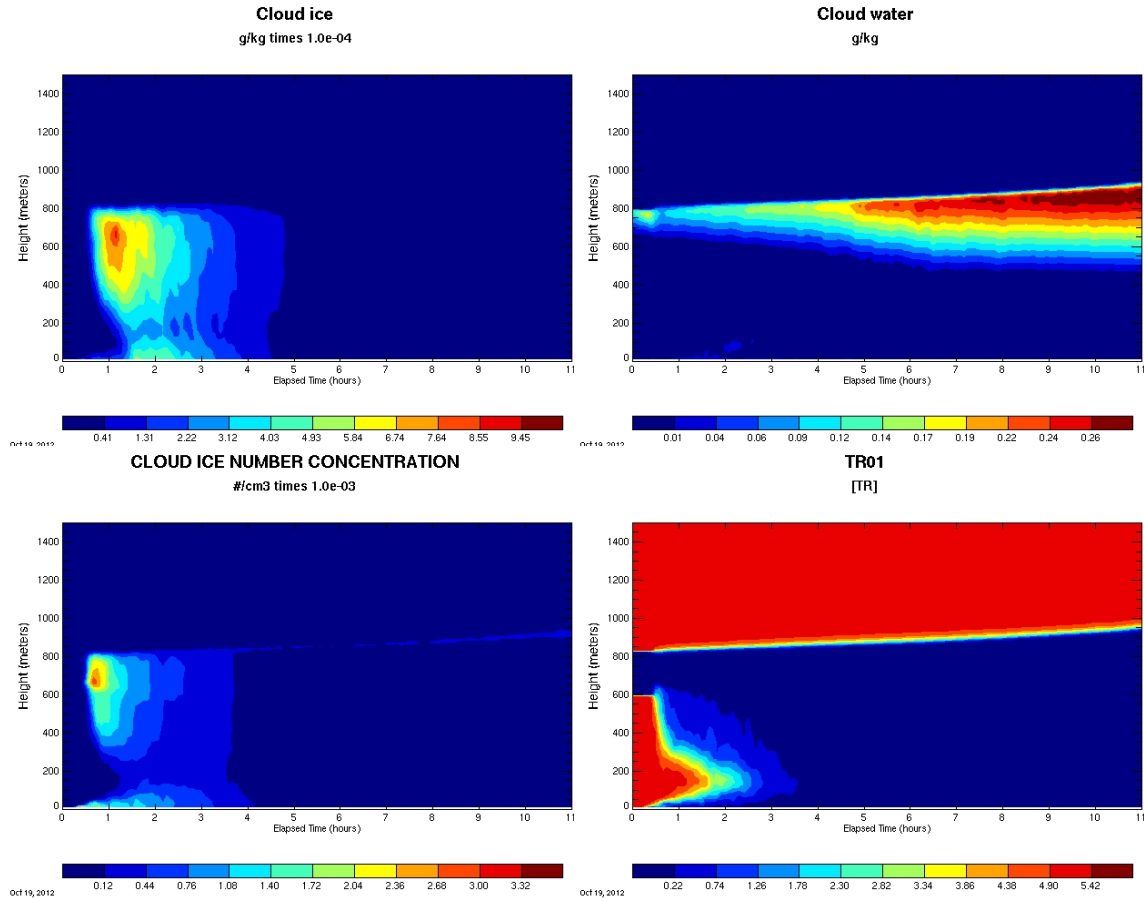


Figure 4.7. Selected SAM output from the prognostic NOSUB simulation (5.0 L^{-1} IN, no IN recycling due to sublimation). The horizontal axis is time, and the vertical axis is height. The upper left is cloud ice mass concentration in g kg^{-1} , the upper right panel is cloud liquid water mass concentration in g kg^{-1} , the lower left panel is cloud ice number concentration in cm^{-3} , and the lower right panel is potential IN concentration (tracer field) in L^{-1} . The color scales are consistent across the prognostic simulations for easy visual comparison.

As seen in the lower right panel of Fig. 4.7, the IN were again introduced into layers just above and below the expected liquid cloud. Once IN began to entrain into the liquid layer, ice rapidly formed and the cloud reached ice water contents of about $9.0 \times 10^{-4} \text{ g m}^{-3}$ at around 1 hour of simulated time, more than a factor of 4 higher than the diagnostic simulations, with the

exception of the DM_10 simulation. At the same time in the simulation, cloud ice number concentrations approached $3.0 \times 10^{-3} \text{ cm}^{-3}$, higher than in the diagnostic simulation and still in agreement with observed ice number concentrations. After 1-2 hours, the ice phase in the cloud rapidly dissipated. This result can be explained by the potential IN field, which showed that IN were depleted in the boundary layer by 4 hours' simulation time. Once the boundary layer was fully depleted of potential IN, the only further activation in the system occurred at the top of the liquid layer, as the cloud continued to entrain a few IN particles and activate up to $4.0 \times 10^{-4} \text{ cm}^{-3}$ ice crystals for the remainder of the 12-hour simulation in the upper-most 20 meters of the remaining liquid layer. The lower left panel of Fig. 4.7 shows that an ice fog formed near the surface early in the simulation, similar to the prognostic simulations conducted for Flight 16. A region of supersaturation developed near the surface, which formed droplets. The droplets then froze as available potential IN were scavenged, similar to the Flight 16 simulations when the prognostic scheme was active.

The SNOSUB simulation (Fig. 4.8) resulted in an extension of the simulated cloud lifetime of about one hour over NOSUB, attributable to low rates of IN replenishment via sublimation early in the simulation. The sublimation process is cut off by the formation of a surface ice fog, limiting the amount of time by which the cloud lifetime could be extended. The fog structure in both Flight 16 and Flight 31 cases is quite similar, and the vertical extent of both fogs increases at about the same rate in the model. Because the below cloud layer was lower in Flight 31, depletion of the potential IN due to the fog before they could impact the cloud layer had a more immediate effect on cloud dissipation, leading to the shorter lifetimes observed.

In SNOSUB_d (Fig. 4.9), the lowest 200 meters of the boundary layer were initialized as completely dried to enhance the sublimation of snow. The most noticeable effects when

compared to SNOSUB occurred after about two hours. The ice fog was prevented from forming as the sublimation was insufficient to provide enough vapor to exceed saturation conditions, allowing for continued sublimation and more effective replenishment of IN. In fact, averaged IN concentrations in some below-cloud regions between 1.5-3 h in the simulation were higher than those originally specified.

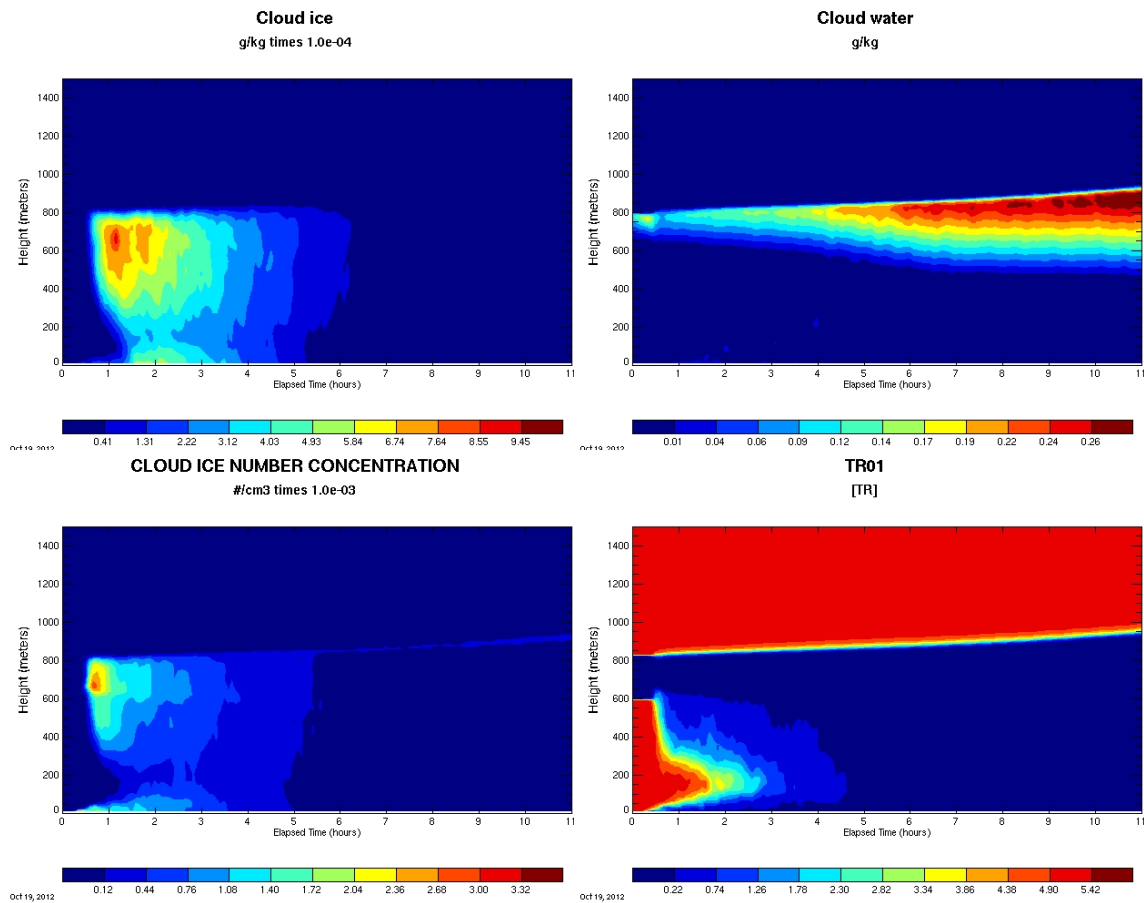


Figure 4.8. Selected SAM output from the prognostic SNOSUB simulation ($5.0 \text{ L}^{-1} \text{ IN}$, including IN recycling due to sublimating snow only). The horizontal axis is time, and the vertical axis is height. All panels as in Fig. 4.7.

On average, the ice water contents in SNOSUB_d were lower than in SNOSUB. Ice number concentrations, however, were slightly higher after about 3.5 hours in the upper region

of the cloud. The potential IN field showed the presence of concentrations up to 0.7 L^{-1} near cloud base until around 9 hours, whereas in SNOSUB potential IN were totally depleted after about 4.5 hours. Liquid water contents of up to 0.12 g m^{-3} were about half those in SNOSUB, but remained relatively stable over the course of the simulation. Overall, ice number concentrations and ice water contents remained well below typical observed values, and liquid water contents, while closer to observations, were still a little more than a factor of ~ 2 higher.

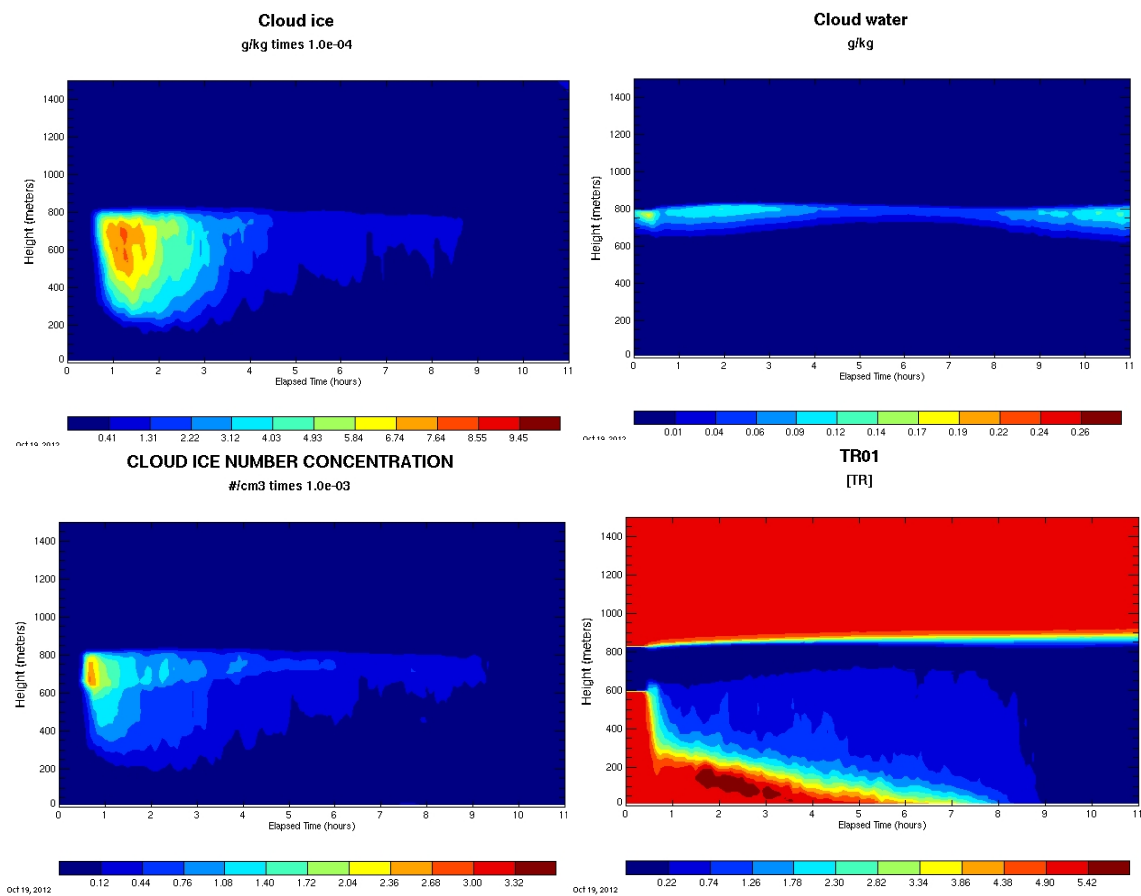


Figure 4.9. Selected SAM output from the prognostic SNOSUB_d simulation (5.0 L^{-1} IN, IN recycling due to sublimating snow only). The lowest 200m of the atmosphere have been totally dried, resulting in the elimination of the surface fog. The horizontal axis is time, and the vertical axis is height. All panels as in Fig. 4.7.

The SUB_LO, SUB_HI, and SUB_HI_d simulations incorporated potential IN recycling from any sublimating ice, including graupel and pristine ice in addition to the snow. Snow comprised, at most, about 76% of the precipitation in the model, early in the simulation, indicating that other ice hydrometeors may again be important to consider when accounting for sublimation effects.

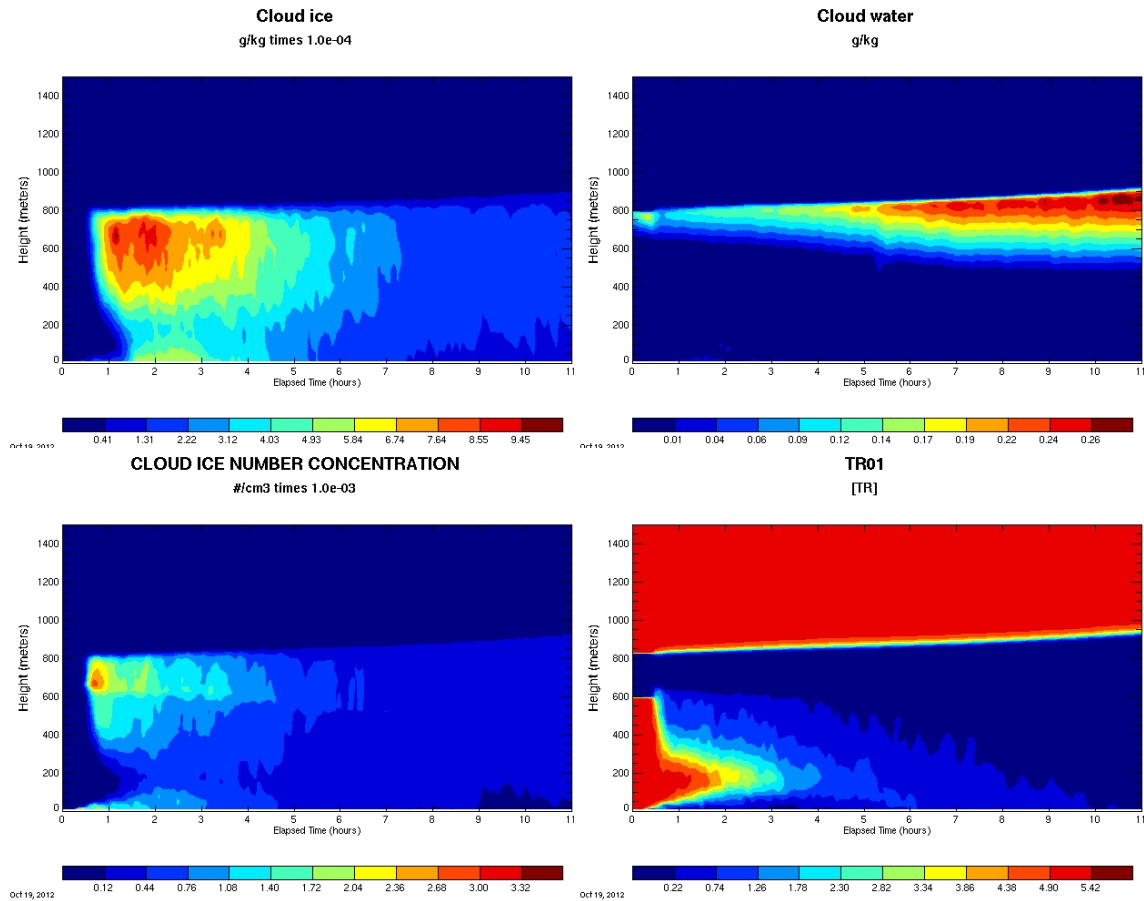


Figure 4.10. Selected SAM output from the prognostic SUB_HI simulation (5.0 L^{-1} IN, IN recycling due to all sublimating ice species). The horizontal axis is time, and the vertical axis is height. All panels as in Fig. 4.7.

When the initial potential IN were set to a factor of 10 increase over the D10 prediction in SUB_HI, but recycling from all hydrometeors was included, the cloud produced more ice than the corresponding SNOSUB run, and persisted for a longer period of time, as was observed with

the same simulations conducted for Flight 16. Interestingly, after about 7 hours, the cloud ice water contents and number concentrations appeared relatively stable, even though ice water contents continued to be much lower than what was observed during the flight, as with all of the Flight 31 simulations. The potential IN field was mostly depleted in the boundary layer by that time, but continued to decline until the end of the simulation, suggesting that persistence of an ice cloud phase past the 12 hour mark was unlikely.

The SUB_LO simulation had ice water contents of about $1.0 \times 10^{-4} \text{ g m}^{-3}$ extending to 8 hours in the simulation, compared to about 6 hours for the SNOSUB simulation, although the initially specified SUB_LO potential IN concentrations were half the amount used in SNOSUB, indicating that sublimation from other ice hydrometeors in addition to snow was important. For the case shown in Fig. 4.10, pristine ice crystal concentrations peaked at $\sim 1.4 \times 10^{-3} \text{ cm}^{-3}$ while peak snow number concentrations were only $\sim 5.0 \times 10^{-4} \text{ cm}^{-3}$.

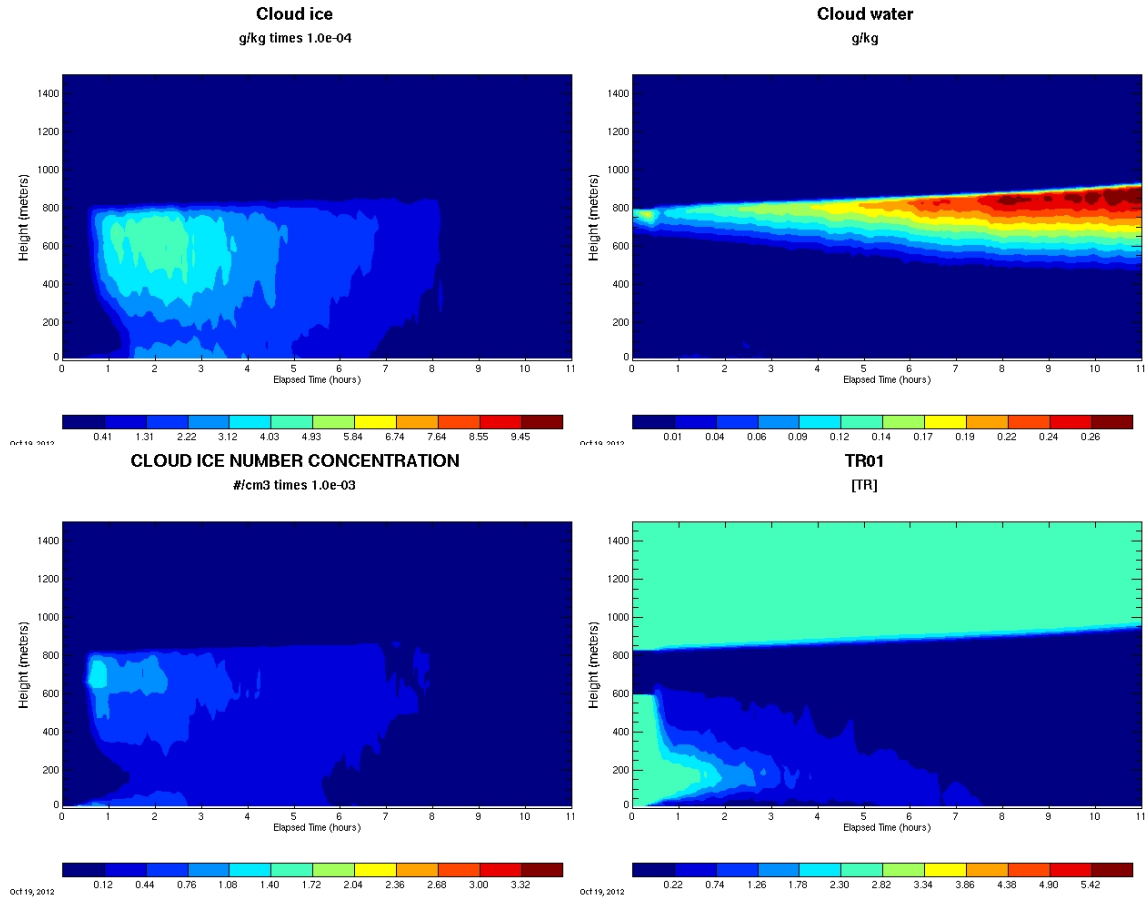


Figure 4.11. Selected SAM output from SUB_LO simulation. The horizontal axis is time, and the vertical axis is height. All panels as in Fig. 4.7.

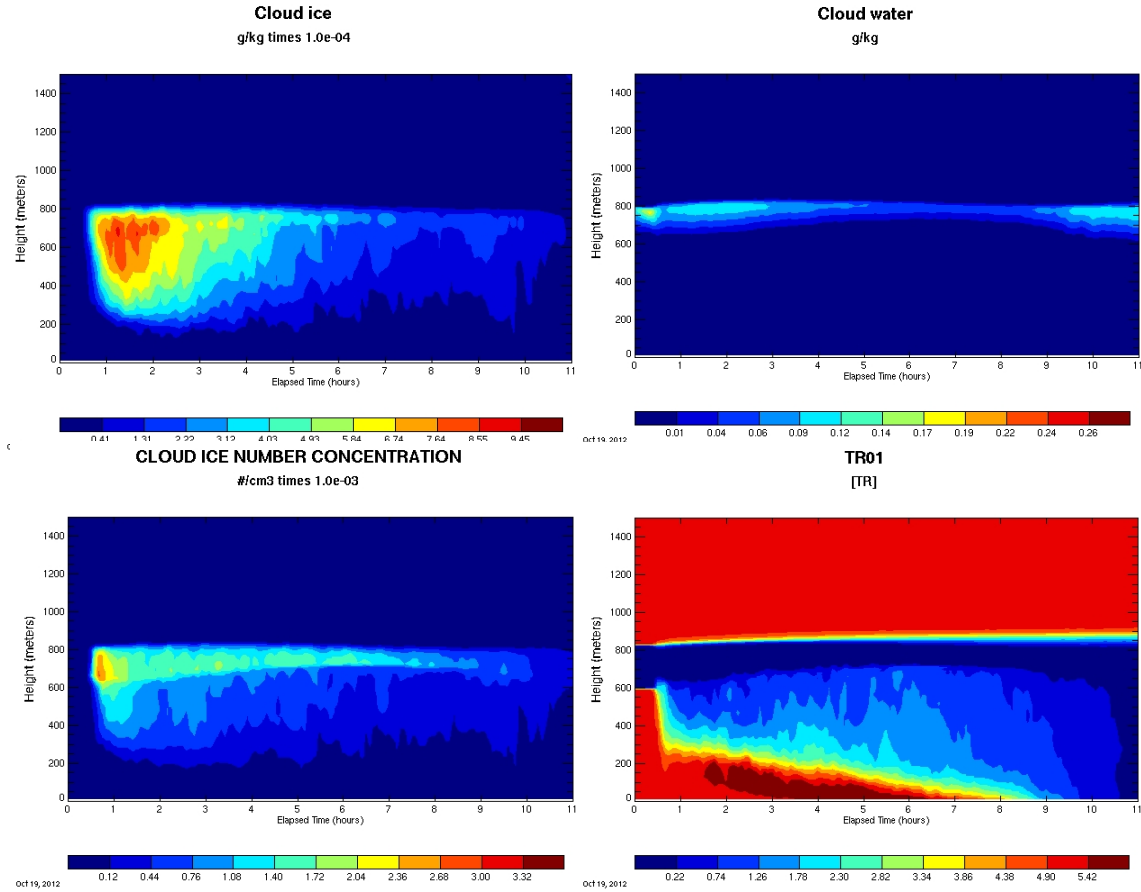


Figure 4.12. Selected SAM output from the prognostic SUB_HI_d simulation ($5.0 \text{ L}^{-1} \text{ IN}$, IN recycling due to all sublimating ice species). The lowest 200m of the atmosphere have been totally dried, resulting in the elimination of the surface fog. All panels as in Fig. 4.7.

The final simulation (SUB_HI_d) was run with the dried profile to enhance further the sublimation of ice in the model. The primary effects were decreased ice water contents on average, but enhanced ice number concentrations in the upper region of the cloud, maintaining concentrations of about $1.0 \times 10^{-3} \text{ cm}^{-3}$ for seven hours, compared to nearly four hours in the non-dried profile. The potential IN field was observed not to deplete as rapidly in previous simulations, primarily due to the drying imposed, which established a larger and more persistent reservoir of potential IN under the cloud than in any other of the simulations. The results from this case show that cloud phase and persistence are very sensitive to the recycling of IN,

particularly since below-cloud IN regenerated close to the surface do not have sufficient time to mix into the supercooled liquid layer to sustain the mixed-phase cloud as they did in the Flight 16 case studies. This is due primarily to potential IN depletion by the fog layer formed near the surface, exhibiting a more profound effect on the simulated clouds for Flight 31 due to the closer proximity to the surface relative to the clouds observed during Flight 16. Additionally, boundary layer relative humidity and moistening due to evaporating precipitation can affect cloud lifetime by modifying the availability of near-surface IN. Figure 4.13 shows individual profiles from several of the simulations for Flight 31 for visual comparison of the individual runs at one time, and the similarity to aircraft observations collected during the flight.

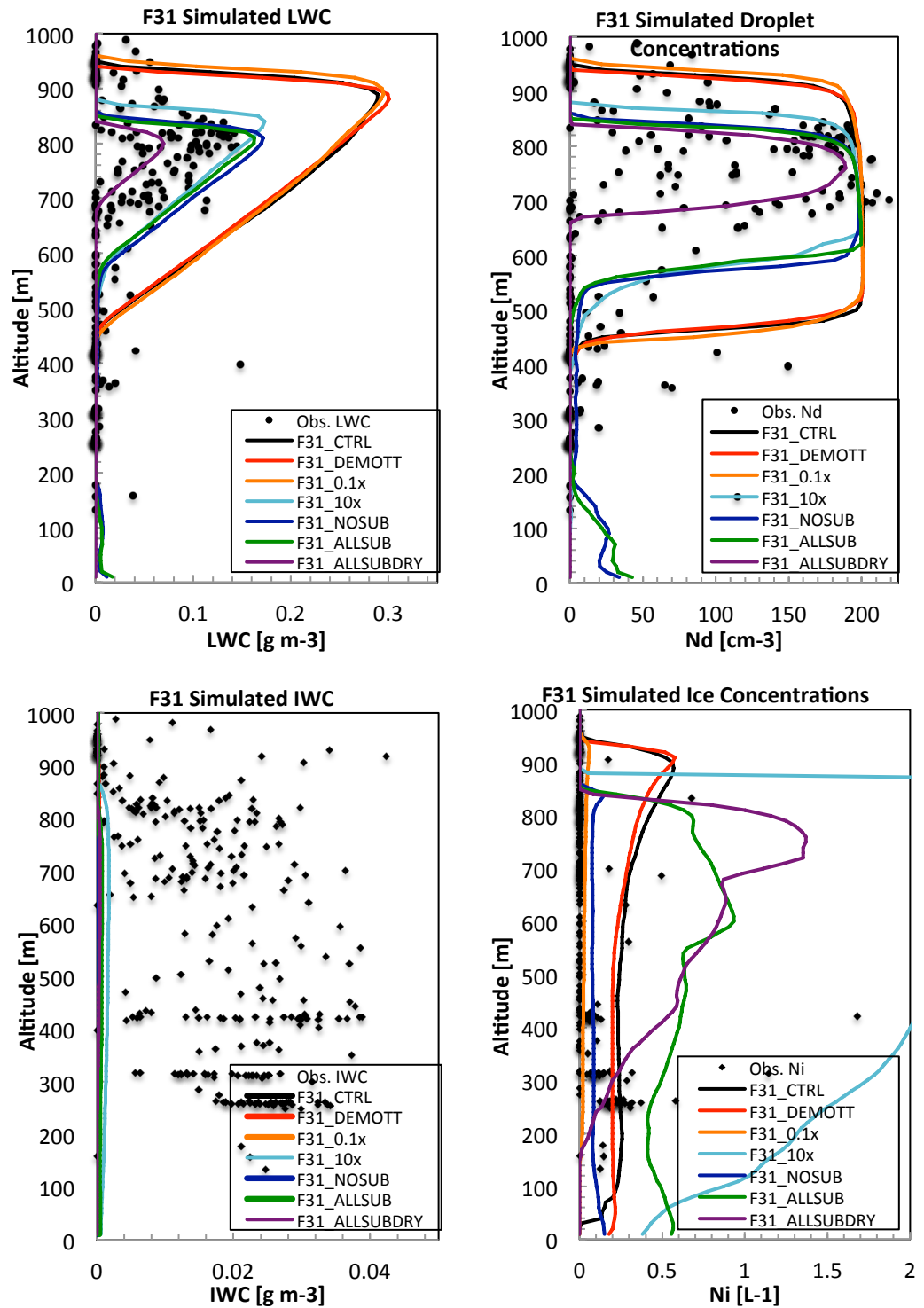


Figure 4.13. Single vertical profiles for selected F31 simulations. Diagnostic simulations are from hour 11, and prognostic simulations from hour 4. Refined aircraft data from G. McFarquhar shown for reference, obtained from DOE-ARM archive.

A prior study that simulated the ISDAC Flight 31 case using the SAM, but in 3-dimensional mode, found that the model tended to overestimate liquid water contents and cloud droplet concentrations, particularly in the upper region of the cloud (*Fan et al.*, 2011). Ice water contents were in better agreement with observations in the uppermost portion of the cloud, but were underestimated closer to the surface. In general, ice water contents in the study were not as poorly estimated as in our simulations. In the study, SAM was set to run with horizontal grid spacing of 100 meters, and vertical spacing of 20 meters, with a 2 second time step, and the model was coupled to a spectral-bin microphysics scheme, with ice nucleation constrained by observed ice number concentrations of about $\sim 0.4 \text{ L}^{-1}$. This difference in microphysical packages most probably explains differences in ice water contents, as the simulations were initialized in the same manner as in this study, however, Fan et al. (2011) cite overestimated fall speeds as a potential culprit, with reduced residence times to permit the growth of ice. They also acknowledge that a near 100% uncertainty in observed ice water contents precludes the possibility of truly knowing whether or not the models underpredicted ice water contents.

Ovchinnikov et al. (2011) also simulated the 26 April case in 3 dimensions with the SAM coupled to the same spectral bin microphysics scheme as in Fan et al. (2011), with a 50 meter horizontal grid spacing, 20 meter vertical spacing, and a 2 second time step. In contrast to our study and to Fan et al., ice microphysical processes were shut off for the first 2 hours of the simulation. Their simulations showed that the cloud exhibited significant sensitivity to the concentration of ice particles; when no ice was present, the liquid layer was able to expand and strengthen in time, but when ice was constrained to values a factor of 4 higher than observed, the liquid layer was depleted continuously, and the cloud nearly glaciated in about 5 hours' simulated time (*Ovchinnikov et al.*, 2011). Consistent with the prognostic simulations presented

here, the cloud liquid layer was observed to begin strengthening after ice production began to decline due to IN consumption.

Despite reasonable predictions of ice number concentrations, ice water contents were generally not well-represented by the SAM for the Flight 31 case study, nor are cloud lifetimes as easily sustained in the prognostic mode as in Flight 16. Liquid water contents were higher than observed, but predicted cloud droplet number concentrations of $\sim 200 \text{ cm}^{-3}$ were slightly higher, but in reasonable agreement with observed values obtained from the DOE-ARM Archive, which differ from values reported in Fan et al. (2011) of around $160 \text{ cm}^{-3} - 175 \text{ cm}^{-3}$. Peak downwelling longwave radiation at the surface between $\sim 267 \text{ W m}^{-2}$ and 269 W m^{-2} severely overestimated observed values for 26 April of $\sim 200 \text{ W m}^{-2}$, following overestimated liquid water content, and representing a potential challenge for attempted climate model simulations for similar events.

Chapter 5

Case Study 3: M-PACE

5.1 Observations

An important contrast to the springtime mixed-phase clouds encountered during the ISDAC campaign, clouds observed in autumn are potentially subject to different aerosol sources and surface fluxes that may fundamentally alter the structure and behavior of the clouds. The ability to correctly model any type of mixed-phase cloud is a crucial test of robustness for the SAM. The following simulations are intended as case studies of a cloud observed on 9 October 2004 during the M-PACE campaign, which also took place near the NSA Barrow research site. The mean concentration of ice nuclei encountered was about $0.16\text{-}0.2\text{ L}^{-1}$, as reported by Fridlind et al. (2007) and Morrison et al. (2008), but several measurements indicated IN concentrations upwards of 10 L^{-1} (Fridlind et al., 2007; Morrison et al., 2008). About 90% of the samples obtained were below the detection limit of the CFDC, and were assumed to be 0, leading to the small mean values.

Analysis of aircraft observations by McFarquhar et al. (2007) showed liquid water contents of $0.193 \pm 0.131\text{ g m}^{-3}$ and ice water contents of $0.025 \pm 0.060\text{ g m}^{-3}$. Average ice number concentrations were measured to be $5.62 \pm 12.10\text{ L}^{-1}$, and thus highly variable and uncertain. Liquid cloud droplet concentrations ranged from 37.8 cm^{-3} to 106.6 cm^{-3} (McFarquhar et al., 2007). All of these values were obtained by averaging values obtained during spirals through the cloud layer. It is important to note that the ice number concentrations

did not exhibit a strong dependence on height within the cloud (McFarquhar *et al.*, 2007), so these averaged values with their large standard deviations will be used as the basis for evaluating each of the SAM simulations. Surface precipitation rates measured over the course of the field campaign reached as high as about 2.5 mm/day, but light snow was experienced nearly every day during the period, and multiple observations of precipitation rates between 0.0 and 1.0 mm/day occurred. The study by Fridlind *et al.* (2007) found that the simulated clouds were relatively insensitive to imposed large-scale forcings, provided that the net effect was a stable cloud top height, as in the observed clouds.

5.2 Model Initialization

Initial profiles of potential temperature, water vapor content, and horizontal winds used for the M-PACE simulations are shown in Figure 5.1, and were derived from a sounding launched at Barrow on 9 October 2004 at 1700Z. The ocean surface possessed less ice coverage, reflected in the prescribed surface sensible and latent heat fluxes of 136.5 W m^{-2} and 107.7 W m^{-2} , respectively. The case-study specific value for $n_{aer,0.5}$ for these simulations was determined to be 3.378 cm^{-3} , representing the cleanest air out of all three cases by a small margin. At cloud top, the predicted concentration of activated ice nuclei was 0.404 L^{-1} . This is double the mean observed concentration, but well within the range over the course of the flight.

Table 5.1. List of M-PACE (9 October 2004) SAM Simulations

| Simulation | Acronym | IN Treatment | Max Initial IN | Activation |
|---------------------------------|----------------|---------------------|---|-------------------|
| Control | CTRL | Diagnostic | T-dependent (500 L ⁻¹ max) | Cooper |
| DeMott | DEMOTT | Diagnostic | 0.404 L ⁻¹ | D10 |
| No Sublimation | NOSUB | Prognostic | 4.04 L ⁻¹ | D10 |
| Snow Sublimation | SNOSUB | Prognostic | 4.04 L ⁻¹ | D10 |
| Snow Sublimation, Dried Profile | SNOSUB_d | Prognostic | 4.04 L ⁻¹ | D10 |
| All Sublimation | SUB_HI | Prognostic | 4.04 L ⁻¹ | D10 |
| All Sublimation, Dried Profile | SUB_HI_d | Prognostic | 4.04 L ⁻¹ | D10 |

A total of ten simulations were conducted following the same conventions set forth in the previous case studies. Results from seven of these runs, as listed in Table 5.1, will be discussed. Results from the sensitivity simulations in diagnostic mode are not presented in this chapter, but showed the same responses as seen in both ISDAC case studies. Additionally, results from the prognostic simulation with a 5x increase over D10-predicted available IN (the equivalent SUB_LO case) are not presented, as this case did not produce any unique information.

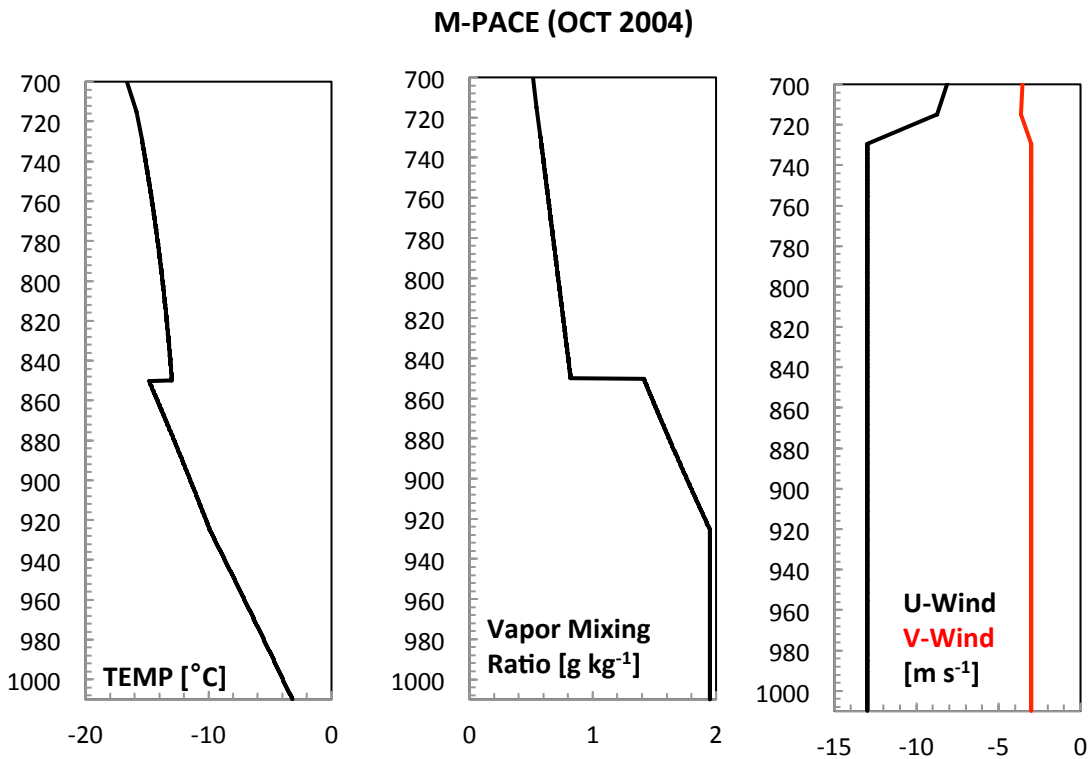


Figure 5.1. Vertical profiles of the initialization data used for M-PACE. SAM is initialized with potential temperature instead of ambient temperature. Also shown are water vapor mixing ratio in g kg^{-1} , and averaged horizontal winds.

5.3 Diagnostic IN Simulations

Figure 5.2 shows the results from the CTRL simulation. CTRL produced a gradually strengthening cloud, indicated by nearly steadily-increasing ice water contents and number concentrations. Near the end of the 12-hour simulation, ice water contents at the top of the cloud were approximately $8.0 \times 10^{-4} \text{ g m}^{-3}$, much lower than observed values. Corresponding ice number concentrations in excess of $1.5 \times 10^{-3} \text{ cm}^{-3}$ were within the range observed. As with the ISDAC Flight 31 CTRL case shown in Chapter 4, the simulations should be carried out to longer times to identify peak ice concentrations and to observe cloud dissipation, if it occurs within a few days of simulated time. Precipitation from the cloud was initially sparse, with measureable

concentrations reaching the ground only after about four hours, and increased to about 0.14 mm/day by the end of the simulation. Peak liquid water contents exceeding 0.36 g m^{-3} are only slightly higher than ($< 1 \text{ g m}^{-3}$) observed values.

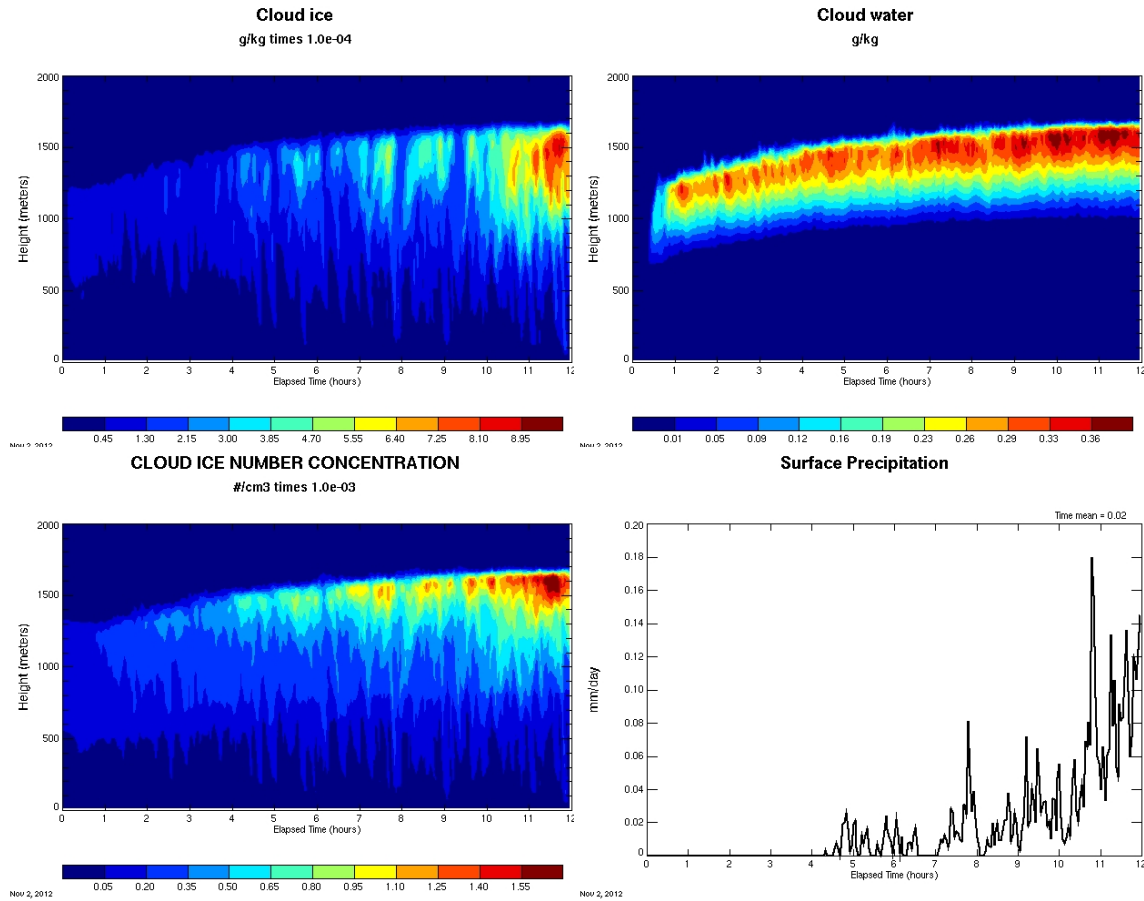


Figure 5.2. Selected SAM output from CTRL. The horizontal axis is time, and the vertical axis is height; all fields were horizontally averaged at each time step to produce these and all subsequent modeled output figures, unless otherwise noted. The upper left panel is cloud ice mass in g/kg, the upper right panel is cloud water mass in g/kg, the lower left panel is cloud ice number concentration in $\#/ \text{cm}^3$, and the lower right panel is surface precipitation in mm/day. Color scales shown are consistent across all diagnostic mode simulations for easy visual comparison.

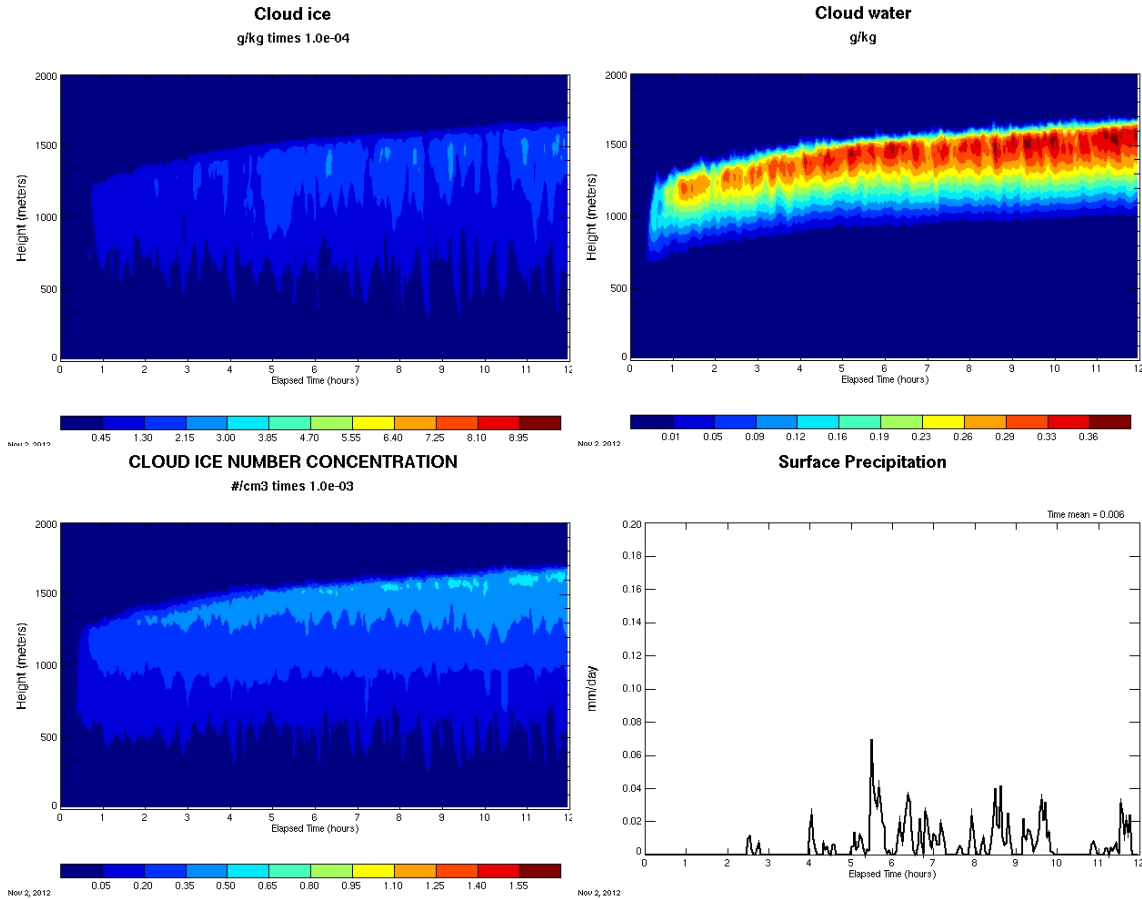


Figure 5.3. Selected SAM output from the DEMOTT simulation. The horizontal axis is time, and the vertical axis is height. All panels as in Fig. 5.2.

The cloud formed in the DEMOTT simulation (Fig. 5.3) generally produced less ice than in CTRL, with cloud top ice water contents of about $2.0 \times 10^{-4} \text{ g m}^{-3}$ and short periods approaching values upwards of $3.0 \times 10^{-4} \text{ g m}^{-3}$, roughly a factor of 3 lower on average than CTRL. Ice number concentrations peaked between $5.0 \times 10^{-4} \text{ cm}^{-3}$ and $6.0 \times 10^{-4} \text{ cm}^{-3}$ near cloud top, also lower than CTRL. These values in the DEMOTT run were lower than the mean of the observations, but remained within the standard deviation. Surface precipitation rates averaged 0.006 mm/day over the 12-hour simulation due to several periods where no ice reached the

surface, and the peak rates near 0.07 mm/day were also lower than in CTRL although not dissimilar from the observations.

5.4 Prognostic IN Simulations

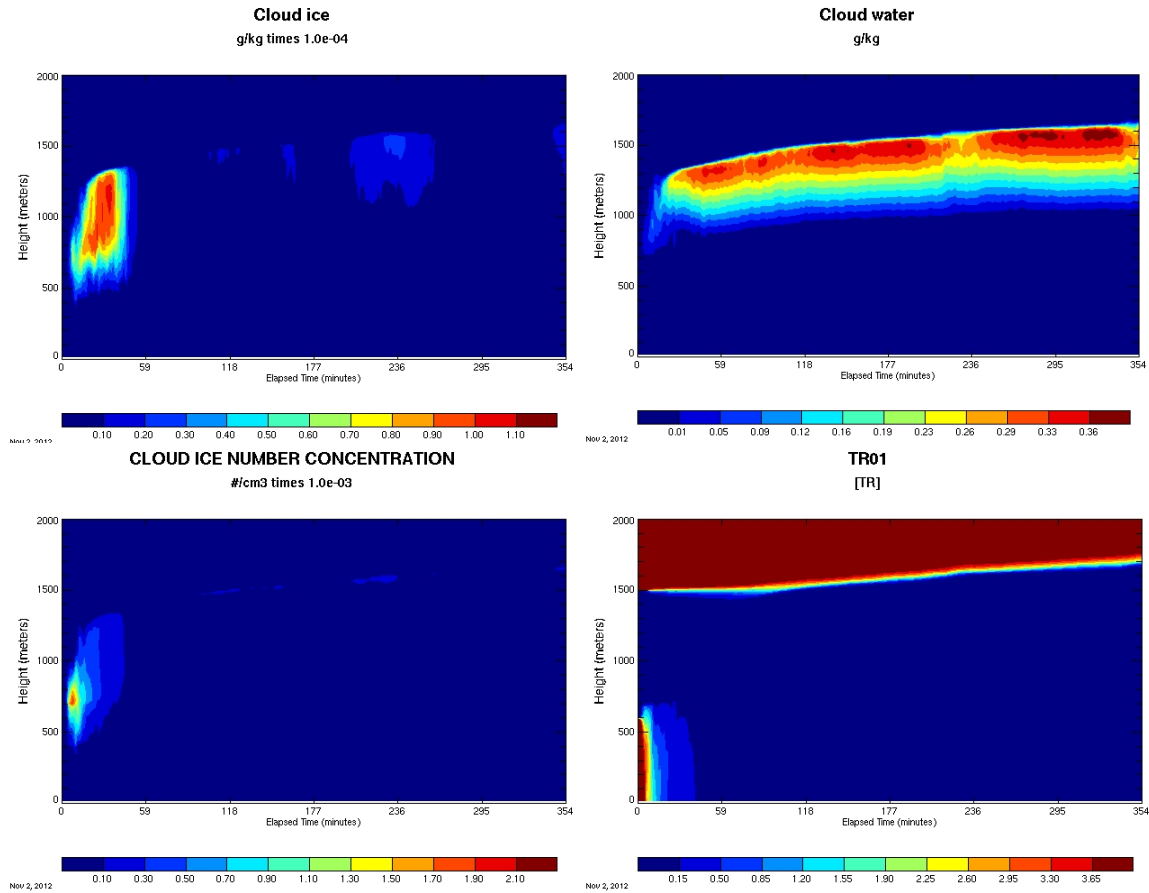


Figure 5.4. Selected SAM output from the prognostic NOSUB simulation ($4.04 \text{ L}^{-1} \text{ IN}$, no IN recycling due to sublimation). The horizontal axis is time, and the vertical axis is height. Upper left panel is cloud ice mass in g/kg, upper right panel is cloud water mass in g/kg, lower left panel is cloud ice number concentration in $\#/cm^3$, and lower right panel is potential IN concentration in $\#/Liter$. The color scales are consistent across the prognostic simulations for easy visual comparison.

Figure 5.4 shows the results obtained when the prognostic scheme was activated, but potential IN recycling due to sublimation was ignored (NOSUB). Note that the time scale of the plots has changed from those presented in other chapters, to just under 6 hours, to enhance the level of detail. The simulated ice phase was short-lived, and the potential IN field showed complete depletion of IN in the lower boundary layer in less than one hour. Peak ice contents of about $1.0 \times 10^{-4} \text{ g m}^{-3}$, a factor of three lower than the DEMOTT simulation, were rapidly reached and extended throughout cloud depth, but rapidly decreased to 0 g m^{-3} , other than for short periods of activity with ice water contents about $2.0 \times 10^{-5} \text{ g m}^{-3}$. Cloud ice number concentrations peaked for a period lasting only minutes at values nearing $1.7 \times 10^{-3} \text{ cm}^{-3}$. Corresponding with the short bursts of further activity, ice number concentrations exhibited periodic increases as the cloud encountered additional potential IN, with concentrations on the order of $3.0 \times 10^{-4} \text{ cm}^{-3}$. These periodic ice concentration increases are similar to concentrations during the DEMOTT run, only about a factor of two lower. Similar to the other prognostic simulations, a liquid cloud was left intact by the end of the simulation, suggesting that ice activation and growth would continue if IN could continuously be supplied at sufficient rates. Peak liquid water contents exceeding 0.36 g m^{-3} remained higher than observed values. Predicted cloud droplet concentrations of 109 cm^{-3} to 124 cm^{-3} also exceeded observed concentrations.

To test whether or not sublimating crystals could have a significant impact on the available supply of potential IN, the model was allowed to return particles if snow sublimated (SNOSUB). Figure 5.5 depicts the results of this change to the model, and shows a nearly identical cloud to the case when sublimation was entirely ignored. The potential IN field depleted quickly, preventing continued ice activation and growth. The primary difference in the simulations was the pulsing behavior of the ice number and mass concentrations and the liquid

water contents; the pulsing is shown to be more pronounced when sublimation effects are included in the model, indicating that the recycling of IN could continue to provide IN to support some periodic ice formation.

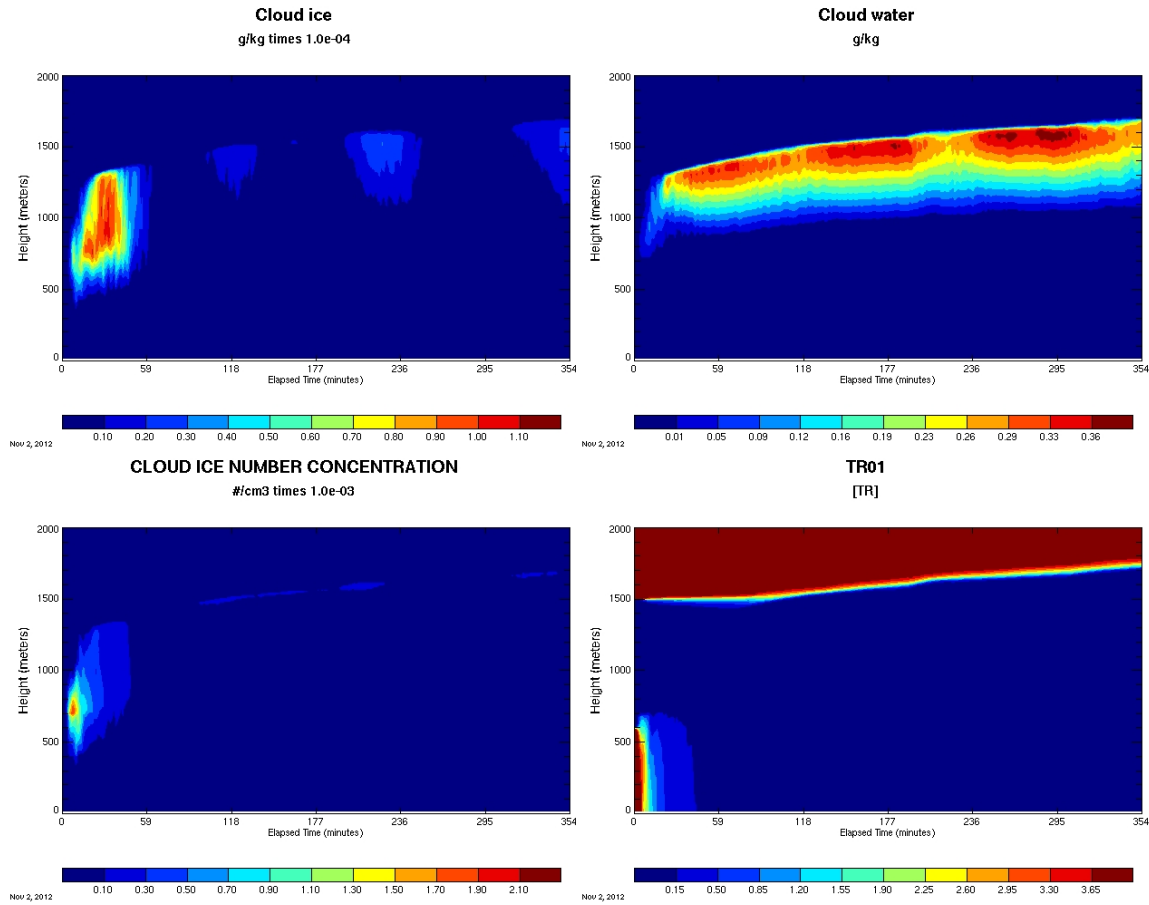


Figure 5.5. Selected SAM output from the prognostic SNOSUB simulation (4.04 L^{-1} IN, IN recycling due to sublimating snow only). The horizontal axis is time, and the vertical axis is height. All panels as in Fig. 5.4.

Particularly for this case study when this behavior was initially observed in the simulated clouds, it was important to attempt to enhance sublimation and consequent potential IN concentrations to see the impacts on the cloud behavior, especially with regards to cloud lifetime. The results of the SNOSUB_d run, shown in Figure 5.6, were surprising. The potential IN field shows that concentrations of near 0.5 L^{-1} were extended at lower levels to almost two hours.

Despite the increase in below-cloud IN, the ice phase near 1 km showed no temporal enhancement, being maintained for only roughly one hour, and exhibiting a shallower depth (less vertical extent below 1 km) relative to the non-dried initial profile.

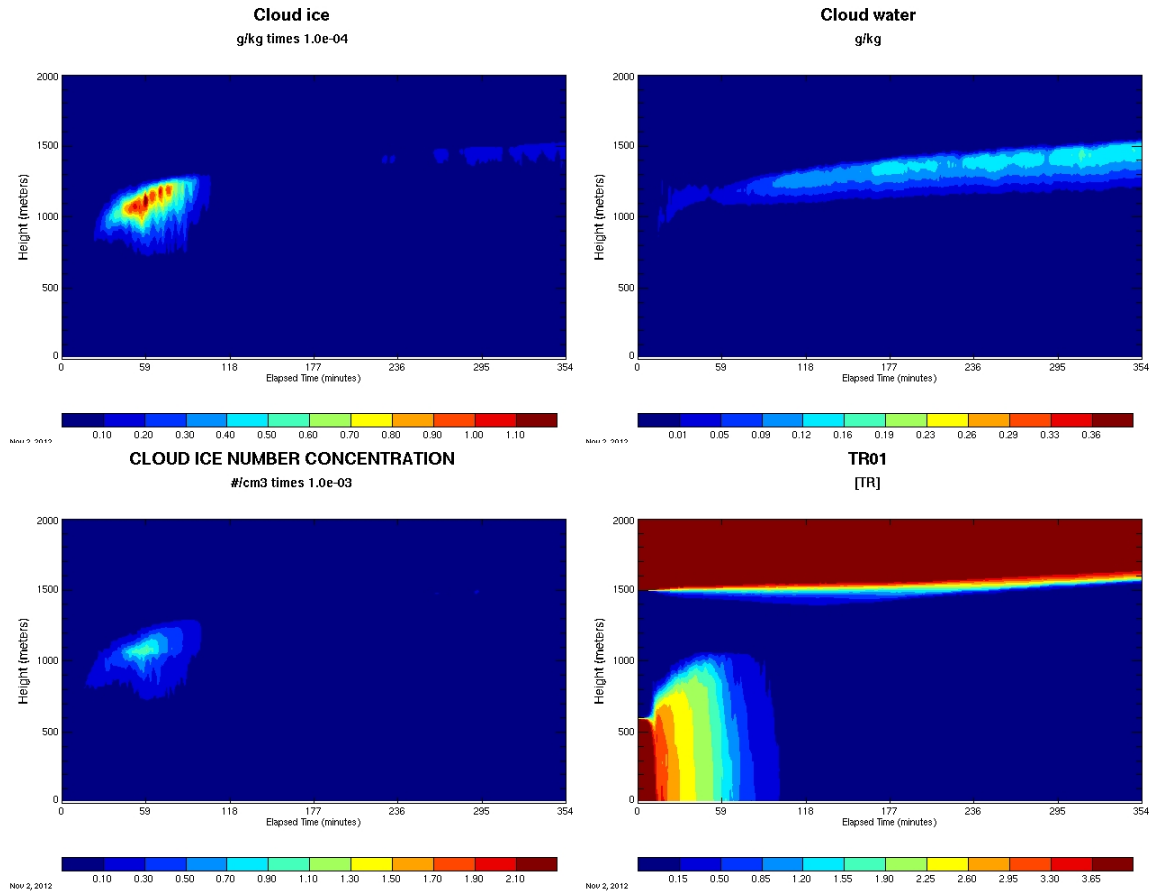


Figure 5.6. Selected SAM output from the prognostic SNOSUB_d simulation ($4.04 \text{ L}^{-1} \text{ IN}$, IN recycling due to sublimating snow only). The lowest 200m of the atmosphere were totally dried in the initialization. All panels as in Fig. 5.4.

Peak ice water contents remained on the order of $1.0 \times 10^{-4} \text{ g m}^{-3}$ as in the previous prognostic simulations, with lower ice number concentrations of nearly $8.0 \times 10^{-4} \text{ cm}^{-3}$, less than half of the peak concentrations in the SNOSUB simulation. Liquid water contents around 0.15 g m^{-3} were also about half those in SNOSUB, but are actually in better agreement with the

observed mean liquid water content. Vapor scavenging in conjunction with overall less available water in the domain due to the imposed drying in the lowest 200 meters is likely responsible.

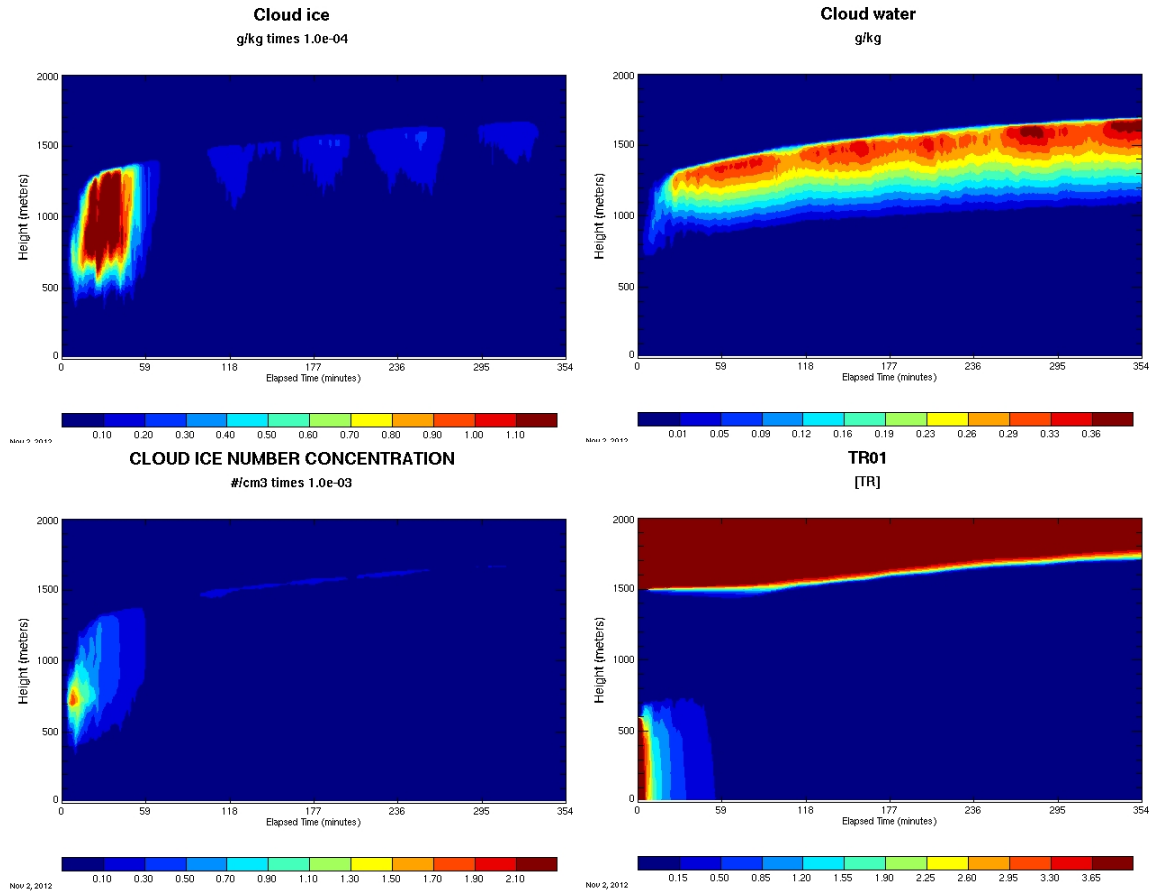


Figure 5.7. Selected SAM output from the prognostic SUB_HI simulation ($4.04 \text{ L}^{-1} \text{ IN}$, IN recycling due to all sublimating ice species). The horizontal axis is time, and the vertical axis is height. All panels as in Fig. 5.4.

When the model was allowed to account for all sublimating ice crystals (SUB_HI), initial ice growth was found to be stronger, shown in Figure 5.7, with cloud ice water contents approaching $1.5 \times 10^{-4} \text{ g m}^{-3}$, a 50% increase over the simulations where only snow sublimation recycled IN. Ice number concentrations, however, were largely unchanged in the same period of time. The effective lifetime of the cloud ice phase remained at around 1 hour.

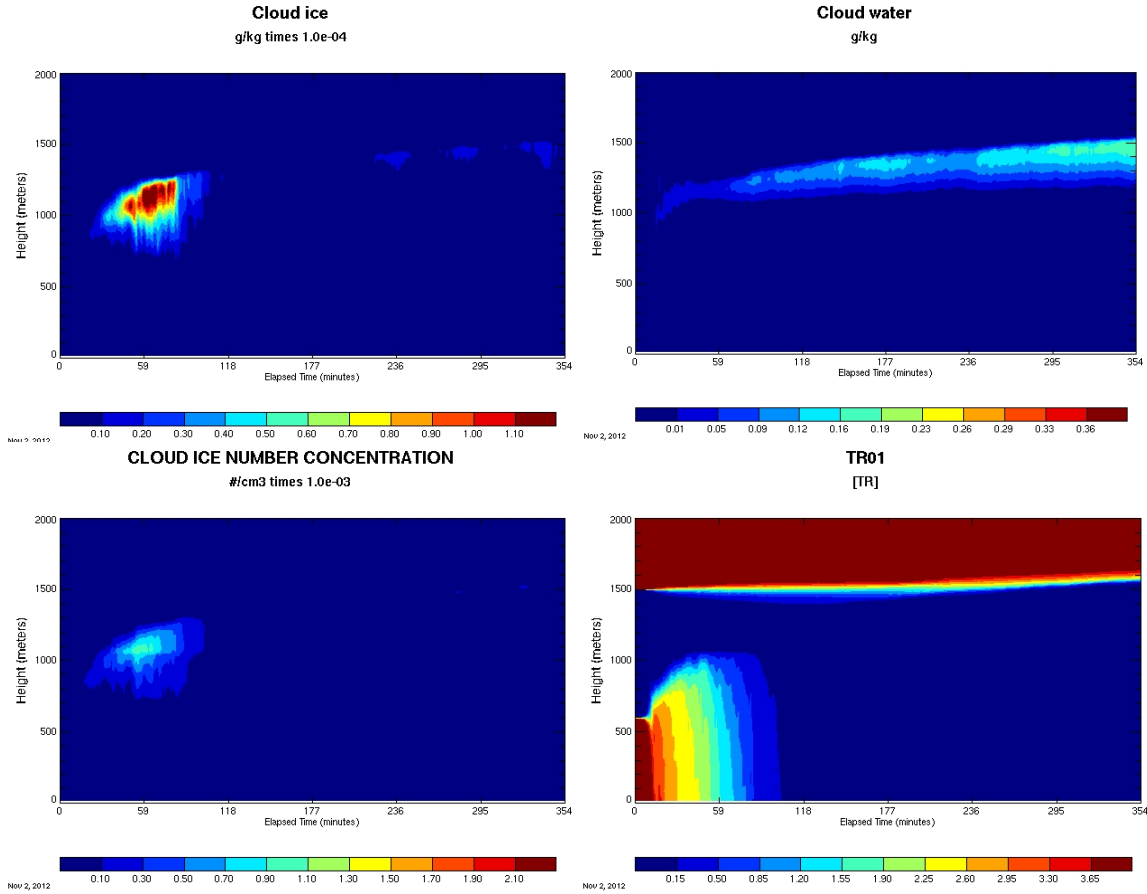


Figure 5.8. Selected SAM output from the prognostic SUB_HI_d simulation (4.04 L^{-1} IN, IN recycling due to all sublimating ice species). The lowest 200m of the atmosphere were totally dried in the initialization. All panels as in Fig. 5.4.

Pulsing variation in cloud ice mass concentrations near the top of the cloud became more evident, but with similar ice and number concentrations as in the other simulations. Potential IN particles continued to be depleted below cloud within the first hour of the simulation, suggesting that ice nucleation near cloud top was primarily initiated by IN entrained from above cloud, as in the other prognostic-IN simulations.

Even after incorporation of all sublimating ice crystals, the simulation with the dried profile (SUB_HI_d), depicted in Figure 5.8, showed similar characteristics to the simulation with a dried profile in which IN recycling only from snow was considered (SNOSUB_d, Fig. 5.6).

The primary differences between these two simulations were a marginally extended ice-phase lifetime when all sublimating ice was considered, and increases in ice water contents to nearly $1.5 \times 10^{-4} \text{ g m}^{-3}$ for a short period of time. The pulsing in ice mass concentration was diminished, as in SNOSUB_d. Again, liquid water contents of about 0.18 g m^{-3} were in good agreement with the observed mean. The reduction in cloud water mass was responsible for a decrease in downward longwave radiation at the surface of 5 W m^{-2} to 9 W m^{-2} from peak values of $\sim 280 \text{ W m}^{-2}$ seen in both diagnostic simulations, an underestimation of the observed radiative flux averaging $\sim 280 \text{ W m}^{-2}$.

Relative to the non-dried profile in which all sublimating ice was considered (SUB_HI, Fig. 5.7), peak ice water contents in SUB_HI_d were similar, but ice number concentrations decreased to about $8.0 \times 10^{-4} \text{ cm}^{-3}$. This same behavior was observed in the corresponding pair of simulations that considered only snow sublimation regeneration of IN. In general, the results of these prognostic simulations indicate that for this M-PACE case study, sublimating ice may serve to increase ice mass in the cloud as vapor re-deposits onto pre-formed crystals, but cannot aid in enhancing cloud lifetimes by replenishing IN, contradicting multiple previous studies and thus likely representing a fault with the model, or with our initialization. Rapid activation serves to deplete the boundary layer of IN within the first hour of the simulations, so additional IN may need to be introduced into the supercooled liquid layer at rates faster than the simulated entrainment and below-cloud turbulence rates can provide them. Additionally, when the lowest 200 meters were dried, no observable extension in the cloud occurred, and it was noted the boundary layer re-humidified at a faster rate than seen in either of the ISDAC simulations, effectively shutting down the sublimation process responsible for recycling the IN.

More previous studies have been conducted for M-PACE than for either of the ISDAC days, most likely due to the fact that M-PACE occurred in 2004, versus 2008. A 2007 study by Prenni et al. (2007) found that whereas simulations from a high-detail model initialized with a common heterogeneous ice formation parameterization produced clouds that rapidly glaciated, simulations initialized with prescribed M-PACE IN concentrations resulted in persistent, mixed-phase clouds featuring a resilient liquid layer at cloud top. In contrast with our results, the Regional Atmospheric Modeling System (RAMS) utilized in the Prenni et al. (2007) study also predicted reasonable ice water contents in the simulated cloud. Furthermore, the study concluded that preventing depletion of IN through precipitation led to rapid glaciation of the cloud; removal of IN through precipitation processes is important for sustaining the cloud lifetime, in agreement with the Harrington and Olsson study from 2001. Another study from 2007 conducted by Fridlind et al. simulated a single-layer, mixed-phase Arctic stratus cloud representative of M-PACE. Consistent with other studies, they found that observed ice nuclei concentrations do not result in accurate simulated ice number concentrations, but multiplicative processes are unlikely to explain the discrepancy. To predict reasonable ice mass, the simulations required IN concentrations in the free troposphere several orders of magnitude greater than observed, or a constant surface flux of IN from the ocean of roughly $\sim 6 \text{ L}^{-1}$ (Fridlind et al., 2007). Similar responses in simulations of mixed-phase Arctic stratus, resulting from rapid depletion of IN, have since been shown (Fridlind et al., 2012). Reducing hydrometeor fall speeds, and thus increasing the amount of time ice crystals spent in a growth regime, was also found to increase cloud ice mass, but number concentrations still remained a factor of two below observed values (Fridlind et al., 2007).

Also published in 2009 was a model intercomparison study simulating a single layer mixed-phase cloud case for M-PACE which compared nine different cloud-resolving models (CRMs), as well as several other single-column models (*Klein et al.*, 2009). The SAM was included as part of the intercomparison, and it was found that variations between all models were sometimes large. In general, models underpredicted liquid water path and this behavior was attributed to interactions between liquid and ice microphysics schemes. In general, improvements in ice representation in Arctic mixed-phase clouds was observed with increasingly complex microphysics schemes, with two-moment schemes performing generally much better than single-moment, temperature dependent treatments. The study found that predicted ice crystal number concentrations varied over five orders of magnitude, and suggested that ice microphysical treatments in particular were crucial when attempting to simulate Arctic mixed-phase clouds.

Morrison et al. (2008) conducted simulations from M-PACE data using the Mesoscale model (MM5) with the then-newly-developed double-moment microphysical scheme (*Morrison et al.*, 2005). The study concluded that while the model reasonably predicted liquid microphysical properties in agreement with observations, the model underpredicted ice crystal number concentrations, similar to this study in most simulations. It was determined that large differences between observed IN concentrations and ice number concentrations implicated additional ice formation processes in the real cloud which were not accounted for in the model. In addition, downwelling longwave radiative fluxes at the surface were overestimated by as much as 20 W m^{-2} (*Morrison et al.*, 2008).

Luo et al. (2008) concluded that the Morrison two-moment microphysical scheme generally performed better than a single-moment scheme in a cloud-resolving model, but

underestimated ice crystal number concentrations, conclusions later replicated in the Weather Research Forecast (WRF) model (*Solomon et al.*, 2009). When IN were increased by a factor of 20, predicted ice number concentrations were more in agreement with observations, but the simulated cloud glaciated, followed by complete dissipation (*Luo et al.*, 2008). Strong sensitivity to ambient IN concentrations has been simulated by other groups (*Avramov et al.*, 2010).

The most recent study simulated both ISDAC and M-PACE cases, similar to this study. As discussed previously, the study utilized the SAM coupled with a spectral bin microphysical scheme (*Fan et al.*, 2009). Unlike most previous studies, the Fan et al. study implemented a prognostic scheme for ice nucleation and they accounted for the effects of sublimating crystals. Like Fridlind et al. (2007), the study tested two hypothetical mechanisms responsible for enhancing ice crystal concentrations, freezing activation of droplet evaporation residues, and contact freezing inside out as drops evaporate (*Fan et al.*, 2009). It was found that simulations which included either of these unproven mechanisms increased ice concentrations by a factor of 10-15 over simulations not including them and were in better agreement with observations. They also concluded that sublimation effects, primarily from below-cloud regions contributed greatly to the ice crystal formation within the cloud, producing ice concentrations 2-3 times higher, and noted that the clouds exhibited extreme sensitivity to IN in early formative stages, such that high IN could cause rapid ice formation, depleting the liquid layer (*Fan et al.*, 2009). This sensitivity likely contributes to the responses observed in our prognostic simulations. We also observed slight increases in ice crystal number concentration when allowing for sublimation effects.

Chapter 6

Summary and Future Work

This work seeks to improve understanding of the processes that maintain long-lived arctic mixed-phase boundary layer stratus clouds. Prior work has demonstrated the high sensitivity of cloud lifetime to moisture availability and to the levels of cloud nucleating particles (*Morrison et al.*, 2011), but the precise way the complex interactions play out in different case studies is not yet well understood. Here, we focus particularly on the role of ice nuclei in creating and maintaining ice in such clouds, using a large-eddy framework with two-moment cloud microphysics to model cloud development and evolution. We also applied the ice nucleation parameterization proposed by DeMott et al. (2010; D10) to constrain the total available potential IN, based on aerosol size distribution observations. The parameterization reproduced measured IN number concentrations during the ISDAC project within measurement uncertainties and standard deviations. The lack of a tight observational constraint on IN in individual cases and historical evidence that observed IN may not be sufficient to explain ice concentrations in Arctic clouds (e.g., missing primary or secondary ice formation mechanisms) led us to vary the predicted IN concentrations by factors of 5-10 to explore the impact on the simulated clouds.

Thirty high-resolution simulations were presented in this study, representing three unique case-studies of spring and fall season clouds. The D10 parameterization successfully produced long-lived mixed-phase stratus clouds that either reached a steady-state condition, or continued to strengthen over the course of the 12-hour simulation. Peak liquid water contents for all simulated clouds while in diagnostic mode ranged from 0.25-0.35 g m⁻³, in good agreement with

ISDAC Flight 16, but higher than typical observed liquid water contents for Flight 31 and M-PACE.

In the case of ISDAC Flight 16 and M-PACE, the D10 parameterization predicted less ice in the cloud than the control (CTRL) simulation using the temperature-dependent but aerosol concentration-independent scheme of Cooper et al. (1984), whereas D10 predicted similar ice mass and concentrations as the CTRL for ISDAC Flight 31. In both ISDAC simulations, the CTRL and D10 simulations predicted reasonable ice number concentrations in agreement with observations. Both the CTRL and D10 diagnostic simulations also predicted ice number concentrations in reasonable agreement with typical values encountered during the M-PACE campaign. In general, using the D10 parameterization constrained by observed total aerosol distributions, reasonable predictions of available IN were made, indicating that linking ice formation to aerosol in the model produces reasonable ice number concentrations and represents a simple, but more realistic treatment for available ice nuclei. In all diagnostic-IN cases, the parameterization could access an essentially unlimited supply of potential ice nuclei, representing a potentially physically unrealistic situation. The simulations represent actual cloud processes only if IN can be supplied to the cloud layer at similar rates than they are removed by nucleation and subsequent fallout of ice hydrometeors. Typically, downwelling longwave radiative fluxes at the surface scaled with predicted peak cloud liquid water contents, and predicted values agreed with observations for ISDAC Flight 16 and M-PACE simulations. When predicted liquid water contents were much higher than observed values, downwelling longwave radiation at the surface was also overestimated, as in ISDAC Flight 31.

In order to investigate a more realistic approach to modeling mixed-phase Arctic clouds, we developed a prognostic scheme, imposing a finite budget on the available ice nuclei. This

prognostic scheme was tested in multiple simulations, ranging from a depletion only scheme, where IN recycling due to sublimation was entirely ignored, to simulations where all sublimating ice crystals returned IN particles to the domain, and additionally with the lowest 200 meters of the boundary completely dried of water to enhance sublimation. When running the model under the prognostic scheme, it was shown in all cases that the model could not sustain clouds for time-scales representative of the longest observed lifetimes. In consideration of the efficacy of the D10 parameterization, and in contrast to a previous study, we found that Flight 16 was as difficult to simulate realistically on the basis of available ice nuclei as for the other cases. Avramov et al. (2012) was able to reasonably simulate the cloud observed during Flight 16 by taking as representative a short period of high (>10 per liter) IN concentration measurements made onboard the aircraft during the flight period. Avramov et al. reasoned that available IN under mixed-phase conditions might have been even higher because the IN measurements were made at substantial water subsaturation. However, these IN concentration measurements were made several degrees colder than the observed cloud temperature, and they are high-valued outliers compared to the relation between IN and aerosol concentrations measured for CFDC processing under mixed-phase conditions during the ISDAC project as a whole, a relation which was shown here to be consistent (average values and variability) with the D10 parameterization. Additionally, the values are inconsistently high compared to IN concentrations measured on other flights on this day with similar aerosol concentrations present. In hindsight, these facts suggest that the values used in Avramov et al. (2012) to infer closure between IN and ice in clouds were potentially suspect for measurement artifacts, and may not have been representative of the average IN concentrations available to the cloud system on this day.

Due to the complex nature of these cloud systems, differences in environmental conditions can strongly influence the clouds. The spring-time ISDAC cloud formed during a period in which sea ice extent was decreasing, potentially increasing fluxes of sensible and latent heat into the boundary layer, fundamentally altering cloud development. M-PACE, on the other hand, sampled clouds from late September through late October, when sea ice is on the rise after reaching minimum extent of coverage in mid-September, and surface fluxes of sensible and latent heats might reasonably be expected to be higher, but decreasing during the study time period. Assumed sensible and latent heat fluxes of 0 W m^{-2} and 10 W m^{-2} used due to observed surface fluxes not being readily available for the two ISDAC case studies were markedly lower than those used for M-PACE (136.5 W m^{-2} and 107.7 W m^{-2} , respectively). Simulations initialized with these assumed values possibly created errors preventing observation of the effects of varying surface fluxes. The prognostic scheme was best at sustaining the case derived from Flight 16, and worst at sustaining the M-PACE cloud, suggesting that there are fundamental differences between the three cases. These differences are particularly noticed between ISDAC and M-PACE, and this may implicate a seasonal pattern, but additional studies are necessary.

In both ISDAC case studies, incorporation of IN recycling due to sublimation was shown to extend cloud lifetimes past what could be accomplished without including sublimation, suggesting that recycled IN may contribute to cloud longevity in reality. Interestingly, in our study the lifetime of the M-PACE cloud could not be appreciably extended regardless of sublimation, indicating an issue with the initialization, or the model itself. For each case-study, the prognostic simulations including all forms of sublimation and an initial potential IN concentration a factor of 10 over what was predicted by equation 2.1 predicted peak ice water contents and number concentrations 2-4 times higher than seen in the diagnostic D10

simulations. These peaks always occurred early in the simulations, and ice water contents and number concentrations almost always steadily decreased afterwards. Despite the increased ice water contents, in all simulations the predicted ice water contents remained several orders of magnitude below observed values. This may indicate an issue with assumptions used in the microphysical treatment of ice, such as the use of spheres with constant, prescribed density. Future simulations should investigate the role of ice crystal growth habits and rates, as well as density variations and fall speeds. The higher peak ice number concentrations in these simulations brought simulated ice numbers closer to those observed during ISDAC Flight 31. For M-PACE, the simulated ice number concentrations remained well within the range of observed values. In the case of ISDAC Flight 16, these peak ice concentration values were only slightly higher than those observed on the aircraft.

Since reproduction of cloud ice concentrations required elevating IN number concentrations by 5-10 times in nearly all cases, it is concluded that understanding of ice formation processes in Arctic mixed phase clouds remains relatively poorly constrained. Inadequacies of present measurements of IN activation properties remain as one potential explanation for discrepancies. IN measurements have been shown to be adequate for describing first ice formation in cold orographic wave clouds (Eidhammer et al. 2010; Field et al. 2012). However, significant unexplained variation of up to five times remains in IN concentration dependence on aerosol concentrations in the DM10 parameterization, with indications that DM10 is biased low at some temperatures when mineral dust particles are the dominant IN source (Niemand et al. 2012). This low bias seems to occur at temperatures colder than present in any of the simulations in this study. A separate low bias in IN measurements with the CFDC could be present based on the need to achieve higher water supersaturations for full IN activation

via immersion freezing in laboratory studies than it is possible to use operationally (Petters et al. 2009; DeMott et al. 2011). Additional potential time dependence of ice nucleation via immersion freezing, unresolved in present measurements, could explain some underestimation of IN concentrations available for the long lifetimes and extent of Arctic stratus, but seems unlikely to provide the level of correction required to sustain observed ice concentrations. No physical evidence yet exists for other unmeasured potential IN mechanisms hypothesized by Fridlind et al. (2007), and no missing secondary ice formation processes of relevance have yet been proposed. It therefore seems unlikely that simply obtaining additional IN measurements in the Arctic will solve these questions, and absent any additional proof that IN are poorly constrained via specialized new measurement methods, attention should likely turn to better constraining IN recycling due to sub-cloud sublimation and blowing snow, and inadequate model treatment of entrainment, mixing, and microphysical processes as other possible sources of the inability to close understanding of ice formation in Arctic clouds.

In sum, the prognostic scheme shows promise despite its simplicity. There is a clear issue with how to initialize IN entry into clouds in all simulations, as placing them in or too close to the cloud-forming layer can artificially deplete IN numbers too rapidly to ensure representative simulations of IN entraining into clouds other than at the edge of the cloud system. The case studies suggest that consideration of IN regeneration in sublimating frozen hydrometeors can be an important mechanism. In reality, additional IN are subject to long-range transport into the Arctic and may also be introduced by surface fluxes of IN and blowing snow into the boundary layer. Neither of these processes are represented by the model in its present state, but can be added in future simulations, if observations exist to quantify them accurately.

As long as sufficient water vapor is present to maintain the supercooled liquid layer, and IN can be continuously supplied to this region, it is not unreasonable to expect the SAM to maintain long lifetimes of the simulated mixed-phase clouds. However, local and remote sources of ice nuclei must be measured for the Arctic in order to reliably quantify these sources and code them into the model; only limited data exist at present. Additional observations of aerosol transport into high latitudes, and of typical ice nuclei concentrations, are needed for the Arctic region in order to better simulate heterogeneous ice formation in mixed-phase boundary layer clouds. Furthermore, accurate representation of mixed-phase boundary layer clouds in the Arctic is essential for increasing the reliability of climate simulations, the primary means of determining the characteristics of future climates, and for exploring mitigation options. To support these efforts, additional and more accurate measurements of cloud properties are needed. Recently suggested were several critical improvements to instrumentation which would improve the ability to observe and quantify mixed-phase cloud properties (*McFarquhar et al.*, 2011). These improvements focus on instrumentation to measure small ice crystals, aerosol properties, and radiative fluxes. Additionally, ground-based remote-sensing instrumentation, which is often easier to implement over long-term measurement periods, has been shown to perform poorly when characterizing liquid microphysical properties, although attempts to improve measurements have shown promise (*Shupe et al.*, 2008b). More accurate measurements will enable better assessment of modeling and predictive capabilities, and ultimately should improve simulations.

References

- Abdul-Razzak, H. and S. J. Ghan (2000), A parameterization of aerosol activation 2. Multiple aerosol types, *Journal of Geophysical Research-Atmospheres*, 105, 6837-6844.
- Archuleta, C. M., P. J. DeMott, S. M. Kreidenweis (2005), Ice nucleation by surrogates for atmospheric mineral dust and mineral dust/sulfate particles at cirrus temperatures, *Atmospheric Chemistry and Physics Discussions*, 5, 3391-3436.
- Avramov, A., and J. Y. Harrington (2010), Influence of parameterized ice habit on simulated mixed phase Arctic clouds, *Journal of Geophysical Research-Atmospheres*, 115.
- Avramov, A., et al. (2011), Toward ice formation closure in Arctic mixed-phase boundary layer clouds during ISDAC, *Journal of Geophysical Research*, 116(D00T08), 25.
- Cooper, W. A. (1986), Ice initiation in natural clouds. Precipitation Enhancement: A Scientific Challenge, *Meteorological Monograph*, No. 43, Amer. Meteor. Soc., 29–32.
- Curry, J. A., W. B. Rossow, D. Randall, and J. L. Schramm (1996), Overview of Arctic cloud and radiation characteristics, *Journal of Climate*, 9(8), 1731-1764.
- DeMott, P. J., A. J. Prenni, X. Liu, S. M. Kreidenweis, M. D. Petters, C. H. Twohy, M. S. Richardson, T. Eidhammer, and D. C. Rogers (2010), Predicting global atmospheric ice nuclei distributions and their impacts on climate, *Proceedings of the National Academy of Sciences of the United States of America*, 107(25), 11217-11222.
- DeMott, P. J., K. Sassen, M. R. Poellot, D. Baumgardner, D. C. Rogers, S. D. Brooks, A. J. Prenni, S. M. Kreidenweis (2003), African dust aerosols as atmospheric ice nuclei, *Geophysical Research Letters*, 30(14).
- Fan, J. W., M. Ovtchinnikov, J. M. Comstock, S. A. McFarlane, and A. Khain (2009), Ice formation in Arctic mixed-phase clouds: Insights from a 3-D cloud-resolving model with size-resolved aerosol and cloud microphysics, *Journal of Geophysical Research-Atmospheres*, 114, 21.
- Fan, J. W., S. Ghan, M. Ovchinnikov, X. H. Liu, P. J. Rasch, and A. Korolev (2011), Representation of Arctic mixed-phase clouds and the Wegener-Bergeron-Findeisen process in climate models: Perspectives from a cloud-resolving study, *Journal of Geophysical Research-Atmospheres*, 116.
- Fridlind, A. M., A. S. Ackerman, G. McFarquhar, G. Zhang, M. R. Poellot, P. J. DeMott, A. J. Prenni, and A. J. Heymsfield (2007), Ice properties of single-layer stratocumulus during the Mixed-Phase Arctic Cloud Experiment: 2. Model results, *Journal of Geophysical Research-Atmospheres*, 112(D24), 25.

Fridlind, A. M., B. van Dierenhoven, A. S. Ackerman, A. Avramov, A. Mrowiec, H. Morrison, P. Zuidema, and M. D. Shupe (2012), A FIRE-ACE/SHEBA Case Study of Mixed-Phase Arctic Boundary Layer Clouds: Entrainment Rate Limitations on Rapid Primary Ice Nucleation Processes, *Journal of the Atmospheric Sciences*, 69(1), 365-389.

Garrett, T. J., and C. F. Zhao (2006), Increased Arctic cloud longwave emissivity associated with pollution from mid-latitudes, *Nature*, 440(7085), 787-789.

Garrett, T. J., M. M. Maestas, S. K. Krueger, and C. T. Schmidt (2009), Acceleration by aerosol of a radiative-thermodynamic cloud feedback influencing Arctic surface warming, *Geophysical Research Letters*, 36.

Harrington, J. Y., P. Q. Olsson (2001), On the potential influence of ice nuclei on surface-forced marine stratocumulus cloud dynamics, *Journal of Geophysical Research*, 106, 27,473-27,484.

Harrington, J. Y., T. Reisin, W. R. Cotton, and S. M. Kreidenweis (1999), Cloud resolving simulations of Arctic stratus - Part II: Transition-season clouds, *Atmospheric Research*, 51(1), 45-75.

Intrieri, J. M., M. D. Shupe, T. Uttal, and B. J. McCarty (2002), An annual cycle of Arctic cloud characteristics observed by radar and lidar at SHEBA, *Journal of Geophysical Research-Oceans*, 107(C10).

Jackson, R. C., G. M. McFarquhar, A. V. Korolev, M. E. Earle, P. S. K. Liu, R. P. Lawson, S. Brooks, M. Wolde, A. Laskin, M. Freer (2012), The dependence of ice microphysics on aerosol concentration in arctic mixed-phase stratus clouds during ISDAC and M-PACE, *Journal of Geophysical Research*, 117.

Jiang, H. L., W. R. Cotton, J. O. Pinto, J. A. Curry, and M. J. Weissbluth (2000), Cloud resolving simulations of mixed-phase Arctic stratus observed during BASE: Sensitivity to concentration of ice crystals and large-scale heat and moisture advection, *Journal of the Atmospheric Sciences*, 57(13), 2105-2117.

Kay, J. E., and A. Gettelman (2009), Cloud influence on and response to seasonal Arctic sea ice loss, *Journal of Geophysical Research-Atmospheres*, 114.

Khairoutdinov, M. F., and D. A. Randall (2003), Cloud resolving modeling of the ARM summer 1997 IOP: Model formulation, results, uncertainties, and sensitivities, *Journal of the Atmospheric Sciences*, 60(4), 607-625.

Khairoutdinov, M. F., D. A. Randall, and Ams (2002), *A cloud resolving model as a cloud parameterization in a GCM: Preliminary results*, 173-174 pp., Amer Meteorological Society, Boston.

- Klein, S. A., et al. (2009), Intercomparison of model simulations of mixed-phase clouds observed during the ARM Mixed-Phase Arctic Cloud Experiment. I: Single-layer cloud, *Quarterly Journal of the Royal Meteorological Society*, 135(641), 979-1002.
- Korolev, A., and P. R. Field (2008), The effect of dynamics on mixed-phase clouds: Theoretical considerations, *Journal of the Atmospheric Sciences*, 65(1), 66-86.
- Larson, V. E., B. J. Nielsen, J. W. Fan, and M. Ovchinnikov (2011), Parameterizing correlations between hydrometeor species in mixed-phase Arctic clouds, *Journal of Geophysical Research-Atmospheres*, 116.
- Lebo, Z. J., N. C. Johnson, and J. Y. Harrington (2008), Radiative influences on ice crystal and droplet growth within mixed-phase stratus clouds, *Journal of Geophysical Research-Atmospheres*, 113(D9).
- Liu, X., J. E. Penner, S. J. Ghan, M. Wang (2007), Inclusion of ice microphysics in the NCAR Community Atmospheric Model version 3 (CAM3), *Journal of Climate*, 20(18).
- Liu, X., S. Xie, J. Boyle, S. A. Klein, X. Shi, Z. Wang, W. Lin, S. J. Ghan, M. Earle, P. Liu, A. Zelenyuk (2011), Testing cloud microphysics parameterizations in NCAR CAM5 with ISDAC and M-PACE observations, *Journal of Geophysical Research. D. (Atmospheres)*, 116.
- Lohmann, U., J. Zhang, and J. Pi (2003), Sensitivity studies of the effect of increased aerosol concentrations and snow crystal shape on the snowfall rate in the Arctic, *Journal of Geophysical Research-Atmospheres*, 108(D11).
- Luo, Y. L., K. M. Xu, H. Morrison, and G. McFarquhar (2008), Arctic mixed-phase clouds simulated by a cloud-resolving model: Comparison with ARM observations and sensitivity to microphysics parameterizations, *Journal of the Atmospheric Sciences*, 65(4), 1285-1303.
- MacBean, G. (2004), Arctic climate: Past and present, *Impacts of a Warming Arctic: Arctic Climate Impacts Assessment*, S. J. Hassol, Ed., Cambridge University Press, 21-60.
- McFarquhar, G., B. Schmid, A. Korolev, J. A. Ogren, P. B. Russell, J. Tomlinson, D. D. Turner, and W. Wiscombe (2011), Airborne instrumentation needs for climate and atmospheric research, *Bulletin of the American Meteorological Society*, 92(9), 1193-1196.
- McFarquhar, G. M., G. Zhang, M. R. Poellot, G. L. Kok, R. McCoy, T. Tooman, A. Fridlind, and A. J. Heymsfield (2007), Ice properties of single-layer stratocumulus during the Mixed-Phase Arctic Cloud Experiment: 1. Observations, *Journal of Geophysical Research-Atmospheres*, 112(D24).
- McFarquhar, G. M., et al. (2011), Indirect and Semi-Direct Aerosol Campaign The Impact of Arctic Aerosols on Clouds, *Bulletin of the American Meteorological Society*, 92(2), 183-+.

Möhler, O., D. G. Georgakopoulos, C. E. Morris, S. Benz, V. Ebert, S. Hunsmann, H. Saathoff, M. Schnaiter, R. Wagner (2008), Heterogeneous ice nucleation activity of bacteria: new laboratory experiments at simulated cloud conditions, *Biogeosciences Discussions*, 5, 1445-1468.

Morrison, H., and J. O. Pinto (2005), Mesoscale modeling of springtime Arctic mixed-phase stratiform clouds using a new two-moment bulk microphysics scheme, *Journal of the Atmospheric Sciences*, 62(10), 3683-3704.

Morrison, H., and A. Gettelman (2008), A new two-moment bulk stratiform cloud microphysics scheme in the community atmosphere model, version 3 (CAM3). Part I: Description and numerical tests, *Journal of Climate*, 21(15), 3642-3659.

Morrison, H., and W. W. Grabowski (2008a), A novel approach for representing ice microphysics in models: Description and tests using a kinematic framework, *Journal of the Atmospheric Sciences*, 65(5), 1528-1548.

Morrison, H., J. A. Curry, and V. I. Khvorostyanov (2005a), A new double-moment microphysics parameterization for application in cloud and climate models. Part I: Description, *Journal of the Atmospheric Sciences*, 62(6), 1665-1677.

Morrison, H., J. A. Curry, M. D. Shupe, and P. Zuidema (2005b), A new double-moment microphysics parameterization for application in cloud and climate models. Part II: Single-column modeling of arctic clouds, *Journal of the Atmospheric Sciences*, 62(6), 1678-1693.

Morrison, H., G. de Boer, G. Feingold, J. Harrington, M. D. Shupe, and K. Sulia (2012), Resilience of persistent Arctic mixed-phase clouds, *Nature Geoscience*, 5(1), 11-17.

Ovchinnikov, M., A. Korolev, and J. W. Fan (2011), Effects of ice number concentration on dynamics of a shallow mixed-phase stratiform cloud, *Journal of Geophysical Research-Atmospheres*, 116.

Phillips, V. T. J., P. J. DeMott, and C. Andronache (2008), An empirical parameterization of heterogeneous ice nucleation for multiple chemical species of aerosol, *Journal of Atmospheric Science*, 65, 2757-2783,

Prenni, A., M. D. Petters, S. M. Kreidenweis, C. L. Heald, S. T. Martin, P. Artaxo, R. M. Garland, A. G. Wollny, U. Poschl (2009a), Relative roles of biogenic emissions and Saharan dust as ice nuclei in the Amazon basin, *Nature Geoscience*, 2, 402-405.

Prenni, A. J., P. J. Demott, D. C. Rogers, S. M. Kreidenweis, G. M. McFarquhar, G. Zhang, and M. R. Poellot (2009b), Ice nuclei characteristics from M-PACE and their relation to ice formation in clouds, *Tellus Series B-Chemical and Physical Meteorology*, 61(2), 436-448.

- Prenni, A. J., J. Y. Harrington, M. Tjernstrom, P. J. DeMott, A. Avramov, C. N. Long, S. M. Kreidenweis, P. Q. Olsson, and J. Verlinde (2007), Can ice-nucleating aerosols affect arctic seasonal climate?, *Bulletin of the American Meteorological Society*, 88(4), 541-+.
- Randall, D., T. Carlson, Y. Mintz (1984),: The sensitivity of a general circulation model to Saharan dust heating, *Aerosols and Their Climatic Effects*, H.E. Gerber and A. Deepak, Eds., A. Deepak Publishing, 123-132.
- Randall, D., M. Khairoutdinov, A. Arakawa, and W. Grabowski (2003), Breaking the cloud parameterization deadlock, *Bulletin of the American Meteorological Society*, 84(11), 1547-+.
- Rogers, D.C. (1988), Development of a continuous flow thermal gradient diffusion chamber for ice nucleation studies, *Atmospheric Research*, 22, 149-181.
- Rogers, D.C., P.J. DeMott, and S.M. Kreidenweis (2001), Airborne measurements of tropospheric ice nucleating aerosol particles in the Arctic Spring, *J. Geophys. Res.*, 106, 15,053-15,063.
- Serreze, M., J. A. Francis (2006), The Arctic amplification debate, *Climate Dynamics*, 76, 241-264.
- Shupe, M. D., and J. M. Intrieri (2004), Cloud radiative forcing of the Arctic surface: The influence of cloud properties, surface albedo, and solar zenith angle, *Journal of Climate*, 17(3), 616-628.
- Shupe, M. D., P. Kollias, P. O. G. Persson, and G. M. McFarquhar (2008a), Vertical motions in arctic mixed-phase stratiform clouds, *Journal of the Atmospheric Sciences*, 65(4), 1304-1322.
- Shupe, M. D., V. P. Walden, E. Eloranta, T. Uttal, J. R. Campbell, S. M. Starkweather, and M. Shiobara (2011), Clouds at Arctic Atmospheric Observatories. Part I: Occurrence and Macrophysical Properties, *Journal of Applied Meteorology and Climatology*, 50(3), 626-644.
- Shupe, M. D., J. S. Daniel, G. de Boer, E. W. Eloranta, P. Kollias, C. N. Long, E. P. Luke, D. D. Turner, and J. Verlinde (2008b), A FOCUS ON MIXED-PHASE CLOUDS The Status of Ground-Based Observational Methods, *Bulletin of the American Meteorological Society*, 89(10), 1549-+.
- Solomon, A., H. Morrison, O. Persson, M. D. Shupe, and J. W. Bao (2009), Investigation of Microphysical Parameterizations of Snow and Ice in Arctic Clouds during M-PACE through Model-Observation Comparisons, *Monthly Weather Review*, 137(9), 3110-3128.
- Verlinde, J., et al. (2007), The mixed-phase Arctic cloud experiment, *Bulletin of the American Meteorological Society*, 88(2), 205-+.
- Walsh, J. E., V. M. Kattsov, W. L. Chapman, V. Govorkova, and T. Pavlova (2002), Comparison of Arctic climate simulations by uncoupled and coupled global models, *J. Clim.*, 15, 1429-1446